University of Sussex

Quantum Gravity and the Renormalisation Group

Theoretical advances and applications

Konstantinos Nikolakopoulos

Submitted for the degree of Doctor of Philosophy

University of Sussex

June 2013

Declaration

I hereby declare that this thesis has not been and will not be submitted in whole or in part to another University for the award of any other degree.

Signature:

Konstantinos Nikolakopoulos

UNIVERSITY OF SUSSEX

Konstantinos Nikolakopoulos, Doctor of Philosophy

Quantum Gravity and the Renormalisation Group

Theoretical advances and applications

Summary

It is well known that quantisation of gravity within the conventional framework of quantum field theory faces challenges. An intriguing novel prospect was put forward by S. Weinberg in 1979 who suggested that the metric degrees of freedom of gravity could be quantised non-pertubatively provided that the theory becomes asymptotically safe (AS) at high energies. In this thesis we put forward a systematic search strategy to test the AS conjecture in four dimensional quantum gravity. Using modern renormalisation group (RG) methods and heat kernel techniques we derive the RG equations for gravitational actions that are formed from powers of the Ricci scalar and powers of the Ricci tensor. The non-linear fixed point equations are solved iteratively and exactly. We develop a sophisticated algorithm to express the fixed point iteratively, and to high order, in terms of its lower order couplings. We also evaluate universal scaling exponents and find that the relevancy of invariants at an asymptotically safe fixed point is governed by their classical mass dimension, providing structural support for the asymptotic safety conjecture. We also apply our findings to the physics of higher dimensional black holes. Most notably, we find that the seminal ultra-spinning Myers-Perry black holes cease to exist as soon as asymptotically safe RG corrections are taken into account. Further results and implications of our findings are discussed.

Acknowledgements

I would like to thank my supervisor Daniel Litim for his guidance and advice during my PhD and for providing me exceptional insights into various aspects of particle physics. I would also like to thank my collaborators, officemates and friends, Kevin Falls and Edouard Marchais for fruitful discussions and for making our office such a pleasant workplace. It was an enjoyment to work together with Christoph Rahmede to whom I owe much of my RG expertise. Am pleased to meet and interact with all the faculty members of the TPP group Mark, Stephan, David, Sebastian and Xavier and it was great to spend time inside and outside the department with Ippocratis, Jorge, Denis, Mike, Jan, Rob, Mafalda, Jonny, Jose Miguel, Clio, Tota, Kingsley, Sussane, Nina, Andrew, Agamemnon, Peter, Ting-Cheng, Dimitri, Glauber, Raul, Miguel and Paul.

I want to thank all my friends back home for the pleasant moments we had together whenever time permitted. To mention only but few, Stavros, Tsiou, Hatzis, Mitsos, Alkiviadis, Panagiotis, Nikitas, Thodoris and Dora. I would like to specially thank Keiko for the joyful times we had and for constant encouragement and inspiration during all these years. Last, but certainly not least, I want to thank my family. My parents, Ilias and Chara for the trust and love they have showed me. Needless to say that without their support this thesis would have never been completed. Many thanks to my lovely sister Adriani for all the happy times we have spent together and of course, my aunt Billy who was always there for me.

This work was supported by A.S. Onassis Public Benefit Foundation under grant number [F-ZG066/2010-2011].

Contents

List of Tables

List of Figures

Chapter 1

Introduction

Among the four fundamental forces of nature, gravity is singled out for its unique properties. Firstly, it is universal in the sense that every particle of matter interacts gravitationally and secondly the gravitational force itself is modified by the presence of matter. Moreover, it is described by a unique mathematical framework which provides the geometrical background for every other interaction. The other three forces of nature, electromagnetism, the weak and the strong nuclear forces are well described within the framework of quantum field theory which arises from the combination of quantum mechanics and of special relativity. The long standing problem of quantising gravity concerns the unification of all four forces in one description. General relativity and quantum field theory have to be combined into a common framework which is consistent and which provides an accurate description of gravity at the quantum level.

Macroscopically, the gravitational force is described by classical general relativity formulated by Einstein in 1915. According to this theory, space and time are not independent but form the four dimensional Lorentzian manifold of spacetime. In addition, every form of matter or energy, curves the spacetime and the trajectories of a test particle under gravitational interaction are simply the geodesics of the manifold. The gravitational force is described in purely geometrical terms which can be summarised by Einstein's field equations

$$R_{\mu\nu} - \frac{1}{2} g_{\mu\nu} R = 8\pi G_N T_{\mu\nu} \,. \tag{1.1}$$

The LHS contains the metric $g_{\mu\nu}$ and geometric quantities such as the Ricci tensor of the manifold $R_{\mu\nu}$, and the Ricci scalar curvature R, which are derived from $g_{\mu\nu}$. Therefore, it describes the curvature of the manifold and consequently the gravitational interactions. The RHS of this equation represents the source of this curvature and is formed by the product of Newton's constant G_N and the energy-momentum tensor $T_{\mu\nu}$, which encodes

all the contributions of matter and energy that in turn determine the geometry of the spacetime.

Since the advent of general relativity there have been significant advances both in theoretical and observational sides. The first experimental verification of the theory came in 1919 with the observation that light rays were bending when passing through strong gravitational fields. Since then many precision tests of general relativity have confirmed its validity to very high accuracy [145]. However, it was the theoretical research which provided insights into its very rich structure. It was only a year after the birth of general relativity when Schwarzschild published the first solution to Einstein's equations [139] in the case where the source of the gravitational potential was a point mass. A striking feature of this solution is the existence of a characteristic length, called the Schwarzschild radius, with the property that no particle, even the photon which is massless, can escape from the gravitational field if it lies inside this radius. This was the first description of a black hole. Improvements to this simplified approach included the addition of the electromagnetic field [129, 119], the extension to rotating spacetimes [88] and more recently to higher dimensions [144, 113]. An important breakthrough in the field of black hole physics came with the suggestion of Bekenstein in 1973 [15] that black holes have entropy and with the discovery by Hawking in 1975 [77] who showed that, despite their property of classically being perfectly absorbing objects, they emit black body radiation due to quantum effects. Consequently they can be assigned with thermodynamic properties such as temperature and entropy and they also obey the four laws of black hole thermodynamics [13]. The theory of general relativity has also vastly contributed to the way that we understand the universe and its history. Modern cosmology, primordial perturbations and inflation are all studied within the framework of general relativity [152].

On the other hand, quantum field theory has also provided significant discoveries during the last century. Within this framework it was possible to successfully describe the remaining three fundamental forces, namely electromagnetic, weak and strong nuclear forces. This description is based on the fundamental axioms of quantum mechanics and of special relativity to give accurate predictions for e.g. scattering experiments through the computation of transition amplitudes and cross sections. Further research revealed the very rich structure of the theory and provided us with some of the most fascinating discoveries. The symmetries of the fields play a fundamental role in quantum field theories. In particular, it was found that local symmetries were able to describe all the known forces as being mediated by gauge bosons which are the carriers of each force. It was

the work of Nambu [114] and Goldstone [64, 65] that shed light on the consequences of symmetry breaking. These advances where applied to the field of elementary particle physics and in 1964 the famous Higgs mechanism [80, 79, 73, 51] was proposed. According to this, the electromagnetism and the weak force are the remaining elements of a broken $SU(2) \times U(1)$ symmetry. With the inclusion of the strong nuclear force all the known elementary particles were grouped in a broken $SU(3) \times SU(2)_L \times U(1)_Y$ symmetry which make up the Standard Model of particle physics. The discovery of the Higgs boson [1, 28] provided the last missing piece of the Standard Model. Numerous extensions of this model have been proposed for energy scales higher than 1 TeV and soon the LHC will provide evidence for their validity.

A very intriguing consequence of quantum field theory is that under the inclusion of quantum effects the coupling constants of a theory are no longer constants but become dependent on the energy scale at which they are probed. A very powerful tool in order to study such phenomena was developed, the renormalisation group [150, 151]. Under infinitesimal changes of the momentum scale k, the evolution of a coupling constant g can be summarised in a differential equation, which is called the beta function

$$\beta(g) = \frac{\partial\, g}{\partial \ln k}. \tag{1.2}$$

The corresponding flow of the coupling with varying momentum is called the renormalisation group flow. With the pioneering work of Kadanoff [85] who introduced the concept of scaling with the block-spin representation and Wilson [156, 155, 154, 157] who introduced a concrete mathematical framework, the ideas of renormalisation group became a standard approach in quantum field theory. The picture of energy dependent running couplings has been thoroughly tested and verified by experiments [83].

It is commonly believed that, in order for a theory to be defined fundamentally, all its couplings should approach a fixed point at very high energies [156], where $k \to \infty$. A very good example of such a theory is that of strong interaction, Quantum Chromodynamics (QCD). It was shown [126, 71] that in the ultraviolet (UV) limit the coupling constant of QCD approaches a non-interacting fixed point under the renormalisation group ($\beta(g) = 0\ ;\ g = 0$), implying that the theory is asymptotically free. Traditionally, quantum field theory in general and consequently the renormalisation group were studied with the techniques of perturbation theory. This supposes that the theory is weakly coupled and therefore that coupling constants are small and beta functions are expressed as power series in g. At high energies, QCD is weakly coupled and perturbation theory works well, but at lower energies the theory becomes strongly coupled. The breakdown of

perturbation theory becomes apparent when we approach the characteristic scale of QCD, i.e. Λ_{QCD}. The perturbative beta function predicts a pole at this scale, while it is known that the theory remains finite but it enters a confinement phase. This indicates the need of a non-perturbative treatment for the system.

Now we return to gravity to find out what happens when we are trying to quantise the theory in the usual way. It is a common belief that, at very short distances the gravitational force should be quantised like the other forces of nature. From the fundamental constants of nature one can form only one energy scale where quantum gravity effects become important and this is known as Planck mass

$$M_P = \sqrt{\frac{\hbar\, c}{G_N}} \approx 1.22 \cdot 10^{19}\,\text{GeV} \tag{1.3}$$

where $\hbar$ is Planck's constant, c is the speed of light and G_N is Newton's constant. In natural units, which we use here, we have $\hbar = c = 1$. The corresponding length is the Planck length $l_P \approx 1.62 \cdot 10^{-35}\,\text{m}$. These energy and length scales are far away from the reach of current experiments. In comparison, the maximum energy that the LHC will reach will be $14 \cdot 10^3\,\text{GeV}$ and the precision tests of general relativity are accurate up to lengths $\sim 10^{-3}\,\text{m}$. However, it has been proposed that the scale of quantum gravity could be much less than $\sim 10^{19}\,\text{GeV}$. This could be the case if there exist extra dimensions which are either very large [7, 5] or they are wrapped [128]. Then, the scale of quantum gravity based on current constrains could be as low as the TeV scale, i.e.

$$M_P \sim \mathcal{O}(\text{TeV}). \tag{1.4}$$

This opens a fascinating prospect that quantum gravity effects could be observed at current experiments like the LHC. If this is the case, experimental data would provide the first evidence of quantum gravity and give invaluable insights about the nature of the theory.

However, it is on the theoretical front that attempts to quantise gravity face their most severe challenges. As it was discussed above, in order for a theory to be defined fundamentally and to be predictive at all scales, it needs to be "renormalisable" in the sense that there are enough parameters in order to cancel the divergences. In perturbation theory there is a simple rule to determine if this is the case just by observing the sign of the mass dimension of the relevant coupling constant. For instance, Newton's constant has negative mass dimension $[G_N] = -2$, indicating that perturbative quantisation of general relativity would not be possible. This was indeed verified by explicit calculations of t' Hooft and Veltman [142] in the case of one loop gravity coupled to matter and of Goroff and Sagnotti [67] in the case of pure two loop gravity.

Even though perturbatively non-renormalisable, one can still make sense of quantum general relativity when treated as an effective field theory. In this approach, quantum effects are encoded in the action with terms which are suppressed by a very high energy scale, the scale at which quantum gravity is manifested. In this way, loop contributions can be calculated as well as low energy quantum corrections to the Newtonian potential which are independent of the details of quantum gravity [21, 20, 24] and take the form

$$V(r) = -G_N \frac{m_1 m_2}{r} \left(1 - \frac{167}{30\pi} \frac{G_N \hbar}{r^2}\right). \tag{1.5}$$

Then, a natural question to ask is up to which energy scale this approach can work. One would expect that, as we approach the Planck mass, the effects of quantum gravity become more important and the UV completion of the theory takes over, making the effective field theory description invalid.

The unsurpassable difficulty of quantising gravity pertubatively has led to extensive research towards a novel theory of quantum gravity and the proposition of many candidates. Among them, probably the most popular and the most studied is string theory [68, 69, 124, 125] where new fundamental degrees of freedom, the strings, are introduced. Every known field is then described as excitations of open and closed strings. In particular, the description of gravity through string theory comes from the closed strings that have spin-2 excitations. Moreover, because of the conformal invariance of the string worldsheet the description of gravity as closed strings is perturbatively renormalisable. However, this picture does not come without a price and string theory has yet to be established as credible theory of quantum gravity since there are still drawbacks and open questions. Among them one should mention the difficulty to construct a viable phenomenological model for particle physics and the choice of one unique vacuum among the vast number of possibilities. Other very popular approaches to the problem of quantum gravity include loop quantum gravity (LQG) [8, 138, 137] and the spin foam models [11] where a non-perturbative formulation of quantum gravity is attempted, again with the introduction of new degrees of freedom. Among the successes of these approaches it is important to mention the accurate description of quantum black hole entropy. Finally, in addition to those quantum gravity candidates, discrete approaches have also been formulated in the context of causal dynamical triangulations (CDT) [4] in a similar fashion to lattice approaches of QCD.

In this thesis we are going to be concerned with an alternative to those approaches aforementioned called "Asymptotic safety" [148, 130]. From a certain point of view, this is the most conservative approach to quantum gravity since, in opposite to most of the

others, it does not require the introduction of any new degrees of freedom. The metric degrees of freedom are the carriers of the gravitational force even at the quantum level and the theory is UV complete. To see how this could be the case consider that, despite the fact that gravity is perturbatively non-renormalisable, there is still the possibility that non-perturbative effects render the theory renormalisable in a similar way that the perturbative pole in the QCD beta function can be understood non-perturbatively. In order for that to be true the beta functions of the couplings should approach a renormalisation group fixed point in the UV and there should also be trajectories of the renormalisation group flow that connect the UV fixed point to the semiclassical regime, so that general relativity is recovered at the low energy limit. Moreover, the number of the couplings that are attracted to the fixed point should remain finite. This is because attractive directions represent free parameters of the theory and in order to retain predictivity there should be only a finite number of them to be fixed by experiment. In summary, the asymptotic safety approach to quantum gravity examines the renormalisation group flow of the theory and tries to determine if these requirements are fulfilled.

In order to be more precise we recall how these requirements are translated when we consider a general gravitational theory [148]. Consider a Wilsonian four-dimensional effective action for Euclidean gravity of the form

$$\Gamma_k = \sum_i \int d^4x \, \bar{\lambda}_i \, \mathcal{O}_i \tag{1.6}$$

where the terms $\mathcal{O}_i$ are built out of the metric field and its derivatives in accordance with diffeomorphism invariance, and $\bar{\lambda}_i$ are the corresponding couplings which carry the energy dependence and therefore are functions of k. Denoting the canonical mass dimension of the couplings as $[\bar{\lambda}_i] = d_i$, we introduce dimensionless couplings $\lambda_i = k^{-d_i}\bar{\lambda}_i(k)$. If the term $\mathcal{O}_i$ in the effective action contains $2\,m_i$ derivatives of the metric field, we have $d_i = 4 - 2\,m_i$. The first requirement for a theory to become asymptotically safe is that at high energies ($k \to \infty$) the renormalisation group flow of the theory is governed by an interacting fixed point λ^*. This means that all the couplings approach a fixed point so that

$$\beta_i \equiv \partial_t(\lambda_i) = 0, \tag{1.7}$$

where we have defined $t = \ln k$. Assuming that this is the case, one has to verify that the number of attractive directions remains finite. For this we linearize the flow in the vicinity of the fixed point

$$\beta_i = \sum_j \mathbb{M}_{ij}(\lambda_j - \lambda_j^*) + O[(\lambda_i - \lambda_i^*)^2] \tag{1.8}$$

where $\mathbb{M}_{ij}$ is the stability matrix given by

$$\mathbb{M}_{ij} = \left.\frac{\partial \beta_i}{\partial \lambda_j}\right|_{\lambda=\lambda^*} . \tag{1.9}$$

The most general solution of (1.8) is given by

$$\lambda_i(k) = \lambda_i^* + \sum_n c_n V_i^n k^{\vartheta_n} \tag{1.10}$$

where ϑ_n are the eigenvalues of $\mathbb{M}_{ij}$, V^n are the corresponding eigenvectors and c_n are free parameters. For the directions with negative eigenvalues $\vartheta_n < 0$, at the ultra-violet limit the couplings approach the fixed point. However, for those with positive eigenvalues $\vartheta_n > 0$ the couplings diverge for $k \to \infty$ and so for a theory to be well defined at that limit one has to demand that the respective parameters c_n vanish. This leaves us with a number of undetermined c_n which correspond to the number of negative eigenvalues. In order for a theory to be predictive and renormalisable in the usual sense, the number of these parameters should be finite and consequently they are to be fixed by experiment. This translates to the second requirement for a theory to be asymptotically safe, namely that the number of ϑ_n which are negative remains finite.

The original conjecture of Weinberg [148] in favour of asymptotic safety scenario was based on the following argument. Provided that an ultra-violet fixed point exists, we can read from the canonical mass dimensions of the couplings the following form for the beta functions

$$\beta_i = -d_i\, \lambda_i + \text{quantum corrections}. \tag{1.11}$$

Assuming a free theory where there are no quantum corrections, the corresponding eigenvalues ϑ_n are given by $-d_i$ and consequently only a finite number of them will be negative. Then, in order to spoil the assumptions of asymptotic safety it would be required that the contribution of quantum corrections is so strong that will change the sign of infinitely many eigenvalues. This is considered highly unlikely, even though only a detailed calculation could verify it.

The first evidence for such a scenario came within perturbation theory in $2+\epsilon$ dimensions [59, 29, 148, 86, 3]. The gravitational flow was computed and a fixed point was found. Even though gravity is trivial in 2 dimensions, it was argued that there might exist a continuation to 4 dimensions so that this picture holds true. However, a value of $\epsilon = 2$ is rather big in order to trust perturbative results in a small ϵ expansion. Moreover, gravity in four dimensions is qualitatively different from that in three, where there are no propagating degrees of freedom and two, where gravity is trivial. With these considerations in mind, it becomes apparent that in order to examine four dimensional quantum

gravity one has to perform a non-perturbative calculation that in every theory is a highly non-trivial and a very involved task.

Inspired by the work of Wilson and Kadanoff a very powerful non-perturbative flow equation for the effective action was formulated by Wetterich [153]. A common approximation scheme within this approach is the restriction of invariants in the fundamental action. Following these advances, the first non-perturbative flow equation was derived in 1998 [130] for Einstein-Hilbert approximation and a year later the UV fixed point was first found in 4 dimensions [141]. Since then, a significant amount of research has been devoted to the asymptotic safety program with many new results which provide further evidence for such a scenario [42, 92, 99, 55, 56, 41]. For the significant advances in this front one has to mention extensions of the operator space by adding higher scalar curvature terms starting with the marginal operator R^2 [91] and continuing with an expansion in powers of R up to order 8 [32, 33, 34, 105]. Investigations have also included the first order contribution of more complicated tensor structures such as the Weyl squared term [16, 17]. Moreover, the renormalisation group for gravity under the inclusion of matter fields has been studied [122, 121, 115, 116, 57, 43, 45, 74, 159], as well as investigations for the quantum effects of the ghost sector [44, 46, 70].

Soon after the establishment of asymptotic safety as a candidate theory for quantum gravity, phenomenological applications attracted a lot of interest. The most well studied concerns the physics of black holes and their modifications if such a scenario is realised. The first application to black holes examined the implications of the running of Newton's constant in the case of a Schwarzschild black hole [23]. It was followed by extensions to rotating spacetimes where the Kerr solution [133, 134] was investigated, and also to higher dimensional spherical symmetric black holes [54] as well as black holes coming from higher derivative gravity [26] or from the inclusion of boundary terms [14]. The asymptotic safety scenario has also been applied to cosmology where again the running of the gravitational coupling was implemented in order to examine consequences on physical quantities [131, 10, 81, 135, 35, 36, 82].

In this thesis we will systematically tackle some of the challenges that arise in the search for asymptotic safety and we will investigate applications to the physics of black holes. Our primary focus will be to test the requirements for asymptotic safety to as high precision as possible. For this, we develop a novel strategy and we perform the most advanced computation up to now by significantly extending the operator space. We are able for the first time to examine polynomials of the Ricci scalar up to order 34 and

to investigate their UV properties. We will also study higher order expansions of more complicated tensor structures such as the Ricci tensor $R_{\mu\nu}$. In this way get new insights about the structure of the theory and we are able to quantitatively investigate the effects that higher order operators have on the asymptotic safety scenario. We will also use the results of asymptotic safety in order to examine their implications to the physics of black holes. We will employ the running of Newton's constant and we will investigate how the properties of black holes are modified due to quantum corrections.

The outline of this thesis is as follows. We begin in Chapter 2 with the theoretical background and we recall the basics of the effective action and of the renormalisation group equation which it obeys. We also go through the construction of the flow equation for gravity, following the original work of [130] and we summarise the calculational setup and the methods that we need to use in order to address such equations. In Chapter 3 we develop the technical machinery that we will use for the derivation of renormalisation group flows. This is done in a general context by developing an algorithm which can be adapted to investigate various gravitational approximations. In Chapter 4 we turn back our attention to the physical problem and we investigate the UV properties of a general function of the Ricci scalar $f(R)$ [33, 105]. We put forward a systematic search strategy in order to test the asymptotic safety conjecture within this approximation and we extend the operator space to the 34th power of the Ricci scalar. The results show great stability as we increase the order of approximation and provide valuable insights into the structure of the UV fixed point. With these findings we are able to revisit Weinberg's original argument and to find strong evidence in favour of the asymptotic safety scenario. In Chapter 5 we examine if this picture is modified when we allow more complicated tensor structures. We choose the gravitational approximation to consist of powers of the Ricci tensor squared and single powers of the Ricci scalar. We derive the renormalisation group flow for this approximation and we investigate its UV properties. We find a self-consistent fixed point and three relevant directions for every order up to order 7 in the expansion. These results provide encouraging evidence that more involved tensor structures do not show the tendency to invalidate the asymptotic safety requirements. Subsequently, we turn our attention to phenomenological applications of the asymptotic safety scenario. In Chapter 6 we use as input the running of the gravitational coupling as dictated by asymptotic safety and we examine its effects on black hole physics in the context of rotating black holes in higher dimensions. After a brief review of classical black hole solutions we examine the implications that the running coupling has to their horizon

structure. Moreover, we investigate how thermodynamic quantities such as temperature and specific heat are affected and we also comment on curvature singularities and the possibility that they are absent in the case of asymptotic safety. Finally, we summarise with our conclusions in Chapter 7.

Chapter 2

The renormalisation group for gravity

2.1 Introduction

In this Chapter we will present the theoretical background that we will subsequently use in this thesis. We will recall the derivation of the flow equation and we will outline the basic steps that we have to take in order to evaluate it, as well as the technical tools that we are going to use.

We begin with the effective action which is going to be the central object of interest for our calculations. The construction and the meaning of the effective action as a functional of the classical field are recalled (for reviews see [25, 123, 149]). Then we adopt the Wilsonian approach [156, 155, 154, 157] where the couplings become momentum-dependent quantities and we re-derive [153] the renormalisation group flow for the simplest case of a scalar field. Some approximation schemes and their dependence on the regulator are discussed and the notion of optimisation is introduced [94, 96].

In the second part of this Chapter we are concerned with the specific form of the renormalisation group flow in the case of gravity (for reviews see [118, 132, 120, 101]). We follow the original work of [130] for the derivation of the flow and we begin with a discussion of the diffeomorphism invariance and of the background field formalism. We incorporate these aspects into our formalism and we outline the derivation of the renormalisation group flow for gravity. We also discuss the approximation schemes that are common and the one that we will employ here. Due to the diffeomorphism invariance the effective average action has to be supplemented by a gauge fixing term which we present as well as the corresponding ghost action. Possible regulator schemes are discussed and we specify the

one that we will use. Subsequently we turn our attention to the techniques that we will use in order to evaluate the renormalisation group flow and we review the basic aspects of the heat kernel methods [9, 63].

2.2 Functional flow

In this section we are going to recap the basics for the effective action and we will recall the derivation of the renormalisation group flow for the effective action [153] in the simplest case of a scalar field ϕ. Here we will follow [62] to which we refer for a complete review together with [112, 136].

2.2.1 Effective action

The most fundamental object that we are interested in is the effective action. Here we are going to review its construction and for simplicity we are going to present the results for a scalar field ϕ. We begin by recalling that in a quantum field theory all the information is stored in n-point functions which are obtained by the *generating functional* which in the Euclidean formalism takes the following form

$$Z[J] = e^{W[J]} = \int \mathcal{D}\phi \exp\left[\int d^4x \left(-\mathcal{L}[\phi]\right) + J\phi\right]. \tag{2.1}$$

Here J is the external source and by $J\phi$ we mean $\int d^4x\, J(x)\phi(x)$. The above quantity is called the generating functional because by taking n functional derivatives of $Z[J]$ at $J = 0$ we obtain the n-point functions of a theory defined by the Lagrangian density $\mathcal{L}$. The functional $W[J]$ which appears as the exponent in (2.1) is called the *generating functional of connected diagrams*. The reason for this name is the same as for the functional $Z[J]$. By taking n derivatives of $W[J]$ with respect to the source J at $J = 0$ the result is the *connected* n-point correlation function. A fundamental quantity coming from $W[J]$ comes by taking only one functional derivative of $W[J]$ with respect to the source J

$$\frac{\delta W[J]}{\delta J} = \frac{1}{Z[J]}\frac{\delta Z[J]}{\delta J} = \langle\phi\rangle_J \equiv \varphi, \tag{2.2}$$

where φ is called *the classical field* and it corresponds to the expectation value of the field ϕ in the presence of the source J. Now we can proceed in order to define the quantity that we are going to use extensively, namely the *effective action*. This is given by the Legendre transform of $W[J]$

$$\Gamma[\phi] = \sup_J \left(\int J\phi - W[J]\right) \tag{2.3}$$

where the notation $\sup_J$ denotes that for every ϕ a special J is singled out such that $\int J\phi - W[J]$ approaches its supremum. By solving (2.3) for J_{sup} we have $\phi = \frac{\delta W[J]}{\delta J} = \varphi$ so that we can write

$$\Gamma[\varphi] = \int J\varphi - W[J]. \tag{2.4}$$

The effective action is an object which is a functional of the classical field φ and thus it incorporates all the quantum fluctuations. The meaning of the effective action becomes clear when we take a functional derivative with respect to its argument

$$\frac{\delta\Gamma[\varphi]}{\delta\varphi} = J(x). \tag{2.5}$$

These are the *quantum equations of motion* by which the effective action $\Gamma[\varphi]$ governs the dynamics of the field expectation value, taking the effects of all quantum fluctuations into account. By taking another functional derivative of the effective action with respect to the classical field φ we arrive to the following expression written in matrix notation

$$\frac{\delta^2\Gamma[\varphi]}{\delta\varphi(x)\delta\varphi(y)} = \left(\frac{\delta^2 W[J]}{\delta J(x)\delta J(y)}\right)^{-1} \equiv G(x,y)^{-1} \tag{2.6}$$

where $G(x,y)$ is the exact propagator of the field ϕ and so that the object $\frac{\delta^2\Gamma[\varphi]}{\delta\varphi(x)\delta\varphi(y)}$ is called the *inverse propagator*.

2.2.2 The flow equation

The first step towards deriving the flow equation for the effective action is to adopt the Wilsonian approach for integrating out momentum modes shell by shell. As a result the effective action and all the couplings of the theory are turned into momentum dependent quantities. The price to pay is that in order to study the flow of the effective action we should include in it all the terms that are consistent with the symmetries of the theory. After adopting the above picture we end up with an interpolating action Γ_k which is called the *effective average action*, such that Γ_k corresponds to the bare action for $k \to \Lambda$ and to the full quantum action for $k \to 0$ (see Figure 2.1). In order to define the effective average action we proceed as before and we start with the definition of the IR regulated generating functional

$$Z_k[J] = e^{W_k[J]} = \int_\Lambda \mathcal{D}\phi\, e^{-S[\phi]-\Delta S_k[\phi]+\int J\phi}, \tag{2.7}$$

which is the generating functional defined in (2.1) plus the regulator term $\Delta S_k[\phi]$ which plays the role of the cutoff at some energy scale k. The regulator term takes the form

$$\Delta S_k[\phi] = \frac{1}{2}\int \frac{d^dq}{(2\pi)^d}\phi(-q)\mathcal{R}_k(q)\phi(q) \tag{2.8}$$

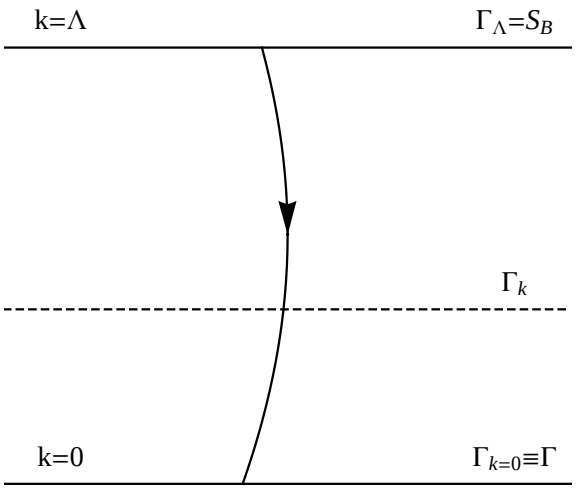

Figure 2.1: The effective average action Γ_k interpolating between the bare action S_B $k \to \Lambda$ and the full quantum effective action Γ for $k \to 0$.

so that it is quadratic in the fields and can be viewed as a momentum dependent mass term. The regulator is in general an arbitrary momentum-dependent function, but in order to implement correctly the IR regularisation and to ensure that the flow equation is finite it should satisfy the following conditions

$$\lim_{q^2/k^2 \to 0} \mathcal{R}_k(q) > 0 \qquad ; \qquad \lim_{k^2/q^2 \to 0} \mathcal{R}_k(q) = 0 \qquad ; \qquad \lim_{k^2 \to \Lambda,\, \Lambda \to \infty} \mathcal{R}_k(q) \to \infty \tag{2.9}$$

The first condition is required so that the regulator term actually implements an IR regularisation and so that no infrared divergences are encountered in the presence of massless modes. The second condition is required in order to recover the full effective action at the infrared limit, $\lim_{k \to 0} \Gamma_k = \Gamma$. Finally, the third is required so that the bare action S_B is recovered at the UV limit $k^2 \to \Lambda$ and $\Lambda \to \infty$. In Figure 2.2 we have plotted a typical smooth regulator and its scale derivative. It follows that the effective average action is defined as

$$\Gamma_k[\phi] = \sup_J \left(\int J\phi - W_k[J] \right) - \Delta S_k[\phi] \tag{2.10}$$

and by repeating the same process as before we have at the supremum of the quantity inside the brackets that $\varphi = \langle \phi \rangle_J = \frac{\delta W_k[J]}{\delta J(x)}$. Consequently for the full propagator we get

$$\frac{\delta \varphi(x)}{\delta J(y)} = \frac{\delta^2 W_k[J]}{\delta J(y) \delta J(x)} \equiv G_k(x-y). \tag{2.11}$$

By taking one functional derivative of the effective average action we have for the quantum equations of motion $J(x) = \frac{\delta \Gamma_k[\varphi]}{\delta \varphi(x)} + \mathcal{R}_k(x)\varphi(x)$ and then by taking another functional

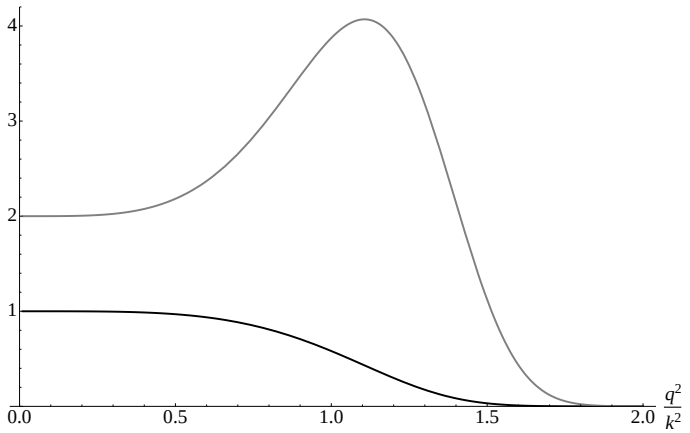

Figure 2.2: A smooth exponential regulator $\mathcal{R}_k$ (black line) and its scale derivative $k\,\partial_k\mathcal{R}_k$ (grey line) as functions of momenta q^2 in units of k^2. By virtue of (2.17) the regulator provides and IR regularisation and its scale derivative a UV regularisation for the flow of the effective average aciton.

derivative we have

$$\frac{\delta J(x)}{\delta\varphi(y)} = \frac{\delta^2\Gamma_k[\varphi]}{\delta\varphi(x)\delta\varphi(y)} + \mathcal{R}_k(x,y). \tag{2.12}$$

This implies in operator notation that the Hessians $\Gamma_k^{(2)} = \frac{\delta^2\Gamma_k[\varphi]}{\delta\varphi(x)\delta\varphi(y)}$ plus the Regulator is the inverse of the full propagator

$$\left(\Gamma_k^{(2)} + \mathcal{R}_k\right)^{-1} = G_k\,. \tag{2.13}$$

What we are really interested in is the cutoff scale dependence of the effective average action. For this we define $t = \ln\frac{k}{\Lambda}$ and $\partial_t = k\frac{d}{dk}$ and we compute the ∂_t derivative of the generating functional of connected diagrams $W_k[J]$

$$\partial_t W_k[J] = -\frac{1}{2}\int \frac{d^dq}{(2\pi)^d}\partial_t\mathcal{R}_k(q)\,\langle\phi(-q)\phi(q)\rangle \tag{2.14}$$

Now we have for the ∂_t derivetive of the $\Delta S_k[\varphi]$ term of the classical field φ

$$\partial_t\Delta S_k[\varphi] = -\frac{1}{2}\int \frac{d^dq}{(2\pi)^d}\langle\phi(-q)\rangle\partial_t\mathcal{R}_k(q)\langle\phi(q)\rangle \tag{2.15}$$

Combining the two expressions above and since we know that the full propagator is given by $G_k(q) = \langle\phi(-q)\phi(q)\rangle - \langle\phi(-q)\rangle\langle\phi(q)\rangle = \langle\phi(-q)\phi(q)\rangle_{\text{conn}}$ we can substitute in (2.14) in order to write

$$\partial_t W_k[J] = -\frac{1}{2}\int \frac{d^dq}{(2\pi)^d}\partial_t\mathcal{R}_k(q)\,G_k(q) + \partial_t\Delta S_k[\varphi]. \tag{2.16}$$

Now we have all the ingredients that we need in order to compute the scale derivative of the average effective action. Then we have

$$\begin{aligned}\partial_t \Gamma_k[\varphi] &= -\,\partial_t W_k[J] - \partial_t \Delta S_k[\varphi] \\ &= \frac{1}{2}\mathrm{Tr}\left[\left(\Gamma_k^{(2)} + \mathcal{R}_k\right)^{-1} \partial_t \mathcal{R}_k\right].\end{aligned} \tag{2.17}$$

Here the trace denotes the sum over all indices and the integration over all momenta. Equation (2.17) is the flow equation for the effective average action and it is central for the study to follow in this thesis. It provides information about infinitesimal changes of the effective average action under the momentum scale and it has the property that is both UV and IR finite. In the UV the scale derivative of the regulator renders this equation finite, while in the IR the regulator itself is used to regulate $\Gamma_k^{(2)}$. Therefore, despite the difficulty to define the effective action one could in principle integrate the flow equation for the effective average action.

2.2.3 Optimisation

The flow equation (2.17) is a very powerful tool for addressing non-perturbative aspects of quantum field theories. However, these problems are often too complex to solve exactly and we have to rely on some kind of approximation scheme. A common approximation scheme that is used is the derivative expansion where the effective average action is expanded in terms of the number of derivatives that act on the field [66]. Similarly one can approximate the effective average action using the vertex expansion where a series in terms of the number of vertices is examined. It is also common to use combination of approximation schemes like the two mentioned here. With these considerations in mind it becomes evident that we need to have a systematic control of the approximation in order to ensure that the dependence of the results on it is minimised.

The truncated flows will in general depend on the regulator in a non-trivial way [12, 93, 6]. Note that this dependence disappears when we go to the infrared limit ($k \to 0$) and we recover the full quantum effective action. However, there can be many trajectories like the one sketched in Figure 2.1 that connect the same endpoints S_B and Γ but have a different renormalisation group flows due to different regulators. The notion of optimisation [94, 97] was then developed by demanding that the regulator is chosen such that the leading order terms of the relevant expansion, will approximate the full flow in an optimised way.

For example, consider the derivative expansion of the $O(N)$ scalar model in $3d$. The physical critical exponents ν_{phys} are expressed as the sum of additional contributions

$\nu_i(RS)$ from each order of the derivative expansion i, with the argument (RS) to indicate the dependence on the regularisation scheme

$$\nu_{\text{phys}} = \nu_0(RS) + \nu_1(RS) + \nu_2(RS) + \dots \tag{2.18}$$

Then it turns out [95], that using a regulator profile function which takes the form

$$R_k(q^2) = (k^2 - q^2)\theta(k^2 - q^2). \tag{2.19}$$

most of the physical information is encoded in $\nu_0(RS_{\text{opt}})$ and that the radius of convergence for such an expansion is maximised. The optimised cutoff (2.19) takes the form of a theta function where for $q^2 > k^2$ vanishes identically, while for $k^2 > q^2$ acts like a momentum dependent mass term. It has been shown that this regulator leads to better stability and convergence properties of the functional flows [94, 96]. It also provides algebraic simplifications for the flows which will become of great importance when we will be concerned with gravity. For a more detailed analysis of the optimised regulator benefits see [104] where the $3d$ Ising model is examined up to the fourth order in the derivative expansion. Since its introduction, the regulator (2.19) has been very popular in the context of quantum gravity and the previous studies of $f(R)$ gravity [33, 105] use this. It is also the regulator profile function that we are going to use in the rest of this thesis.

2.3 Functional flow for gravity

In the first part of this Section we collect the elements in order to derive the renormalisation group flow for gravity following the original work of [130]. In what follows we will review the basic ingredients that we will need to use in order to derive renormalisation group flows for gravity without relying on specific ansatz. Finally we recap the heat kernel methods which we are going to use for the calculation of the functional trace in (2.17).

2.3.1 Diffeomorphism invariance

In order to construct the functional renormalisation group flow for gravity we have to take into account the symmetries of the theory. In gravity this means that the effective action is invariant under the general coordinate transformation

$$\delta g_{\mu\nu} = \mathcal{L}_v g_{\mu\nu} \tag{2.20}$$

where $\mathcal{L}_v$ is the Lie derivative with respect to the vector field v^μ. In gauge theories this is usually implemented with the aid of the Ward identities. These are expressed in the form

of an identity for the functional Γ that satisfies an equation $W[\Gamma] = 0$. When we adopt the Wilsonian picture and we turn to the effective average action Γ_k the Ward identities become momentum dependent $W_k[\Gamma_k] = 0$ and the requirement that $\lim_{k\to 0} W_k[\Gamma_k] = W[\Gamma]$ is automatically satisfied provided that Γ_k obeys the flow equation (2.17) (see [102] for a complete discussion in the context of QCD).

However, in gravity it is common that one makes approximations for the effective average action and therefore there is no guarantee that the Ward identities are still satisfied. In order to implement diffeomorphism invariance in our study we employ the background field method [2]. According to this we decompose our original field into an arbitrary fixed background and a fluctuation field which transforms under quantum gauge transformations and also becomes the integration variable in the path integral. In the case of gravity we decompose the metric field $\gamma_{\mu\nu}(x)$ into an arbitrary constant background $\bar{g}_{\mu\nu}(x)$ and a fluctuation $h_{\mu\nu}(x)$ according to

$$\gamma_{\mu\nu}(x) = \bar{g}_{\mu\nu}(x) + h_{\mu\nu}(x). \tag{2.21}$$

Then we can replace the integration over $\gamma_{\mu\nu}(x)$ with an integration over $h_{\mu\nu}(x)$. For a complete discussion about the construction of Wilsonian flows using the background field methods see [58]. As is discussed in the first application of the background field method in RG gravity studies [130] the effective action Γ_k should be invariant under the general coordinate transformation

$$\Gamma_k[\chi + \mathcal{L}_v\chi] = \Gamma_k[\chi], \tag{2.22}$$

where χ stands collectively for all the fields that Γ_k depends on and the Lie derivative is with respect to the background gauge transformations. Because of the gauge symmetry the action should be supplemented with a gauge fixing term and the respective ghost term, the specific form of which will be presented in Section 2.3.3. Then, the background field method guarantees that the effective average action remains gauge invariant apart from the terms that explicitly break the symmetry.

2.3.2 The flow equation for gravity

For the construction of the flow equation for gravity we follow [130] and we start by writing down the most general scale-dependent partition function

$$Z_k[J] = \int \mathcal{D}h_{\mu\nu}\mathcal{D}C^\mu\mathcal{D}\bar{C}_\mu \exp\left[-S_{\rm gr}[\bar{g}+h] - S_{\rm gf}[h;\bar{g}] - S_{\rm gh}[h,C,\bar{C};\bar{g}] - S_{\rm source} - \Delta S_k\right] \tag{2.23}$$

where $S_{\rm gr}$ is our ansatz for the gravitational action, S_{gf} is the gauge fixing term, $S_{\rm gh}$ is the ghost term and $S_{\rm source}$ is the source action. The fields C and $\bar{C}$ are the Faddeev-Popov ghosts. Now, in analogy with the classical scalar field φ discussed in the previous section, we define the classical counterparts of the metric and the ghost fields to be respectively $g_{\mu\nu}$ and c, $\bar{c}$. Now the classical metric is split to the background and the classical fluctuation $\bar{h}$ as $g_{\mu\nu}(x) = \bar{g}_{\mu\nu}(x) + \bar{h}_{\mu\nu}(x)$. Consequently, we write the effective average action in terms of the classical fields

$$\Gamma_k[g, c, \bar{c}\,; \bar{g}]. \tag{2.24}$$

The conventionally defined effective action is then obtained at the limit

$$\Gamma[g_{\mu\nu}] = \lim_{k\to 0} \Gamma_k[g_{\mu\nu}, 0, 0; g_{\mu\nu}] \tag{2.25}$$

and it follows that $\Gamma[g_{\mu\nu}]$ is invariant under the gauge transformations $\delta g_{\mu\nu} = \mathcal{L}_v g_{\mu\nu}$. For the renormalisation group flow of the effective average action we then have [130]

$$\begin{aligned}\partial_t \Gamma_k[\bar{h}, c, \bar{c}\,; \bar{g}] =& \frac{1}{2}\mathrm{Tr}\left[\left(\Gamma_{\rm k}^{(2)} + \mathcal{R}_{\rm k}\right)^{-1} \partial_{\rm t}\mathcal{R}_{\rm k}\right]_{\bar{\rm h}\bar{\rm h}} + \frac{1}{2}\mathrm{Tr}\left[\left(\Gamma_{\rm k}^{(2)} + \mathcal{R}_{\rm k}\right)^{-1} \partial_{\rm t}\mathcal{R}_{\rm k}\right]_{\bar{\rm c}\rm c} \\ &- \frac{1}{2}\mathrm{Tr}\left[\left(\Gamma_{\rm k}^{(2)} + \mathcal{R}_{\rm k}\right)^{-1} \partial_{\rm t}\mathcal{R}_{\rm k}\right]_{\rm c\bar{c}}\end{aligned} \tag{2.26}$$

with the following definition for the second variation $\Gamma_k^{(2)}$ of two fields χ_i and χ_j

$$\left(\Gamma_k^{(2)}\right)_{\chi_i\chi_j} \cdot \mathbb{I} \cdot \delta(x-y) = \frac{1}{\sqrt{\bar{g}(x)}} \frac{\delta}{\delta\chi_i(x)} \frac{1}{\sqrt{\bar{g}(y)}} \frac{\delta\Gamma_k}{\delta\chi_j(y)} \tag{2.27}$$

and $\mathbb{I}$ being the unit element on the space of fields χ_i and χ_j carrying the appropriate index structure. Note that the second variation involves derivatives of the fluctuating field at a fixed value of the background field.

Now we have to make an appropriate choice of ansatz for the effective average action Γ_k in order to solve the above flow equation. At this point there is the necessity to rely on some approximation schemes so that we make the equation tractable. Here we describe the three steps of approximation and the resulting flow equation. First, for the gravitational effective action one has to truncate the theory space in order to have a system of finite number of differential equations. Secondly, one has to address the issue of quantum effects coming from the ghost action and having to solve bimetric equations. For this we make an approximation ansatz for Γ_k as

$$\Gamma_k[\bar{h}, c, \bar{c}\,; \bar{g}] = \bar{\Gamma}_k[\bar{g} + \bar{h}] + \hat{\Gamma}_k[\bar{h}\,; \bar{g}] + S_{\rm gf}[\bar{h}; \bar{g}] + S_{\rm gh}[\bar{h}, c, \bar{c}; \bar{g}], \tag{2.28}$$

where we have defined

$$\bar{\Gamma}_k[\bar{g} + \bar{h}] = \Gamma_k[\bar{g}, 0, 0\,; \bar{g}] \tag{2.29}$$

and $\hat{\Gamma}_k[g,\bar{g}]$ encodes all the terms that violate the split symmetry of Γ_k for $g \neq \bar{g}$. Then the last step of approximation is to set $\hat{\Gamma}_k = 0$. In this way one ends up with an equation which is function only of one metric. To clarify further the benefits of this simplification note that now the second variation (2.27) is a variation of only fluctuating fields which makes the calculation considerably simpler. By virtue of the modified Ward identities it was shown [130] that this is a good leading order approximation. Moreover, results with the ghost sector included [44, 46, 70] indicate that the quantitative impact that this has is not important. Recently, also bimetric truncations for gravity have been considered [106, 107, 108]. The final form for the approximation of the effective average action will then be

$$\Gamma_k[g,\bar{g},c,\bar{c}] = \bar{\Gamma}_k[g] + S_{\rm gf}[h;\bar{g}] + S_{\rm gh}[h,c,\bar{c};\bar{g}]. \tag{2.30}$$

Then, the flow equation that we are interested in is given by

$$\partial_t \bar{\Gamma}_k[g] = \frac{1}{2}\mathrm{STr}\left[\left(\Gamma_k^{(2)} + \mathcal{R}_k\right)^{-1}_{\chi_i\chi_j} \partial_t\left(\mathcal{R}_k\right)_{\chi_j\chi_i}\right], \tag{2.31}$$

where χ_i stand collectively for the metric and ghost degrees of freedom.

2.3.3 Gauge fixing and ghosts

Because of the diffeomorphism invariance of the metric field the effective action has to be supplemented with a gauge fixing term so that only the physical modes of the field are taken into account. Following [130] it is convenient to choose a gauge fixing term of the form

$$S_{\rm gf} = \frac{1}{2\alpha}\int d^dx\sqrt{\bar{g}}\,\bar{g}^{\mu\nu}\mathcal{F}_\mu\mathcal{F}_\nu \tag{2.32}$$

with the gauge fixing condition $\mathcal{F}_\mu = 0$. Here we will choose the function $\mathcal{F}_\mu$ to be given by [121]

$$\mathcal{F}_\mu = \sqrt{2}\kappa\left(\bar{\nabla}^\nu h_{\mu\nu} - \frac{1+\rho}{d}\bar{\nabla}_\mu h\right), \tag{2.33}$$

with $\kappa = (32\pi G_N)^{-1/2}$ and $h = h^{\mu\nu}\bar{g}_{\mu\nu}$ being the trace of the fluctuation. The gauge fixing condition that was originally used in [130] corresponds to $\rho = \frac{d}{2} - 1$. Here and from now on barred geometrical quantities such as $\bar{\nabla}$ above, mean that they are constructed by the background metric $\bar{g}_{\mu\nu}$. Then, by substituting $\mathcal{F}_\mu$ into the gauge fixing action we get

$$S_{\rm gf} = \frac{\kappa^2}{\alpha}\int d^dx\sqrt{\bar{g}}\left[\bar{\nabla}^\rho h_{\mu\rho}\bar{\nabla}^\lambda h^\mu_\lambda - \left(\frac{1+\rho}{d}\right)^2 h\bar{\nabla}^2 h + 2\frac{1+\rho}{d}h\bar{\nabla}_\mu\bar{\nabla}^\rho h^\mu_\rho\right]. \tag{2.34}$$

The corresponding ghost action for the above gauge fixing is

$$S_{\rm gh} = -\sqrt{2}\int d^dx\sqrt{\bar{g}}\bar{C}^\mu M_{\mu\nu}C^\nu, \tag{2.35}$$

where in the first order of the expansion the Faddeev-Popov operator is given by

$$M_{\mu\nu} = \bar{\nabla}^{\rho}\bar{g}_{\mu\nu}\bar{\nabla}_{\rho} + \bar{\nabla}^{\rho}\bar{g}_{\rho\nu}\bar{\nabla}_{\mu} - 2\frac{1+\rho}{d}\bar{\nabla}_{\mu}\bar{g}^{\rho\sigma}\bar{g}_{\rho\nu}\bar{\nabla}_{\sigma}. \tag{2.36}$$

In Chapter 3 we are going to compute the second variation of the ghost fields from (2.35) and the contribution to the gravitational second variation coming from the gauge fixing term (2.35).

2.3.4 Regulator schemes

The last ingredient of the flow equation consists of the regulator term. In general the second variation for each component field will be a function of some differential operator $\mathcal{O}$. The general prescription is that the regulator term $\mathcal{R}_k^{\phi_i\phi_j}$ for an inverse propagator $\left(\Gamma_k^{(2)}\right)^{\phi_i\phi_j}$ is chosen such that it leads to the replacement

$$\mathcal{O} \to \mathcal{O} + R_k(\mathcal{O}) \tag{2.37}$$

where $R_k(\mathcal{O})$ is the regulator profile function. At this stage we have some freedom for choosing the cutoff scheme by choosing different definitions for the differential operator $\mathcal{O}$. As has been extensively discussed in the literature [34] we split the differential operator according to $\mathcal{O} = -\nabla^2 + \mathbf{E}$, where ∇^2 represents the covariant derivative for both diffeomorphism invariance and all other possible gauge symmetries and $\mathbf{E}$ is a linear map acting on the field. In turn we split the potential term as $\mathbf{E} = \mathbf{Q} + \mathbf{E}_k$ where $\mathbf{Q}$ is independent of the couplings and $\mathbf{E}_k$ depends on the couplings of the theory. Then we discriminate between three different cases for the differential operator $\mathcal{O}$. If it contains only the covariant derivatives of the theory we call this regulator scheme as *Type I cutoff*. This was the cutoff first used in [130]. If the regulator term contains the covariant derivatives plus a coupling independent term $\mathbf{Q}$ we then call it *Type II cutoff*. This was the case investigated in [34] where the potential $\mathbf{Q}$ was chosen as $\frac{R}{d}$ for the gravity part and as $R_{\mu\nu}$ for the ghost fields. Finally, if in addition to ∇^2 and $\mathbf{Q}$ the regulator scheme also contains a potential term which depends on the couplings as $\mathbf{E}_k$, then it is called *Type III cutoff*. This type of cutoff was again introduced in the context of Einstein-Hilbert truncation in [34] by stripping out the gravitational regulator from the wavefunction renormalisation. In what follows we are going to use a Type I cutoff for our calculations.

2.3.5 Choice of background

Up to now we have left the background metric undetermined. In order to calculate the renormalisation group flow we will use the heat kernel methods which are described in

2.3.6. To use these techniques we eventually have to make a choice for the background metric $\bar{g}_{\mu\nu}$. For our purposes and in order to make the evaluation of the flow simpler we will choose our background to be a sphere. Then we have the following identities

$$\bar{R}_{\mu\nu} = \frac{\bar{R}}{d}\bar{g}_{\mu\nu} \qquad ; \qquad \bar{R}_{\mu\nu\rho\sigma} = \frac{\bar{R}}{d(d-1)}\left(\bar{g}_{\mu\rho}\bar{g}_{\nu\sigma} - \bar{g}_{\mu\sigma}\bar{g}_{\nu\rho}\right). \tag{2.38}$$

This choice of background amounts to projecting all the tensorial structures to the scalar curvature $\bar{R}$. However, a non-trivial dependence of the various tensors comes into consideration through the evaluation of the second variation. For a more detailed discussion about the background dependence see [106].

2.3.6 Heat Kernel techniques

Here we are going to recall the general methods for evaluating the flow equation using the heat kernel techniques [9, 63]. The RHS of the flow equation (2.17) consists of the functional trace over the quantity $\partial_t \mathcal{R}_k(\Gamma_k^{(2)} + \mathcal{R}_k)^{-1}$. As mentioned, the functional trace has the meaning of the sum over all indices and the integration over all momenta. In general, the functional trace of a function $W(\mathcal{O})$ of an operator $\mathcal{O}$ is given by the sum

$$\mathrm{Tr}_s\, W(\mathcal{O}) = \sum_i W(\lambda_i), \tag{2.39}$$

where λ_i are the eigenvalues of the operator. By introducing the Laplace anti-transform $\tilde{W}(t)$ we express $W(t) = \int ds\, e^{-ts}\tilde{W}(t)$ and we substitute back in (2.39) in order to write

$$\mathrm{Tr}W(\mathcal{O}) = \int_0^\infty dt\, \tilde{W}(t)\, \mathrm{Tr}_s e^{-t\mathcal{O}} \tag{2.40}$$

where $K(t) = e^{-t\mathcal{O}}$ is the heat kernel of the operator $\mathcal{O}$. In equation (2.40) the subscript s denotes the spin of the field which the operator $\mathcal{O}$ acts on and takes the values 0 for scalars, 1 for vectors and 2 for 2-tensors. The trace of the heat kernel has a well known early time ($t \to 0$) asymptotic expansion given by [9]

$$\begin{aligned}\mathrm{Tr}_s e^{-t\mathcal{O}} = \frac{1}{(4\pi)^{d/2}} \int d^dx\sqrt{g}\, \Big[&\mathrm{tr}_s\mathbf{b}_0(\mathcal{O})t^{-\frac{d}{2}} + \mathrm{tr}_s\mathbf{b}_2(\mathcal{O})t^{-\frac{d}{2}+1} + \dots \\ &+\mathrm{tr}_s\mathbf{b}_d(\mathcal{O}) + \mathrm{tr}_s\mathbf{b}_{d+2}(\mathcal{O})t + \dots\Big].\end{aligned} \tag{2.41}$$

The coefficients $\mathbf{b}_n$ are called the heat kernel coefficients and they are linear combinations of curvature tensors and their derivatives of order $2n$. The trace of the coefficients that we will need in this thesis evaluated in the spherical background metric can be read in Appendix B. Now we define $B_n = \int d^dx\sqrt{g}\,\mathrm{tr}_s\mathbf{b}_n(\mathcal{O})$ and $Q_n[W] = \int_0^\infty dt\, t^{-n}\tilde{W}(t)$, so that we can write equation (2.40) in the following form

$$\mathrm{Tr}W(\mathcal{O}) = \frac{1}{(4\pi)^{d/2}} \sum_{n=0}^{\infty} Q_{\frac{d}{2}-n} B_{2n}(\mathcal{O}). \tag{2.42}$$

Now the functional trace is expressed as the early time expansion for the heat kernel of the operator $\mathcal{O}$ instead of the spectral sum (2.39). One of the great benefits of this representation is that by using the optimised cutoff (2.19) the series truncates because all the $Q_n[W]$ vanish for $n < -d$. Therefore with a finite number of heat kernel coefficients we can derive the full flow. This becomes apparent when we make use of the Mellin transform and we express the functional $Q_n[W]$ in terms of the original function $W(z)$. Then we have that for every $n > 0$

$$Q_n[W] = \frac{1}{\Gamma(n)} \int_0^\infty dz\, z^{n-1} W(z) \tag{2.43}$$

and similarly for Q_{-n} with $n \geq 0 \in \mathbb{Z}$ we have

$$Q_{-n}[W] = (-1)^n \left. \frac{d^n W(z)}{dz^n} \right|_{z=0} . \tag{2.44}$$

In Chapter 3 we will develop a general algorithm for computing these functionals just with the knowledge of the second variation. It will then become clear that the usage of the optimised cutoff truncates the series and we end up with an exact flow.

As will become clear later, there are some cases where we have to exclude certain modes from the trace computation due to constraints that some fields obey. Here we are going to state the general mechanism of how this is taken into account. More details about the specific exclusions that we are going to use can be found in the Appendix B. Since the trace of an arbitrary smooth function $W(\mathcal{O})$ can be represented as its spectral sum, the general rule for omitting the missing modes from the trace of an operator valued function is

$$\mathrm{Tr}_s^{\prime\cdots\prime}[W(-\nabla^2)] = \mathrm{Tr}_s[W(-\nabla^2)] - \sum_{l=1}^{l=m} D_l(d,s) W(\Lambda_l(d,s)) \tag{2.45}$$

where the m primes on the LHS indicate the number of modes to be subtracted and $D_l(d,s)$ are the degeneracies of the eigenvalues $\Lambda_l(d,s)$. For the operator $-\nabla^2$ acting on scalars, transverse vectors and transverse-traceless symmetric tensors $D_l(d,s)$ and $\Lambda_l(d,s)$ are given in Table B.1 of Appendix B.

2.4 Summary

In this Chapter we have summarised the theoretical background of this thesis and we have gathered together all the ingredients that we will need in order to proceed with the evaluation of the renormalisation group flow for gravity. We have briefly reviewed the fundamental aspects of the effective average action and the equation which it obeys

under the renormalisation group. We then discussed the choice of the regulator function according to the optimisation principle.

In the second part we reviewed the derivation and the form of the flow for a gravitational theory and we presented the form of the gauge fixing and ghost actions. Subsequently we reviewed the regulator schemes that are common and we chose the one that we will use for our computations. Finally we recalled the heat kernel methods which are used in order to evaluate the trace which enters the flow equation.

Chapter 3

Flow derivation

3.1 Introduction

The functional equation (2.31) provides a powerful tool for the investigation of the renormalisation group flow for gravity. For the derivation of such a flow we need to divide the calculation into separate steps and to develop some technical machinery. In this chapter we present some computational techniques for the two main elements of the flow calculation, namely, the evaluation of the second variation and of the functional trace. The results of this chapter are kept general and they will subsequently be used in Chapter 4 and Chapter 5 for the derivation of the gravitational flow in different approximations.

In the first part we are concerned with the derivation of the second variation. It is important to choose a representation for our field in such a way that the resulting second variation is a function of operators with known heat kernel coefficients. For this reason we decompose the metric field into its transverse traceless components [158, 42]. This is a change of integration variables in the path integral which leads to the appearance of auxiliary fields through the determinants of the transformation. After performing the decomposition we determine the second variation for the gauge fixing action and the corresponding ghost action. In this way we compute the Hessians for all the parts of the effective average action (2.30) apart from the gravitational anstaz $\bar{\Gamma}_k$ which will be computed in the corresponding chapters.

In the second part of this chapter we are interested in the functional trace that appears in (2.31). We develop a general algorithm for the evaluation of the trace which has as input the Hessian of a field and as output a closed expression for the functions $Q_n[W]$ in the heat kernel expansion (2.42). We write the Hessians as power series of the operator ∇^2 and we adopt the choice of cutoff type and of regulator profile as outlined in Chapter

2. Then we proceed step by step and we derive analytic expressions for all the functions $Q_n[W]$. The flow equation is then obtained simply by summing the appropriate terms in the heat kernel expansion.

The rest of this chapter is organised as follows. In Section 3.2 we present the derivation of the Hessians. We start in 3.2.1 by discussing the transverse traceless decomposition of the metric field and the transverse decomposition of the ghost fields. We then substitute in the gauge fixing action and in 3.2.2 we find the contribution to the Hessian due to the gauge fixing. Similarly in 3.2.3 we compute the Hessian of the ghost action. Then, in 3.2.4 we examine the metric and ghost decomposition to determine the contributions in the action of the auxiliary fields and to compute their Hessians. In Section 3.3 we present the algorithm for the computation of the functional trace. In 3.3.1 we determine the regulator term for a *Type I cutoff* and in 3.3.2 we compute the coefficients $Q_n[W]$ for the diagonal piece of the Hessian. In 3.3.3 we compute $Q_n[W]$ for the non-diagonal piece of the Hessian where we have a mixing between two components and in 3.3.4 we investigate the case where certain modes have to be excluded from the trace. Finally, in Section 3.4 we summarise our results.

3.2 Computing the Hessians

Here we are going to derive the Hessians for all the fields that contribute to the flow equation apart from the gravitational part which will be derived in the next chapters according to the ansatz chosen. As explained in 2.3.2 the effective average action takes the form

$$\Gamma_k[g, \bar{g}, c, \bar{c}] = \bar{\Gamma}_k[g] + S_{\rm gf}[h; \bar{g}] + S_{\rm gh}[h, c, \bar{c}; \bar{g}]. \tag{3.1}$$

Here $\bar{\Gamma}_k[g]$ encodes the gravity part which we leave undetermined for now, $S_{\rm gf}[h; \bar{g}]$ is the contribution from the gauge fixing term and $S_{\rm gh}[h, c, \bar{c}; \bar{g}]$ is the contribution from the ghosts. The results of this section are commonly used in studies of RG gravity and they can be found in numerous previous works [130, 91, 42, 33, 105].

3.2.1 Decompositions

In order to calculate the trace with the heat kernel methods we have to bring the second variation into a form where $\Gamma_k(z)$ is a function of the D'Alembertian. For this reason we decompose our original field $h_{\mu\nu}$ into its transverse traceless decomposition [158] which was first introduced in the context of the functional renormalisation group in [42]

$$h_{\mu\nu} = h^T_{\mu\nu} + \bar{\nabla}_\mu \xi_\nu + \bar{\nabla}_\nu \xi_\mu + \bar{\nabla}_\mu \bar{\nabla}_\nu \sigma - \frac{1}{d} \bar{g}_{\mu\nu} \bar{\nabla}^2 \sigma + \frac{1}{d} \bar{g}_{\mu\nu} h, \tag{3.2}$$

with the various new fields that appear being subject to the constraints

$$\bar{g}^{\mu\nu} h^T_{\mu\nu} = 0, \qquad \bar{\nabla}^\mu h^T_{\mu\nu} = 0, \qquad \bar{\nabla}^\mu \xi_\mu = 0, \qquad h = \bar{g}_{\mu\nu} h^{\mu\nu}. \tag{3.3}$$

Here $h = \bar{g}^{\mu\nu} h_{\mu\nu}$ is the trace of the fluctuation, $h^T_{\mu\nu}$ denotes the transverse-traceless part of $h_{\mu\nu}$, ξ_μ is a transverse vector that together with the scalar σ make up the longitudinal-traceless part of $h_{\mu\nu}$ according to (3.2). Such a decomposition is also advantageous because it leads to partial diagonalisation of the propagator (except between h and σ) and therefore it becomes possible to analytically invert it.

Note that after decomposing our original field $h_{\mu\nu}$ into its transverse traceless decomposition it does not receive any contributions from the modes of the σ field that obey the conformal Killing equation

$$\bar{\nabla}_\mu \bar{\nabla}_\nu \sigma + \bar{\nabla}_\nu \bar{\nabla}_\mu \sigma = \frac{2}{d} \bar{g}_{\mu\nu} \bar{\nabla}^2 \sigma \tag{3.4}$$

and similarly from the modes of the ξ^μ field that obey the Killing equation

$$\bar{\nabla}_\mu \xi_\nu + \bar{\nabla}_\nu \xi_\mu = 0. \tag{3.5}$$

These modes, when evaluated on the sphere, correspond to the lowest two modes of σ and the lowest mode of ξ^μ respectively and therefore they should be excluded from the trace evaluation. For details of the heat kernel coefficients of the constrained fields as well as for the exclusion of lowest modes see Appendix B.

As with the metric fluctuations, it is convenient to decompose the ghost fields into transverse (C^T_μ and $\bar{C}^T_\mu$) and longitudinal (η and $\bar{\eta}$) parts

$$C_\mu = C^T_\mu + \bar{\nabla}_\mu \eta, \qquad \bar{C}_\mu = \bar{C}^T_\mu + \bar{\nabla}_\mu \bar{\eta}. \tag{3.6}$$

Here the modes that are unphysical and should be excluded from the trace evaluation are the lowest modes of the scalars η and $\bar{\eta}$. Moreover, by relating the spectrum of the transverse fields to that of the original field and of the scalar we conclude that we should also exclude the lowest mode of C^T_μ and $\bar{C}^T_\mu$ as well as the second lowest mode of η and $\bar{\eta}$. Again, more details about this construction can be found in the Appendix B.

3.2.2 Gauge fixing part

The gauge fixing action (2.34) is already quadratic in the fields. Now we can substitute the metric decomposition (3.2) into (2.34) to express S_{gf} in terms of the metric components

as

$$\begin{aligned} S_{\rm gf} =& \frac{\kappa^2}{\alpha}\int d^dx\sqrt{\bar g}\left\{\xi_\nu\left[\bar\Box^2+2\frac{\bar R}{d}\bar\Box+\frac{\bar R^2}{d^2}\right]\xi^\nu\right. \\ &-\sigma\left[\left(\frac{d-1}{d}\right)^2\bar\Box^3+2\frac{\bar R}{d^2}(d-1)\bar\Box^2+\frac{\bar R^2}{d^2}\bar\Box\right]\sigma \\ &\left.+\frac{2}{d^2}h\left[(d-1)\rho\bar\Box^2+\rho\bar R\,\bar\Box\right]\sigma-\frac{\rho^2}{d^2}h\bar\Box h\right\}, \end{aligned} \tag{3.7}$$

where we have defined $\Box = g_{\mu\nu}\nabla^\mu\nabla^\nu$. It follows that the contributions to the Hessians (2.27) coming from the gauge fixing action take the form

$$\left(\Gamma_k^{(2)}\right)^{\xi\xi}_{\rm gf} = \frac{\kappa^2}{\alpha}\left(\Box^2+2\frac{R}{d}\Box+\frac{R^2}{d^2}\right) \tag{3.8}$$

$$\left(\Gamma_k^{(2)}\right)^{\sigma\sigma}_{\rm gf} = \frac{\kappa^2}{\alpha}\left(-\left(\frac{d-1}{d}\right)^2\Box^3-2\frac{R}{d^2}(d-1)\Box^2-\frac{R^2}{d^2}\Box\right) \tag{3.9}$$

$$\left(\Gamma_k^{(2)}\right)^{hh}_{\rm gf} = \frac{\kappa^2}{\alpha}\left(-\frac{\rho^2}{d^2}\Box\right) \tag{3.10}$$

$$\left(\Gamma_k^{(2)}\right)^{h\sigma}_{\rm gf} = \frac{\kappa^2}{\alpha}\left(\rho\frac{2}{d^2}(d-1)\Box^2+\rho\frac{2}{d^2}R\,\Box\right) \tag{3.11}$$

where we have dropped the bars for notational simplicity, since after computing the Hessians we set $g_{\mu\nu}=\bar g_{\mu\nu}$ and therefore it remains only one metric field. However, it should be kept in mind that all the geometric quantities are constructed with the background metric.

3.2.3 Ghost part

We now turn our attention to the ghost action. By taking two functional derivatives of (2.35) with respect to the metric field we observe that it gives no contribution to the Hessians

$$\frac{\delta^{(2)}S_{\rm gh}}{\delta g_{\mu\nu}\delta g_{\alpha\beta}}=0. \tag{3.12}$$

Consequently the only contribution comes from the part which is quadratic in the ghost fields C_μ and $\bar C_\nu$. After substituting the ghost decomposition (3.6) into the ghost action (2.35) we have

$$S_{\rm gh}=-\sqrt{2}\int d^dx\sqrt{\bar g}\left\{\bar C^{\mu T}M_{\mu\nu}C^{\nu T}+\bar C^{\mu T}M_{\mu\nu}\bar\nabla^\nu\eta+\bar\nabla^\mu\bar\eta\,M_{\mu\nu}C^{\nu T}+\bar\nabla^\mu\bar\eta\,M_{\mu\nu}\bar\nabla^\nu\eta\right\}. \tag{3.13}$$

Now we substitute the Faddeev-Popov operator (2.36) into the above equation and we perform the second variation in order to get for the Hessians of each ghost component

field

$$\left(\Gamma_k^{(2)}\right)^{\bar{C}^T C^T} = -\sqrt{2}\,\Box - \sqrt{2}\frac{R}{d} \tag{3.14}$$

$$\left(\Gamma_k^{(2)}\right)^{\bar{\eta}\eta} = \frac{2\sqrt{2}}{d}\left[d-\rho-1\right]\Box^2 + \frac{2\sqrt{2}}{d}R\,\Box\,, \tag{3.15}$$

where again we have dropped the bars after setting $g_{\mu\nu} = \bar{g}_{\mu\nu}$.

3.2.4 Auxiliary fields

The metric decomposition (3.2) is merely a coordinate transformation and as such it induces the Jacobian of the transformation $J_{\rm gr}$. Here we are going to determine this quantity and we will follow the Faddeev-Popov trick so that we transform the contributions from the determinants into contributions from auxiliary fields. We begin by writing the following relation between the original field $h_{\mu\nu}$ and the components of the transverse traceless decomposition

$$\int d^dx\sqrt{\bar{g}}\,h_{\mu\nu}h^{\mu\nu} = \int d^dx\sqrt{\bar{g}}\left\{h^T_{\mu\nu}h^{T\mu\nu} + \frac{1}{d}hh - 2\,\xi_\nu\left[\bar{\Box}+\frac{\bar{R}}{d}\right]\xi^\nu + \sigma\left[\left(\frac{d-1}{d}\right)\bar{\Box}^2 + \frac{\bar{R}}{d}\bar{\Box}\right]\sigma\right\}. \tag{3.16}$$

Then, at the level of the path integral the Jacobian of the field transformation takes the following form

$$J_{\rm gr} = \left(\det M_{(0)}\right)^{1/2}\left(\det M_{(1T)}\right)^{1/2} \tag{3.17}$$

with the operators $M_{(0)}$ and $M_{(1T)}$ coming from the contributions of the scalar σ and the transverse vector ξ^μ respectively and having the following form

$$M_{(0)} = \left(\frac{d-1}{d}\right)\bar{\Box}^2 + \frac{\bar{R}}{d}\bar{\Box} \tag{3.18}$$

$$M_{(1T)} = \bar{\Box} + \frac{\bar{R}}{d}\,. \tag{3.19}$$

The terms containing the transverse-traceless field $h^T_{\mu\nu}$ and the trace field h do not contribute to the transformation Jacobian since they do not involve operators and under the path integral they are simple gaussian integrals contributing only a constant. Now, we would like to express these determinants as new contributions to the action in terms of auxiliary fields. For this, we follow the Faddeev-Popov trick and write them as gaussian integrals. We start with the determinant of the scalar field

$$\left(\det M_{(0)}\right)^{1/2} = \frac{\det M_{(0)}}{\left(\det M_{(0)}\right)^{1/2}} = \int \mathcal{D}\lambda\mathcal{D}\bar{\lambda}\mathcal{D}\omega\cdot\exp\left[-\int d^dx\sqrt{\bar{g}}\left\{\bar{\lambda}M_{(0)}\lambda + \omega M_{(0)}\omega\right\}\right] \tag{3.20}$$

where λ and $\bar{\lambda}$ are complex Grassmann fields coming from the numerator of the above expression and ω is a real field coming from the denominator. Thus the action for the

scalar auxiliary fields reads $S_{\text{aux}(0)} = \int d^dx\sqrt{g}\left[\bar{\lambda}M_0\lambda + \frac{1}{2}\omega M_0\omega\right]$ and the Hessians for $\bar{\lambda}$, λ and ω are given, after dropping the bars, by

$$\left(\Gamma_k^{(2)}\right)^{\bar{\lambda}\lambda} = \left(\Gamma_k^{(2)}\right)^{\omega\omega} = \left(\frac{d-1}{d}\right)\Box^2 + \frac{R}{d}\Box\,. \tag{3.21}$$

Similarly for the determinant $\det M_{(1T)}$ coming from the contribution of the transverse vector we have

$$\left(\det M_{(1T)}\right)^{1/2} = \frac{\det M_{(1T)}}{\left(\det M_{(1T)}\right)^{1/2}} = \int \mathcal{D}c_\mu^T\mathcal{D}\bar{c}^{T\mu}\mathcal{D}\zeta_\mu^T\cdot\exp\left[-\int d^dx\sqrt{\bar{g}}\left\{\bar{c}_\mu^T M_{(1T)}c^{T\mu} + \frac{1}{2}\zeta_\mu^T M_{(1T)}\zeta^{T\mu}\right\}\right] \tag{3.22}$$

with c_μ^T and $\bar{c}_\mu^T$ being complex Grassmann transverse vector fields coming from the numerator of the above expression and ζ_μ^T a real transverse vector field coming from the denominator. The corresponding Hessians, after dropping the bars become

$$\left(\Gamma_k^{(2)}\right)^{\bar{c}^Tc^T} = \left(\Gamma_k^{(2)}\right)^{\zeta^T\zeta^T} = \Box + \frac{R}{d}. \tag{3.23}$$

In the same way that the metric decomposition (3.2) induces the Jacobian of the transformation we get contributions J_{gh} from the decomposition of the ghost fields (3.6). Now, the original ghost fields C_μ and $\bar{C}_\mu$ obey the following identity with the components $C^{T\mu}$, $\bar{C}^{T\mu}$, η and $\bar{\eta}$

$$\int d^dx\sqrt{\bar{g}}\,\bar{C}_\mu C^\mu = \int d^dx\sqrt{\bar{g}}\left\{\bar{C}_\mu^T C^{T\mu} - \bar{\eta}\bar{\Box}\eta\right\}. \tag{3.24}$$

The fields C_μ^T and $\bar{C}_\mu^T$ do not involve operators and thus they contribute only a constant. Now, in the level of path integral the Jacobian of the transformation comes only from the scalars η and $\bar{\eta}$ and after performing the gaussian integral it can be written

$$J_{\text{gh}} = \left(\det\left[-\bar{\Box}\right]\right)^{-1} \tag{3.25}$$

As before we express this in terms of the contribution to the action of auxiliary fields, so that it takes the form

$$J_{\text{gh}} = \int \mathcal{D}\bar{s}\mathcal{D}s\exp\left[-\int d^dx\sqrt{\bar{g}}\bar{s}\left[-\bar{\Box}\right]s\right], \tag{3.26}$$

where now the fields $\bar{s}$ and s are complex conjugate scalars. The corresponding Hessian for this auxiliary field, after dropping the bars, is given by

$$\left(\Gamma_k^{(2)}\right)^{\bar{s}s} = -\Box. \tag{3.27}$$

3.3 Trace computation algorithm

For the computation of the functional trace in (2.31) we will use the heat kernel techniques. Here we present an algorithm for computing the trace having as input the general form of

the second variation. We then determine the form that the regulator term should have, we move on by implementing the optimised cutoff and finally we evaluate the integrals for the functions $Q_n[W]$ defined in (2.43) and (2.44). We also evaluate these functions for the case that we have off diagonal terms in the second variation with the mixing of two components. Finally, we compute the two lowest excluded modes for a scalar and the lowest excluded mode for a vector.

3.3.1 The Regulator term

The most general form of the second variation will take is in the form of power series in terms of an operator $\triangle$ with maximum power p. Then we write

$$\left(\Gamma_k^{(2)}\right)^{\phi_i\phi_j} = \sum_{m=0}^{p} \mathcal{A}_m^{\phi_i\phi_j} \triangle^m \,, \tag{3.28}$$

where unless is needed we will drop the $\phi_i\phi_j$ indices and the coefficients $\mathcal{A}_m$ will depend on the momentum scale k through the couplings of the theory. The next step is the definition of the regulator term $\mathcal{R}_k^{\phi_i\phi_j}$. For our purposes it is enough to determine the regulator just for *type I cutoff*. However, the process described here has a straightforward generalisation to the other types of cutoffs. For *Type I cutoff* we define the regulator (see 2.3.4) by demanding that the addition of the regulator term $\mathcal{R}_k^{\phi_i\phi_j}$ to the Hessian of the corresponding field, leads everywhere to the replacement of the operator $\triangle$ by $\triangle + R_k(\triangle)$ where $R_k(\triangle)$ is the profile function. So we have

$$\sum_{m=0}^{p} \mathcal{A}_m(\triangle + R_k)^m = \sum_{m=0}^{p} \mathcal{A}_m \triangle^m + \mathcal{R}_k^{\phi_i\phi_j} \tag{3.29}$$

or solving for $\mathcal{R}_k^{\phi_i\phi_j}$

$$\mathcal{R}_k^{\phi_i\phi_j} = \sum_{m=1}^{p} \mathcal{A}_m(\triangle + R_k)^m - \sum_{m=1}^{p} \mathcal{A}_m \triangle^m. \tag{3.30}$$

Now that we have an explicit form for the regulator term we can proceed to determine its scale derivative, which is an essential component of the flow equation (2.31). In *type I cutoff* the operator $\triangle$ does not contain any couplings and thus it does not have any momentum dependence. Therefore the ∂_t derivative of the regulator reads

$$\partial_t \mathcal{R}_k^{\phi_i\phi_j} = C_1 \partial_t R_k + C_2 \tag{3.31}$$

where C_1 is the coefficient of the profile function scale derivative and C_2 contains all the remaining momentum dependence coming form the couplings of the theory. By applying

∂_t to (3.30) we have for these coefficients the following

$$C_1 = \sum_{m=1}^{p} m\mathcal{A}_m(\triangle + R_k)^{m-1} \tag{3.32}$$

$$C_2 = \sum_{m=1}^{p} \partial_t\mathcal{A}_m(\triangle + R_k)^m - \sum_{m=1}^{p} \partial_t\mathcal{A}_m\triangle^m\,. \tag{3.33}$$

3.3.2 The diagonal piece

Now, we have all the ingredients that we need in order to evaluate the trace of the flow equation. For this split the FRGE into two parts according to (3.31). The equation for the diagonal part reads

$$\frac{1}{2}\mathrm{Tr}\left[\partial_t\mathcal{R}_k^{\phi_i\phi_j}\left(\left(\Gamma_k^{(2)}\right)^{\phi_i\phi_j} + \mathcal{R}_k^{\phi_i\phi_j}\right)^{-1}\right] = \frac{1}{2}\mathrm{Tr}\left[\frac{C_1}{D}\partial_t R_k\right] + \frac{1}{2}\mathrm{Tr}\left[\frac{C_2}{D}\right] \tag{3.34}$$

where we have defined as D the denominator of the above expressions after adding the regulator term to the Hessian. In terms of the coefficients $\mathcal{A}_m$ and the profile function R_k it takes the form

$$D = \sum_{m=0}^{p} \mathcal{A}_m(\triangle + R_k)^m. \tag{3.35}$$

In order to evaluate the integrals $Q_n[W]$ defined in (2.43) and (2.44) we have to make a specific choice for the profile function which determines the way that momentum modes are cut off. For the the rest of this thesis we will adopt the optimised cutoff profile function [94, 97] given by

$$R_k(y) = (k^2 - y)\theta(k^2 - y). \tag{3.36}$$

In the present setup, the use of the optimised profile function has the additional advantage that it makes the heat kernel expansion to truncate for even dimensions. We will explicitly see how this happens when we evaluate $Q_n[W]$. Now we take the scale derivative of the profile function which reads

$$\partial_t R_k(y) = 2k^2\theta(k^2 - y) + 2k^2(k^2 - y)\delta(k^2 - y). \tag{3.37}$$

It is easy to observe that both the above integrals in (3.34) will be overall multiplied by the step function $\theta(k^2 - y)$ and therefore we can change the integral limits from $\int_0^\infty$ to $\int_0^{k^2}$ and replace everywhere the step functions by 1. Then we have for the coefficients C_1, C_2 and the denominator D after substituting $\triangle = y$

$$C_1 = \sum_{m=1}^{p} m\mathcal{A}_m k^{2m-2} \;\;;\;\; C_2 = \sum_{m=1}^{p} \partial_t\mathcal{A}_m(k^{2m} - y^m) \;\;;\;\; D = \sum_{m=0}^{p} \mathcal{A}_m k^{2m} \tag{3.38}$$

Now we turn our attention to the evaluation of the integrals $Q_n[W]$ for a positive n. Then, from (2.43) we have that

$$Q_n[W] = \frac{1}{\Gamma(n)} \int_0^\infty dy\, y^{n-1} W(y). \tag{3.39}$$

The integrand $W(y)$ of the above equation can be split in two parts according to (3.34). Then we define $W_1 = \frac{1}{2}\frac{C_1}{D}\partial_t R_k$ and $W_2 = \frac{1}{2}\frac{C_2}{D}$ and we evaluate the corresponding integrals $I_n^i = Q_n[W_i]$ separately. Note that both of these integrals are overall multiplied by the step function $\theta(k^2 - y)$ so we can change the integral limits from $\int_0^\infty$ to $\int_0^{k^2}$ and replace everywhere the step functions by 1. Moreover, the W_1 integral has a term which is proportional to $2k^2(k^2 - y)\delta(k^2 - y)$. Upon integration this term will vanish and so we will drop it from now on. Now we have

$$I_n^1 = \frac{k^{2n}}{\Gamma(n)} \frac{1}{n} \frac{\sum_{m=1}^p m \mathcal{A}_m k^{2m}}{\sum_{m=0}^p \mathcal{A}_m k^{2m}} \qquad ; \qquad I_n^2 = \frac{k^{2n}}{2\Gamma(n)} \frac{1}{n} \frac{\sum_{m=1}^p \frac{m}{m+n} \partial_t \mathcal{A}_m k^{2m}}{\sum_{m=0}^p \mathcal{A}_m k^{2m}}. \tag{3.40}$$

By summing the two contributions above we get an expression for the coefficients Q_n of the heat kernel expansion for positive n

$$Q_n = \frac{k^{2n}}{2\, n\, \Gamma(n)} \cdot \frac{1}{\sum_{m=0}^p \mathcal{A}_m k^{2m}} \left[2 \sum_{m=1}^p m \mathcal{A}_m k^{2m} + \sum_{m=1}^p \frac{m}{m+n} \partial_t \mathcal{A}_m k^{2m} \right], \qquad n > 0. \tag{3.41}$$

For the evaluation of the trace in the flow equation (2.31) we also need the expression for $Q_n[W]$ when n is a negative integer. For a negative integer the Mellin transforms are given by

$$Q_{-n} = (-1)^n \frac{d^n W(y)}{dy^n}\bigg|_{y=0}, \qquad n \in \mathbb{N}. \tag{3.42}$$

where the y-dependence of $W(y)$ comes through the $\partial_t \mathcal{R}_k^{\phi_i \phi_j}$ term so it is enough to compute the derivative of this term. In the previous sections we have disregard the explicit form of the $\theta(k^2 - y)$-functions, since they were overall multiplied our functions and it was an easy interpretation just by changing the integral limits and putting $\theta(k^2 - y) = 1$. For the purposes of evaluating this quantity we note that the product of two $\theta(k^2 - y)$ distributions will result another $\theta(k^2 - y)$ distribution, so for our calculation purposes we will substitute any $\theta(k^2 - y)^n$ by $\theta(k^2 - y)$.The derivatives which hit the $\theta(k^2 - y)$ will become $\delta(k^2 - y)$ and by taking the limit $y = 0$ it will vanish, as long as $k^2 \neq 0$. Moreover, the overall multiplication with $\theta(k^2 - y)$ will give just 1 in the limit $y = 0$. Then we have

$$\frac{d^n \partial_t \mathcal{R}_k^{\phi_i \phi_j}}{dy^n} = \left[- \sum_{m=1}^p \frac{m!}{(m-n)!} \partial_t \mathcal{A}_m y^{m-n} \right] \tag{3.43}$$

so after evaluating this expression for $y = 0$ the only term that survives is the one with $m = n$. Therefore we have for the coefficients Q_n

$$Q_{-n} = (-1)^{n+1}\frac{1}{2}\frac{n!}{\sum_{m=0}^{p}\mathcal{A}_m k^{2m}}\cdot(\partial_t\mathcal{A}_n)\ , \qquad n > 0. \tag{3.44}$$

3.3.3 The non-diagonal piece

When there are off-diagonal components of the second variation $\left(\Gamma_k^{(2)}\right)^{\phi_i\phi_j}$ we have to find the inverse of this sub-matrix. For the case where the mixing is just between two components ϕ_1 and ϕ_2 the inverse of $\left(\Gamma_k^{(2)}\right)^{\phi_i\phi_j}$ is given by

$$\left(\left(\Gamma_k^{(2)}\right)^{\phi_i\phi_j} + \mathcal{R}_k^{\phi_i\phi_j}\right)^{-1} = \frac{1}{\mathrm{Det}\left[\left(\Gamma_k^{(2)}\right)^{\phi_i\phi_j} + \mathcal{R}_k^{\phi_i\phi_j}\right]}\cdot\mathbb{M} \tag{3.45}$$

with the matrix $\mathbb{M}$ given by

$$\mathbb{M} = \begin{pmatrix} \left(\Gamma_k^{(2)}\right)^{\phi_2\phi_2} + \mathcal{R}_k^{\phi_2\phi_2} & -\left(\Gamma_k^{(2)}\right)^{\phi_1\phi_2} - \mathcal{R}_k^{\phi_1\phi_2} \\ -\left(\Gamma_k^{(2)}\right)^{\phi_2\phi_1} - \mathcal{R}_k^{\phi_2\phi_1} & \left(\Gamma_k^{(2)}\right)^{\phi_1\phi_1} + \mathcal{R}_k^{\phi_1\phi_1} \end{pmatrix} \tag{3.46}$$

It follows that the trace takes the form

$$\frac{1}{2}\mathrm{Tr}\left[\partial_t\mathcal{R}_k^{\phi_i\phi_j}\left(\tilde{\Gamma}^{(2)}_{\phi_i\phi_j}\right)^{-1}\right] = \frac{1}{2}\mathrm{Tr}\left[\frac{1}{\mathrm{Det}\left[\tilde{\Gamma}^{(2)}_{\phi_i\phi_j}\right]}\mathcal{M}\right] \tag{3.47}$$

with the expression $\mathcal{M}$ given by

$$\mathcal{M} = \left(\tilde{\Gamma}^{(2)}_{\phi_2\phi_2}\partial_t\mathcal{R}_k^{\phi_1\phi_1} - \tilde{\Gamma}^{(2)}_{\phi_1\phi_2}\partial_t\mathcal{R}_k^{\phi_2\phi_1} - \tilde{\Gamma}^{(2)}_{\phi_2\phi_1}\partial_t\mathcal{R}_k^{\phi_1\phi_2} + \tilde{\Gamma}^{(2)}_{\phi_1\phi_1}\partial_t\mathcal{R}_k^{\phi_2\phi_2}\right) \tag{3.48}$$

where we have used the abbreviation $\tilde{\Gamma}^{(2)}_{\phi_i\phi_j} = \left(\Gamma_k^{(2)}\right)^{\phi_i\phi_j} + \mathcal{R}_k^{\phi_i\phi_j}$. The regulator (3.30) and the coefficients of the expansion (3.31) remain the same, but now we restore the indices $\phi_i\phi_j$ in all the expressions. After substituting for the regulator we have $\tilde{\Gamma}^{(2)}_{\phi_i\phi_j} = D^{\phi_i\phi_j}$ where $D^{\phi_i\phi_j}$ is given by the expression (3.35) for D with all the coefficients $\mathcal{A}$ replaced by $\mathcal{A}^{\phi_i\phi_j}$. In the following we assume that the second variation $\left(\Gamma_k^{(2)}\right)^{\phi_i\phi_j}$ is symmetric. Then, by adopting the optimised cutoff we have everything as before multiplied by the step function. Thus we change the integration limits and substitute $\theta(k^2 - y)$ with 1. Then, the expressions for $\left(\Gamma_k^{(2)}\right)^{\phi_i\phi_j}$ are just constants which do not enter the integration over y. The integration over $\partial_t\mathcal{R}_k^{\phi_i\phi_j}$ is known from the previous section and gives

$$\mathcal{I}^{\phi_i\phi_j} = \frac{k^{2n}}{n}\left[2\sum_{m=1}^{p} m\mathcal{A}_m^{\phi_i\phi_j}k^{2m} + \sum_{m=1}^{p}\frac{m}{m+n}\partial_t\mathcal{A}_m^{\phi_i\phi_j}k^{2m}\right] \tag{3.49}$$

so that the coefficients Q_n for the non-diagonal piece are given by

$$Q_n = \frac{1}{2\,\Gamma(n)}\cdot\frac{1}{D^{\phi_1\phi_1}D^{\phi_2\phi_2} - (D^{\phi_1\phi_2})^2}\cdot\left[D^{\phi_2\phi_2}I^{\phi_1\phi_1} - 2D^{\phi_1\phi_2}I^{\phi_1\phi_2} + D^{\phi_1\phi_1}I^{\phi_2\phi_2}\right]. \tag{3.50}$$

Similarly for the non-diagonal piece of the trace for a negative integer we get

$$Q_{-n} = (-1)^{n+1}\frac{1}{2}\frac{n!}{D^{\phi_1\phi_1}D^{\phi_2\phi_2} - (D^{\phi_1\phi_2})^2} \cdot \left[D^{\phi_2\phi_2}\mathcal{K}^{\phi_1\phi_1} - 2D^{\phi_1\phi_2}\mathcal{K}^{\phi_1\phi_2} + D^{\phi_1\phi_1}\mathcal{K}^{\phi_2\phi_2}\right] \tag{3.51}$$

with $n > 0$ in the above equation and

$$\mathcal{K}^{\phi_i\phi_j} = \partial_t \mathcal{A}_n^{\phi_i\phi_j}. \tag{3.52}$$

3.3.4 Excluded modes

As explained in 2.3.6 we often encounter the trace of a function where some eigenmodes of the $-\nabla^2$ operator have to be excluded. For example we saw in 3.2.1 that after performing the decomposition of the fluctuation $h_{\mu\nu}$ into its components through the transverse traceless decomposition, the lowest mode of ξ^μ and the two lowest modes of σ have to be excluded. In order to incorporate this into the evaluation of the traces we follow the general rule

$$\mathrm{Tr}_s^{'\cdots'}[W(-\nabla^2)] = \mathrm{Tr}_s[W(-\nabla^2)] - \sum_{l=1}^{l=m} D_l(d,s)W(\Lambda_l(d,s)) \tag{3.53}$$

where $\Lambda_l(d,s)$ are the eigenvalues of the operator and $D_l(d,s)$ their multiplicities given in Table B.1. Here the primes denote the number of the lowest modes to be excluded. For our calculation we will need the form of $\mathrm{Tr}_{(0)}^{'}$, $\mathrm{Tr}_{(0)}^{''}$and $\mathrm{Tr}_{(1T)}^{'}$. We start with the lowest mode of a scalar. According to Table B.1 in the Appendix B for the lowest mode of a scalar field we have

$$\mathrm{Tr}_{(0)}^{'}[W(-\nabla^2)] = \mathrm{Tr}_{(0)}[W(-\nabla^2)] - W(0). \tag{3.54}$$

The part $W(0)$ of the above equation which has to be excluded from the scalar trace is simply evaluated by setting $y = 0$ in the expression for $W(y)$. Then we denote the lowest excluded mode of a scalar as $X_{(0)}^{'}$ and we have

$$X_{(0)}^{'} = W(0) = \frac{\sum_{m=1}^{p}\partial_t\mathcal{A}_m k^{2m}}{\sum_{m=0}^{p}\mathcal{A}_m k^{2m}} + \frac{\sum_{m=1}^{p} m\mathcal{A}_m k^{2m}}{\sum_{m=0}^{p}\mathcal{A}_m k^{2m}} \tag{3.55}$$

Similarly for the exclusion of the two lowest modes of a scalar field we have according to the table B.1

$$\mathrm{Tr}_{(0)}^{''}[W(-\nabla^2)] = \mathrm{Tr}_{(0)}[W(-\nabla^2)] - W(0) - (d+1)\,W\left(\frac{1}{d-1}R\right) \tag{3.56}$$

In general the result will involve theta functions coming from the choice of the profile function and more precisely from (3.36) and (3.37). For the specific expression under

consideration the theta functions are of the form $\theta(k^2 - \frac{R}{d-1})$. Since in the following we are going to focus to an expansion in small $\frac{R}{k^2}$ we can evaluate these theta functions at the limit $\frac{R}{k^2} \ll 1$ in order to get for the exclusion of the two lowest scalar modes

$$X''_{(0)} = X'_{(0)} + (d+1)\frac{1}{\sum_{m=0}^{p}\mathcal{A}_m k^{2m}}\left[2\sum_{m=1}^{p} m\mathcal{A}_m k^{2m} + \sum_{m=1}^{p}\partial_t\mathcal{A}_m\left(k^{2m} - \frac{R^m}{(d-1)^m}\right)\right]. \tag{3.57}$$

Finally we have to determine the exclusion for lowest mode of a transverse vector. Again, by reading the multiplicities and the eigenvalues from Table B.1 we have

$$\mathrm{Tr}'_{(1T)}[W(-\nabla^2)] = \mathrm{Tr}_{(1T)}[W(-\nabla^2)] - \frac{d(d+1)}{2}W\left(\frac{R}{d}\right) \tag{3.58}$$

As before we evaluate the theta functions coming from the profile function for the limit $\frac{R}{k^2} \ll 1$ and we have for the lowest exclusion mode of the vector

$$X'_{(1T)} = \frac{d(d+1)}{2}\frac{1}{\sum_{m=0}^{p}\mathcal{A}_m k^{2m}}\left[2\sum_{m=1}^{p} m\mathcal{A}_m k^{2m} + \sum_{m=1}^{p}\partial_t\mathcal{A}_m\left(k^{2m} - \frac{R^m}{d^m}\right)\right]. \tag{3.59}$$

3.4 Summary

In this Chapter we have summarised the technical tools that we will use in order to derive flow equations. We divided our calculation into two parts and we kept the content general so that it can be applied to different approximations for the gravitational effective average action. The results of this Chapter considerably simplify the derivation of flow equations and their application to specific gravitational approximations is used in Chapter 4 and Chapter 5.

In the first half we derived all the Hessians for the effective average action (2.30) apart from those coming from the gravitational anstaz $\bar{\Gamma}_k$ which will be computed at the corresponding chapters. We decomposed the metric field according to the transverse traceless decomposition and the second variation of the gauge fixing action was computed. Similarly we decomposed the ghost vector fields to their transverse decomposition and we evaluated the Hessians of the ghost action. These transformations resulted to the appearance in the action of auxiliary fields and their Hessians were presented.

In the second part we presented an algorithm for computing the functions $Q_n[W]$ that appear in the heat kernel expansion (2.42). We start with the second variation of each component field by writing it as power series of the operator ∇^2 and we end up with explicit expressions for $Q_n[W]$ in terms of the coefficients of the ∇^2 expansion. We also calculated the same quantities in the case where the Hessians are not completely diagonal,

but they have a mixing between two components. Finally we presented the case where distinct modes are excluded from the functional trace.

Chapter 4

The f(R) approximation

4.1 Introduction

Now that we have all the technical tools at our disposal we return to the physical problem that we are interested in. Our aim is to test the asymptotic safety conjecture using the renormalisation group methods developed in Chapter 2 and Chapter 3. A reasonable question to ask is how we can get insights given that we have to rely to an approximation, even if this is non-perturbative. If we consider for example an asymptotically free theory such as QCD, we know that because the theory is non-interacting at the UV, operators with increasing mass dimension scale according to their canonical mass dimensions and become increasingly irrelevant. Therefore, making an expansion in such operators results in a well defined approximation scheme. For an asymptotically safe theory however, the UV fixed point is interacting and there is no a-priori ordering principle for the scaling of the operators. Recall from (1.11) that the critical exponents are affected by non-trivial interactions at the UV fixed point and moreover in order for the theory to be asymptotically safe these quantum corrections should not be strong enough to turn infinitely many eigenvalues negative. Here we are going to tackle these questions by adopting a bootstrap approach [52]. We will make the hypothesis that even for the case of a non-trivial fixed point the operators become increasingly irrelevant with increasing mass dimension and that therefore an expansion in powers of the operators is a reasonable approximation. Subsequently, we perform a systematic search order by order to test the hypothesis and by extending our technique to very high order we are able for the first time to provide quantitative information about the validity of the approximation, such as results for the radius of convergence and a full stability analysis.

In this chapter we will apply this method to the case where the gravitational effective

average action is given by an arbitrary function of the scalar curvature R. Accordingly, the approximation ansatz takes the form

$$\bar{\Gamma}_k[g] = \int d^d x \sqrt{g}\, F_k(R). \tag{4.1}$$

Classically, modifications of Einstein gravity of the form $S = \int d^d x \sqrt{g}\, f(R)$ have been considered for a long time and have proven very popular with many applications in Cosmology [37]. At the quantum level investigating, the behaviour of a general function $F(R)$ is of great importance in order to check the validity of the low order approximations. In practice, the investigation of the properties of such a function is performed by expanding $F(R)$ as a power series of the Ricci scalar up to a maximum order N

$$\bar{\Gamma}_k[g] = \int d^d x \sqrt{g} \sum_{n=0}^{N-1} \bar{\lambda}_n R^n. \tag{4.2}$$

In this context the requirements for the theory to become asymptotically safe are that the dimensionless couplings $\lambda_i = k^{-d_i} \bar{\lambda}_i$, approach fixed point values at the UV limit and that the number of negative critical exponents remains finite. Within the approximation (4.2) we will apply our bootstrap approach in order to systematically test the requirements of asymptotic safety at every order up to $N_{\max} = 35$ [52]. Our results show that a self-consistent UV fixed point exists at every order of the approximation and that the number of negative eigenvalues is always three. More interestingly, it is found that curvature invariants become increasingly irrelevant with increasing mass dimension and that their critical exponents take almost gaussian values. These findings justify the original approximation hypothesis a-posteriori, by performing a detailed examination of the properties of $F(R)$ quantum gravity.

Previous studies that are concerned with powers of the Ricci scalar have a long and successful history in the context of asymptotic safety. The first results in favour of the asymptotic safety conjecture [148] were obtained in the Einstein-Hilbert approximation for the effective action [130, 141] where a UV fixed point with two attractive directions was discovered. Within this approximation the dependence of the fixed point structure was examined under the inclusion of matter fields [42], under variations of the regulator scheme [92] and also when we consider higher dimensional gravity [99, 55, 56]. However, the Einstein-Hilbert truncation is only a leading order approximation since in the Wilsonian approach for the effective average action we should include all the operators that are compatible with the symmetry of diffeomorphism invariance. Therefore, extensions of the operator space were examined by adding higher scalar curvature terms [91, 32, 33, 34, 105, 41] as well as Weyl squared terms [16, 17]. Moreover, the renormalisation group for gravity

under the inclusion of matter fields has been studied [122, 121, 115, 116, 57, 43, 45, 74, 159], as well as investigations for the quantum effects of the ghost sector [44, 46, 70]. Here we are going to focus on the inclusion of scalar curvature operators in the effective action.

The flow equation for the $f(R)$ quantum gravity in a closed form was first obtained in [33, 105]. For analysing the results a polynomial expansion of $F(R)$ in terms of the scalar curvature was performed and a UV fixed point was found in every order, up to a maximum order R^6. Moreover, for every order greater than R^2 a three dimensional critical surface was observed. These results were extended [34] to order R^8 were again the UV fixed point and the three relevant directions were found and to order R^{10} [22] were only the fixed point values were calculated. Already in these orders, a consistency of the results and a relative stability of the fixed point values was observed, providing evidence that the low order results of Einstein-Hilbert and R^2 gravity were good leading order approximations. However, some of the open questions that remained concerned the behaviour of the system at higher orders, a full stability analysis for the fixed points and a detailed examination of the critical exponents in the light of asymptotic safety conjecture by Weinberg [148]. Here, we perform an analysis of the flow equation of $F(R)$ gravity and we compute fixed point values and critical exponents for every order in the approximation up to R^{34}. We also estimate the radius of convergence for the expansion and we present a stability analysis for both the fixed points and the critical exponents. Finally we use our results to examine the ordering principle of the eigenvalues and to determine their deviation from gaussianity.

The rest of this Chapter is organised as follows. In Section 4.2 we will compute the second variation of the ansatz (4.1) and present the Hessians for the effective average action. In Section 4.3 we will choose a specific gauge fixing and we will concentrate to the case $d = 4$ in order to re-derive the flow equation for the function $F(R)$ [33, 105] using the computational algorithm for the trace evaluation that was developed in Section 3.3. In Section 4.4 we will develop a new method which will allow us to compute the fixed point values for high orders and in Section 4.5 we will construct the corresponding method for the critical exponents. In Section 4.6 we will present the results of our analysis starting from the values of the fixed points and their convergence and proceeding with the radius of convergence for the full $F(R)$ function, the anomalous dimension, the critical exponents, the stability analysis of the results and finally we comment on the possibility of de-Sitter solutions. In Section 4.7 we perform a detailed analysis for the critical exponents and we make links with the canonical power counting. We conclude this chapter with a summary in Section 4.8.

4.2 Computing the Hessians

Here we are going to derive the Hessians for all the fields that contribute to our ansatz as the first step towards calculating the renormalisation group flow of the theory. As explained in 2.3.2 the effective average action takes the form

$$\Gamma_k[g,\bar{g},c,\bar{c}] = \bar{\Gamma}_k[g] + S_{gf}[h;\bar{g}] + S_{gh}[h,c,\bar{c};\bar{g}]. \tag{4.3}$$

The Hessians for the ghost fields and the contribution from the gauge fixing action were computed in Chapter 3 and are given in 3.2.2 for the gauge fixing and in 3.2.3 for the ghost part. The missing element is the computation of the second variation for the gravitational part.

4.2.1 Gravity part

We proceed with the second variation of the gravitational part given by (4.1). In order to compute $\bar{\Gamma}_k^{(2)}$ we make an expansion

$$\bar{\Gamma}_k[\bar{g}+\bar{h};\bar{g}] = \bar{\Gamma}_k[\bar{g};\bar{g}] + \mathcal{O}(\bar{h}) + \frac{1}{2}\bar{\Gamma}_k^{\text{quad}}[\bar{g}+\bar{h};\bar{g}] + \mathcal{O}(\bar{h}^3) \tag{4.4}$$

and we extract the quadratic part. Then we get

$$\bar{\Gamma}_k^{\text{quad}} = \int d^dx \left\{ \delta^{(2)}(\sqrt{g})F_k(R) + 2\delta(\sqrt{g})\delta(R)F_k'(R) + \sqrt{g}\delta^{(2)}(R)F_k'(R) + \sqrt{g}F_k''(R)\delta(R)\delta(R) \right\}, \tag{4.5}$$

where here and form now on the primes denote derivatives with respect to the argument. Now we substitute the expressions from Appendix A for the various variations appearing above to get

$$\begin{aligned}
\bar{\Gamma}_k^{\text{quad}} = \int d^dx\,\sqrt{g}\Bigg\{ & h^{\mu\nu}\left[-\frac{1}{2}F(R) + \frac{d-2}{d-1}\frac{R}{d}F'(R)\right]h_{\mu\nu} \\
& + h\left[F''(R)\,\nabla^4 - \frac{1}{2}F'(R)\,\nabla^2 + \frac{1}{4}F(R) - \frac{d-2}{d-1}\frac{R}{d}F'(R) + \frac{R^2}{d^2}F''(R)\right]h \\
& + h\left[-2F''(R)\,\nabla^2 + F'(R) - 2\frac{R}{d}F''(R)\right]\nabla_\mu\nabla_\nu h^{\mu\nu} \\
& + (\nabla^\mu h_{\mu\alpha})\;F'(R)\;(\nabla_\nu h^{\nu\alpha}) + (\nabla^\mu\nabla^\nu h_{\mu\nu})\;F''(R)\;\left(\nabla^\alpha\nabla^\beta h_{\alpha\beta}\right)\Bigg\}.
\end{aligned} \tag{4.6}$$

In order to compute the trace we have to bring the second variation into a form where it is a function of the D'Alembertian ∇^2. For this we use the metric field decomposition as defined in Section 3.2.1 and we find the Hessians in terms of each component field. These are given in Appendix A. In Table 4.1 we summarise the contribution from each individual component field after adding the contributions from the gauge fixing part, the ghost part and the auxiliary fields.

Component $\phi_i\phi_j$	The Hessian $\Gamma^{(2)}_{\phi_i\phi_j}$
$h^{T\mu\nu}h^T_{\mu\nu}$	$\frac{1}{2}F'_k(R)\Box - \frac{1}{2}F_k(R) - \frac{d-2}{d(d-1)}R\,F'_k(R)$
$\xi^\mu\xi_\mu$	$\frac{1}{\alpha}\Box^2 + \left[\frac{2}{\alpha}\frac{R}{d} + F_k(R) - 2F'_k(R)\frac{R}{d}\right]\Box + \frac{1}{\alpha}\frac{R^2}{d^2} + F_k(R)\frac{R}{d} - 2F'_k(R)\frac{R^2}{d^2}$
$\sigma\sigma$	$\frac{(d-1)^2}{d^2}\Box^4 - \frac{d-1}{2d^2}\left[\frac{d-1}{\alpha} + (d-2)F'_k(R) - 4RF''_k(R)\right]\Box^3$ $-\frac{1}{2d^2}\left[4R\frac{(d-1)}{\alpha} + d(d-1)F_k(R) - R(d\,F'_k(R) + 2RF''_k(R)\right]\Box^2$ $-\left[\frac{R^2}{d^2}\frac{1}{\alpha} + R\,(d\,F_k(R) - 2RF'_k(R))\right]\Box$
hh	$\frac{(d-1)^2}{d^2}F''_k(R)\Box^2 - \frac{1}{4d^2}\left[4\frac{\rho^2}{\alpha} + 2(d-1)\left((d-2)F'_k(R) - 4R\,F''_k(R)\right)\right]\Box$ $+\frac{1}{4d^2}\left[(d-2)(d\,F_k(R) - 4RF'_k(R)) + 4R^2F''_k(R)\right]$
$h\sigma$	$-\frac{(d-1)^2}{d^2}F''_k(R)\Box^3 + \frac{(d-1)}{d^2}\left[\frac{\rho}{\alpha} + \frac{(d-2)}{2}F'_k(R) - 2RF''_k(R)\right]\Box^2$ $+\frac{1}{d^2}\left[\frac{\rho}{\alpha} + \frac{(d-2)}{2}F'_k(R) - RF''_k(R)\right]R\Box$
$\bar{C}^T_\mu C^{T\mu}$	$-\sqrt{2}\Box - \sqrt{2}\frac{R}{d}$
$\bar{\eta}\eta$	$\frac{2\sqrt{2}}{d}\left[d-\rho-1\right]\Box^2 + \frac{2\sqrt{2}}{d}R\Box$
$\bar{\lambda}\lambda$	$\left[1-\frac{1}{d}\right]\Box^2 + \frac{R}{d}\Box$
$\omega\omega$	$\left[1-\frac{1}{d}\right]\Box^2 + \frac{R}{d}\Box$
$\bar{c}^T_\mu c^{T\mu}$	$\Box + \frac{R}{d}$
$\zeta^T_\mu\zeta^{T\mu}$	$\Box + \frac{R}{d}$
$\bar{s}s$	$-\Box$

Table 4.1: Summary of the decomposed second variation for the $F_k(R)$ action

4.3 The flow equation

In this Section we will use the techniques we have developed in order to evaluate the renormalisation group flow for $F(R)$ quantum gravity. For RG studies it is convenient to introduce dimensionless variables. In previous studies where only the first few orders were examined, it was common to introduce the dimensionless Newton's coupling and the dimensionless cosmological constant through

$$g = G_k\,k^{d-2} \qquad ; \qquad \lambda = k^{2-d}\Lambda_k \tag{4.7}$$

Here, we are going to treat Newton's coupling and the cosmological constant just as coming from the first two orders of the expansion of $F(R)$. We start by introducing the dimensionless Ricci scalar

$$\rho = \frac{R}{k^2} \tag{4.8}$$

and the dimensionless $f_k(R)$ function defined as

$$f_k(R) = 16\pi\,k^{-d}F_k\left(\frac{R}{k^2}\right) \tag{4.9}$$

It follows for the derivatives of the function that

$$f_k'(R) = 16\pi\, k^{-d+2} F_k'\left(\frac{R}{k^2}\right) \qquad ; \qquad f_k''(R) = 16\pi\, k^{-d+4} F_k''\left(\frac{R}{k^2}\right) \tag{4.10}$$

and for its scale derivatives that

$$\begin{aligned} 16\pi\, \partial_t F_k(R) =& k^d \left(d f_k(\rho) + \partial_t f_k(\rho) - 2\rho f_k'(\rho)\right) \\ 16\pi\, \partial_t F_k'(R) =& k^{d-2} \left((d-2) f_k'(\rho) + \partial_t f_k'(\rho) - 2\rho f_k''(\rho)\right) \\ 16\pi\, \partial_t F_k''(R) =& k^{d-4} \left((d-4) f_k''(\rho) + \partial_t f_k''(\rho) - 2\rho f_k'''(\rho)\right) \end{aligned} \tag{4.11}$$

Thus the LHS of the flow equation in four dimensions simply reads

$$\partial_t \bar{\Gamma}_k = \frac{24\pi}{\rho^2}\left[\partial_t f(\rho) - 2\rho f'(\rho) + 4 f(\rho)\right] \tag{4.12}$$

Now, we can turn to the RHS and calculate the traces using the heat kernel methods. The flow equation in terms of the traces of the various components reads

$$\begin{aligned} \partial_t \bar{\Gamma}[\bar{g},\bar{g}] =& \frac{1}{2}\mathrm{Tr}_{(2T)}\left[\frac{\partial_t \mathcal{R}_k^{h^T h^T}}{\bar{\Gamma}^{(2)}_{h^T h^T}}\right] + \frac{1}{2}\mathrm{Tr}'_{(1T)}\left[\frac{\partial_t \mathcal{R}_k^{\xi\xi}}{\bar{\Gamma}^{(2)}_{\xi\xi}}\right] + \frac{1}{2}\mathrm{Tr}''_{(0)}\left[\frac{\partial_t \mathcal{R}_k^{\sigma\sigma}}{\bar{\Gamma}^{(2)}_{\sigma\sigma}}\right] + \frac{1}{2}\mathrm{Tr}_{(0)}\left[\frac{\partial_t \mathcal{R}_k^{hh}}{\bar{\Gamma}^{(2)}_{hh}}\right] \\ &+ \mathrm{Tr}''_{(0)}\left[\frac{\partial_t \mathcal{R}_k^{\sigma h}}{\bar{\Gamma}^{(2)}_{\sigma h}}\right] - \mathrm{Tr}'_{(1T)}\left[\frac{\partial_t \mathcal{R}_k^{\bar{C}^T C^T}}{\bar{\Gamma}^{(2)}_{\bar{C}^T C^T}}\right] - \mathrm{Tr}''_{(0)}\left[\frac{\partial_t \mathcal{R}_k^{\bar{\eta}\eta}}{\bar{\Gamma}^{(2)}_{\bar{\eta}\eta}}\right] - \mathrm{Tr}''_{(0)}\left[\frac{\partial_t \mathcal{R}_k^{\bar{\lambda}\lambda}}{\bar{\Gamma}^{(2)}_{\bar{\lambda}\lambda}}\right] \\ &+ \frac{1}{2}\mathrm{Tr}''_{(0)}\left[\frac{\partial_t \mathcal{R}_k^{\omega\omega}}{\bar{\Gamma}^{(2)}_{\omega\omega}}\right] - \mathrm{Tr}'_{(1T)}\left[\frac{\partial_t \mathcal{R}_k^{\bar{c}^T c^T}}{\bar{\Gamma}^{(2)}_{\bar{c}^T c^T}}\right] + \frac{1}{2}\mathrm{Tr}'_{(1T)}\left[\frac{\partial_t \mathcal{R}_k^{\zeta^T \zeta^T}}{\bar{\Gamma}^{(2)}_{\zeta^T \zeta^T}}\right] + \mathrm{Tr}''_{(0)}\left[\frac{\partial_t \mathcal{R}_k^{\bar{s}s}}{\bar{\Gamma}^{(2)}_{\bar{s}s}}\right] \end{aligned} \tag{4.13}$$

In order to continue and compute the traces we have to fix the gauge and focus on a specific spacetime dimension. For what follows we make the following choices

$$d = 4 \qquad ; \qquad \alpha \to 0 \qquad ; \qquad \rho = 0. \tag{4.14}$$

This choice of gauge results in two simplifications of the flow equation. Since we take the limit $\alpha \to 0$ the gauge fixing terms are tending to ∞. However, since terms proportional to $\frac{1}{\alpha}$ are also included in the regulator, when we take the limit $\alpha \to 0$ at the level of the FRGE only the terms proportional to $\frac{1}{\alpha}$ survive.

As a result the non-diagonal term σh vanishes since it has no dependence on α (for $\rho = 0$) while the denominator involves the components hh and $\sigma\sigma$ and it goes to ∞. The second simplification which occurs is that the gravity and the gauge degrees of freedom and the gravity degrees of freedom totally decouple. The gravity d.o.f. are encoded in $h^T h^T$ and hh, while the gauge d.o.f. are in $\xi\xi$ and $\sigma\sigma$.

Now we are in the position to use the machinery developed in Section 3.3 in order to calculate the trace. The result for the renormalisation group flow equation of $f(R)$ quantum gravity reads

$$\partial_t f(\rho) - 2\rho f'(\rho) + 4f(\rho) = I[f](\rho)\,. \tag{4.15}$$

The RHS encodes the contributions from fluctuations and arises from the operator trace (5.13) over all propagating fields. It generically splits into several parts,

$$I[f](\rho) = I_0[f](\rho) + \partial_t f'(\rho)\, I_1[f](\rho) + \partial_t f''(\rho)\, I_2[f](\rho)\,. \tag{4.16}$$

The additional flow terms proportional to $\partial_t f'(\rho)$ and $\partial_t f''(\rho)$ arise through the Wilsonian momentum cutoff $\partial_t R_k$, which we have chosen to depend on the background field. Furthermore, the terms $I_0[f](\rho)$, $I_1[f](\rho)$ and $I_2[f](\rho)$ depend on $f(\rho)$ and its field derivatives $f'(\rho)$, $f''(\rho)$ and $f'''(\rho)$. There are no flow terms $\partial_t f'''(\rho)$ or higher because the momentum cutoff R_k is proportional to the second variation of the action. A dependence on $f'''(\rho)$ in $I_0[f]$ results completely from rewriting $\partial_t F''(R)$ in dimensionless form. In the following expressions, we will suppress the argument ρ.

All three terms $I_0[f]$, $I_1[f]$, $I_2[f]$ arise from tracing over the fluctuations of the metric field for which we have adopted a transverse traceless decomposition. The term $I_0[f]$ also receives f-independent contributions from the ghosts and from the Jacobians originating from the split of the metrical fluctuations into tensor, vector and scalar parts. To indicate the origin of the various contributions in the expressions below, we use superscipts T, V, and S to refer to the transverse traceless tensorial, vectorial, and scalar origin. The specific form of $I_0[f]$, $I_1[f]$, $I_2[f]$ depends on the gauge (here the same as in section 7 in [34]) and regulator choice (with the optimized cutoff [94, 97]).

With these considerations in mind, we write the various ingredients in (4.15) as

$$I_0[f] = c\left(\frac{P_c^V}{D_c^V} + \frac{P_c^S}{D_c^S} + \frac{P_0^{T1} f' + P_0^{T2}\,\rho\, f''}{D^T} + \frac{P_0^{S1} f' + P_0^{S2} f'' + P_0^{S3}\,\rho\, f'''}{D^S}\right) \tag{4.17}$$

$$I_1[f] = c\left(\frac{P_1^T}{D^T} + \frac{P_1^S}{D^S}\right) \tag{4.18}$$

$$I_2[f] = c\,\frac{P_2^S}{D^S}\,. \tag{4.19}$$

The numerical prefactor reads $c = 1/(24\pi)$. It arises from our normalisation factor 16π introduced in (4.9), divided by the volume of the unit 4-sphere, $384\pi^2$. Note that the factor is irrelevant for the universal exponents at the fixed point. The first two terms in (4.17) arise from the ghosts (V) and the Jacobians (S), while the third and fourth arise from the tensorial (T) and scalar (S) metric fluctuations, respectively. Both (4.18) and (4.19) only have contributions from the tensorial and scalar metric fluctuations. The

various denominators appearing in (4.17), (4.18) and (4.19) are given by

$$D^T = 3f - (\rho - 3)f' \tag{4.20}$$

$$D^S = 2f + (3 - 2\rho)f' + (3 - \rho)^2 f'' \tag{4.21}$$

$$D_c^V = (4 - \rho) \tag{4.22}$$

$$D_c^S = (3 - \rho)\,. \tag{4.23}$$

The numerators in (4.17), (4.18) and (4.19) are polynomials in ρ. They arise through the heat kernel expansion of the traces, and are given by

$$P_c^V = \frac{607}{15}\rho^2 - 24\rho - 144 \tag{4.24}$$

$$P_c^S = \frac{511}{30}\rho^2 - 12\rho - 36 \tag{4.25}$$

$$P_0^{T1} = \frac{311}{756}\rho^3 - \frac{1}{3}\rho^2 - 90\rho + 240 \tag{4.26}$$

$$P_0^{T2} = -\frac{311}{756}\rho^3 + \frac{1}{6}\rho^2 + 30\rho - 60 \tag{4.27}$$

$$P_0^{S1} = \frac{37}{756}\rho^3 + \frac{29}{15}\rho^2 + 18\rho + 48 \tag{4.28}$$

$$P_0^{S2} = -\frac{37}{756}\rho^4 - \frac{29}{10}\rho^3 - \frac{121}{5}\rho^2 - 12\rho + 216 \tag{4.29}$$

$$P_0^{S3} = \frac{181}{1680}\rho^4 + \frac{29}{15}\rho^3 + \frac{91}{10}\rho^2 - 54 \tag{4.30}$$

$$P_1^T = \frac{311}{1512}\rho^3 - \frac{1}{12}\rho^2 - 15\rho + 30 \tag{4.31}$$

$$P_1^S = \frac{37}{1512}\rho^3 + \frac{29}{60}\rho^2 + 3\rho + 6 \tag{4.32}$$

$$P_2^S = -\frac{181}{3360}\rho^4 - \frac{29}{30}\rho^3 - \frac{91}{20}\rho^2 + 27\,. \tag{4.33}$$

From the explicit expressions it is straightforward to confirm that $I_0[f]$ has homogeneity degree zero in f, $I_0[a\,f] = I_0[f]$ for any $a \neq 0$, whereas $I_1[f]$ and $I_2[f]$ have homogeneity degree -1, $I_i[a \cdot f] = a^{-1}\, I_i[f]$ $(i = 1, 2)$. This establishes that $I[f]$ (4.16) has homogeneity degree zero.

4.4 The fixed point equation

Having derived the renormalisation group flow equation for $f(R)$ gravity (4.16), the next step is to look for fixed point solutions. This means that we need to find solutions of the function $f(\rho)$ for the equation

$$4f(\rho) - 2\,\rho\, f'(\rho) = I_0[f](\rho)\,. \tag{4.34}$$

This is a third order, non-linear differential equation and finding an analytical solution would be a prohibited task. For this, we have to rely to some kind of approximation with

the most common one in the literature being a polynomial expansion of the function $f(\rho)$

$$f(\rho) = \sum_{n=0}^{N-1} \lambda_n \, \rho^n, \tag{4.35}$$

where N is the order at which we truncate the function $f(\rho)$. Consequently, we make a series expansion of the fixed point equation (4.34) and we equate the expressions with the same power of the dimensionless scalar curvature ρ.

It turns out that instead of computing at every order the series coefficient and solve N equations with N unknowns there is an iterative process which allows us to reach very high orders in the polynomial expansion and also to solve the system of the equations. This is based on the observation that at each order n of the expanded fixed point equation (4.34), the highest coefficient of the expanded $f(\rho)$ function (4.35) is always λ_{n+2} and moreover it is always linear. Therefore we can always analytically solve to get an expression

$$\lambda_{n+2} = \mathcal{G}_n(\lambda_0, \lambda_1, \cdots, \lambda_{n+1}) \tag{4.36}$$

Thus, starting from the zeroth order ($n = 0$) we get an equation of λ_2 in terms of λ_0 and λ_1. For the first order ($n = 1$) we get an equation of λ_3 in terms of λ_0, λ_1 and λ_2 and by substituting the results of the zeroth order we end up with an equation of λ_3 in terms of λ_0 and λ_1 only. In this fashion we can get all the coupling in terms of the first two

$$\lambda_n = \mathcal{F}_n(\lambda_0, \lambda_1) \qquad , \qquad n \geq 2. \tag{4.37}$$

The last two equations for the expanded fixed point equation (4.34) will then provide us with equations for the coupling λ_N and λ_{N+1}. In agreement with the truncation (4.35) we have to set these two to zero

$$\begin{aligned} \lambda_N &= 0 \\ \lambda_{N+1} &= 0. \end{aligned} \tag{4.38}$$

Solving these two equations we find the fixed point values for λ_0 and λ_1 and consequently, by substituting into (4.37) we find the fixed point values for all the other couplings. Therefore, we have reduced the problem of solving a system of N equations to a recursive relation plus solving a system of two equations. In what follows we are going to explicitly derive the recursive relation for the fixed point equation.

4.4.1 General considerations

In order to find the relation for the highest coefficient in terms of all the rest it is convenient to start by writing the fixed point equation (4.34) in one line. The crucial observation at

this point, is that by putting the fixed point equation under this form, we can make use of the Leibniz rule to obtain an explicit expression for the n-th derivative of (4.34) [109]. Then, in terms of the various polynomials we have

$$L\,D^c\,D^T\,D^S - c\,N^S\,D^T\,D^c - c\,N^T\,D^S\,D^c - c\,N^c\,D^S\,D^T = 0, \tag{4.39}$$

where we used the denominators as defined in (4.23). We have also defined the combined denominator of the constant mode D^c and the left hand side of the fixed point equation L as

$$D^c = \rho^2 - 7\rho + 12 \tag{4.40}$$

$$L = 4f - 2\,\rho\,f'. \tag{4.41}$$

Finally, we have defined the numerators in terms of the polynomials as

$$N^S = P_0^{S1} f' + P_0^{S2} f'' + P_0^{S3}\,\rho\,f''' \tag{4.42}$$

$$N^T = P_0^{T1} f' + P_0^{T2}\,\rho\,f'' \tag{4.43}$$

$$N^c = -\frac{115}{2}\rho^3 + \frac{3383}{15}\rho^2 + 60\rho - 576. \tag{4.44}$$

The strategy that we are going to follow is to determine the form of the fixed point equation (4.39) at each order of the series expansion. This boils down to finding the n-th derivative of it. We start with the series expansion of the function $f(\rho)$, which takes the form

$$f(\rho) = \sum_{n=0}^{N-1} \frac{1}{n!}\, f^{(n)}\Big|_{\rho=0} \rho^n, \tag{4.45}$$

where here and from now on $f^{(n)}$ denotes the n-th derivative of f with respect to ρ. It turns out to be more convenient to perform the calculation in terms of $f^{(n)}$ instead of λ_n. However, these two are simply related by $\lambda_n = \frac{1}{n!} f^{(n)}$. Now, we write down the form for the n-th derivative of the following expression when evaluated at $\rho = 0$

$$\left(\rho^k f^{(m)}\right)^{(n)}\Big|_{\rho=0} = \frac{n!}{(n-k)!} f^{(m+n-k)}. \tag{4.46}$$

Using this it becomes straightforward to find the form of all the expressions that contribute to the fixed point equation (4.39). Then we have

$$\left(D^S\right)^{(n)} = \left(n^2-3n+2\right) f^{(n)} + 3(1-2n) f^{(n+1)} + 9 f^{(n+2)} \tag{4.47}$$

$$\left(D^T\right)^{(n)} = (3-n) f^{(n)} + 3 f^{(n+1)} \tag{4.48}$$

$$(L)^{(n)} = (2-n) f^{(n)} \tag{4.49}$$

$$\begin{aligned}\left(N^S\right)^{(n)} = {} & (216-54n) f^{(n+2)} + (48-12n) f^{(n+1)} \\ & + n\left[18 - \frac{121}{5}(n-1) + \frac{91}{10}(n-1)(n-2)\right] f^{(n)} \\ & + n(n-1)\left[\frac{29}{15} - \frac{29}{10}(n-2) + \frac{29}{15}(n-2)(n-3)\right] f^{(n-1)} \\ & + n(n-1)(n-2)\left[\frac{37}{756} - \frac{37}{756}(n-3) + \frac{181}{1680}(n-3)(n-4)\right] f^{(n-2)}\end{aligned} \tag{4.50}$$

$$\begin{aligned}\left(N^T\right)^{(n)} = {} & -60(n-4) f^{(n+1)} + 30n(n-4) f^{(n)} + \frac{1}{6} n(n-1)(n-4) f^{(n-1)} \\ & - \frac{311}{756} n(n-1)(n-2)(n-4) f^{(n-2)}\end{aligned} \tag{4.51}$$

If an expression X from those above is multiplied with a term which does not contain f, as N^c and D^c, then it contributes only a coefficient. To see this in more detail we use the generalised Leibniz rule and we write the contributions for coming from these terms after taking n derivatives and evaluating at $\rho = 0$

$$\begin{aligned}\left(X \cdot N^c\right)^{(n)}\Big|_{\rho=0} = {} & -576 X^{(n)} + 60\, n X^{(n-1)} + \frac{3383}{15} n(n-1) X^{(n-2)} \\ & - \frac{115}{2} n(n-1)(n-2) X^{(n-3)}\end{aligned} \tag{4.52}$$

$$\left(X \cdot D^c\right)^{(n)}\Big|_{\rho=0} = 12 X^{(n)} - 7\, n X^{(n-1)} + n(n-1) X^{(n-2)}. \tag{4.53}$$

Now we have all the ingredients we need in order to expand the fixed point equation (4.39) and to find the recursive relation of the highest coupling in terms of all the rest.

4.4.2 The highest coefficient

As we can observe from the form of (4.39) the highest coefficient will always be $f^{(n+2)}$ and it always comes linearly. The terms that contribute to it are $9 f^{(n+2)}$ from D^S and $(216-54n) f^{(n+2)}$ from N^S. Now we introduce some notation in order to write the recursive relation in an as compact form as possible.

First, we write the n-th derivative of an expression X in terms of its coefficients of the f derivatives. Then we have

$$X^{(n)} = \sum_i x_i\, f^{(n+i)}, \tag{4.54}$$

where for all the expressions appearing above the index i runs from -2 to 2. Here the coefficients are denoted with the respective small letter x_i. For example, the coefficients of

the expression $\left(D^S\right)^{(n)}$ will be denoted by d_i^S. The main tool that we need to use in order to expand the fixed point equation and find the highest coupling is the generalised Leibniz rule for two functions $(f\cdot g)^{(n)}=\sum_{k=0}^{n}\binom{n}{k}f^{(k)}g^{(n-k)}$. Now we introduce the shorthand expression

$$\mathcal{L}(f;g)^n=\sum_{k=0}^{n-1}\binom{n}{k}f^{(n)}g^{(n-k)}. \tag{4.55}$$

Now it is straightforward to apply n derivatives to the fixed point equation and single out the contributions to $f^{(n+2)}$. Then, the highest coefficient will be given by terms involving (4.55) and some other single terms. The terms involving the modified Leibniz rule (4.55) are coming from all the terms that do not involve n derivatives of D^S or N^S. These will not produce a coefficient $f^{(n+2)}$ and for this it is now justified the modified upper limit in (4.55) as $n-1$ instead of n. The single terms come from the terms with n derivatives acting on D^S and N^S but not containing $f^{(n+2)}$. Finally, the denominators that appear are just the coefficients of $f^{(n+2)}$. The final result reads

$$\begin{aligned}f^{(n+2)}=&\frac{-\mathcal{L}(D^S;L\,D^T\,D^c)^n+c\,\mathcal{L}(N^S;D^T\,D^c)^n+c\,\mathcal{L}(D^S;N^T\,D^c)^n+c\,\mathcal{L}(D^S;D^T\,N^c)^n}{d^S_{n+2}L\,D^T\,D^c-c\,n^S_{n+2}D^T\,D^c-c\,d^S_{n+2}N^T\,D^c-c\,d^S_{n+2}D^T\,N^c}\\&+\frac{-\sum_{i=-2}^{1}d_i^S f^{(n+i)}\left[L\,D^T\,D^c-c\,N^T\,D^c-c\,D^T\,N^c\right]+\sum_{i=-2}^{1}c\,n_i^S f^{(n+1)}D^T\,D^c}{d^S_{n+2}L\,D^T\,D^c-c\,n^S_{n+2}D^T\,D^c-c\,d^S_{n+2}N^T\,D^c-c\,d^S_{n+2}D^T\,N^c}\end{aligned} \tag{4.56}$$

with the various Leibniz terms having analytic expressions given by

$$\begin{aligned}\mathcal{L}(D^S;L\,D^T\,D^c)^n=&\sum_{k=0}^{n-1}(D^S)^{(k)}\left\{12\sum_{l=0}^{n-k}c_1\,f^{(l)}\left[(3-n+k+l)f^{(n-k-l)}+3f^{(n-k-l+1)}\right]\right.\\&-7\sum_{l=0}^{n-k-1}c_2\,f^{(l)}\left[(4-n+k+l)f^{(n-k-l-1)}+3f^{(n-k-l)}\right]\\&\left.+\sum_{l=0}^{n-k-2}c_3\,f^{(l)}\left[(5-n+k+l)f^{(n-k-l-2)}+3f^{(n-k-l-1)}\right]\right\}\end{aligned} \tag{4.57}$$

with $c_1=\frac{(2-l)\,n!}{k!l!(n-k-l)!}$, $c_2=\frac{(2-l)n!}{k!l!(n-k-l-1)!}$ and $c_3=\frac{(2-l)n!}{k!l!(n-k-l-2)!}$. The other three Leibniz terms are considerably simpler

$$\begin{aligned}\mathcal{L}(N^S;D^T\,D^c)^n=&\sum_{k=0}^{n-1}\binom{n}{k}(N^S)^{(k)}\left[36f^{(n-k+1)}+(36-33n+33k)f^{(n-k)}\right.\\&\left.+(n-k)(10n-10k-31)f^{(n-k-1)}-(n-k)(n-k-1)(n-k-5)f^{(n-k-2)}\right]\end{aligned} \tag{4.58}$$

and

$$\begin{aligned}\mathcal{L}(D^S;N^T\,D^c)^n=&\sum_{k=0}^{n-1}\binom{n}{k}(D^S)^{(k)}\Big[-720(c_4-4)f^{(c_4+1)}+60c_4(13c_4-59)f^{(c_4)}\\&-2c_4(134c_4^2-835c_4+701)f^{(c_4-1)}\\&+\frac{1}{126}c_4\left(3011c_4^3-28490c_4^2+64393c_4-38914\right)f^{(c_4-2)}\\&+\frac{1}{108}c_4\left(329c_4^4-3637c_4^3+13597c_4^2-20267c_4+9978\right)f^{(c_4-3)}\\&+\frac{311}{756}c_4(c_4^5-16c_4^4+95c_4^3-260c_4^2+324c_4-144)f^{(c_4-4)}\Big]\end{aligned}\tag{4.59}$$

with $c_4=n-k$ and finally

$$\begin{aligned}\mathcal{L}(D^S;D^T\,N^c)^n=&\sum_{k=0}^{n-1}\binom{n}{k}(D^S)^{(k)}\Big[-1728^{(c_4+1)}+108(7c_4-16)f^{(c_4)}+\frac{1}{5}c_4(3083c_4-2183)f^{(c_4-1)}\\&-\frac{1}{30}(11941c_4^2-56121c_4+44180)f^{(c_4-2)}+\frac{115}{2}c_4(c_4-1)(c_4-2)(c_4-6)f^{(c_4-3)}\Big].\end{aligned}\tag{4.60}$$

Combining all the above we have an analytic expression for the highest coupling λ_{n+2} for the polynomial expansion and even though the final expression looks rather complicated it allows us to reach much higher order than what we would with the conventional techniques. In order to tackle the recursive relation we created an application using a code written in the programming language $C++$. After running the code we managed to find all the couplings up to order

$$N=35.\tag{4.61}$$

The limitations of the computing memory was the main obstacle to go to even higher orders of the approximation. The results of this calculation will be presented in the sections to follow.

4.5 The critical exponents

Having established a systematic way to solve the fixed point equation we turn our attention to the second important quantity that we have to compute, the critical exponents. In this section we will follow the techniques developed in the previous section in order to find an efficient way to compute the critical exponents.

Now we have to re-introduce the scale derivative terms and to examine the full flow equation. We keep working with the form of the equation where everything is put in one line and we have

$$U+D^c\,D^T\,D^S\,\partial_t f-c\,P_1^S\,D^T\,D^c\partial_t f'-c\,P_2^S\,D^T\,D^c\partial_t f''-c\,P_1^T\,D^S\,D^c\partial_t f'=0,\tag{4.62}$$

where U denotes the fixed point equation in one line

$$U = L\, D^c\, D^T\, D^S - c\, N^S\, D^T\, D^c - c\, N^T\, D^S\, D^c - c\, N^c\, D^S\, D^T. \tag{4.63}$$

Now we follow the same strategy as we did with the fixed points and we try to determine the form of the flow equation (4.62) after taking n derivatives. This will be given by

$$\begin{aligned} U^{(n)} + \sum_{l=0}^{n} \binom{n}{l} V_0^{(l)} \partial_t f^{(n-l)} = \\ = c \left[\sum_{l=0}^{n} \binom{n}{l} V_1^{(l)} \partial_t f^{(n-l+1)} + \sum_{l=0}^{n} \binom{n}{l} V_2^{(l)} \partial_t f^{(n-l+2)} + \sum_{l=0}^{n} \binom{n}{l} V_3^{(l)} \partial_t f^{(n-l+1)} \right] \end{aligned} \tag{4.64}$$

where we have defined the coefficients of the scale derivatives as

$$V_0 = D^c\, D^T\, D^S \tag{4.65}$$

$$V_1 = P_1^S\, D^T\, D^c \tag{4.66}$$

$$V_2 = P_2^S\, D^T\, D^c \tag{4.67}$$

$$V_3 = P_1^T\, D^S\, D^c \tag{4.68}$$

Now it is convenient to define $\beta_i \equiv \partial_t f^{(i)}$ and write the flow equation (4.62) in matrix form

$$\vec{\boldsymbol{\beta}} = \mathbb{V}^{-1} \cdot \vec{\boldsymbol{U}}, \tag{4.69}$$

with $\vec{\boldsymbol{\beta}}$ being the vector of the beta functions β_i, the vector $\vec{\boldsymbol{U}}$ being the vector of the fixed point equation at each order of the expansion $U^{(j)}$ and $\mathbb{V}$ being the matrix for the coefficients of $\partial_t f^{(i)}$ at each order of the series expansion j. The entries of V_{ij} will be given in the rest of this section.

In order to compute the critical exponents, we have to linearise the flow in the vicinity of the fixed point g_*. Then we keep only the lowest order and we have

$$\vec{\boldsymbol{\beta}} = \cancelto{0}{\vec{\boldsymbol{\beta}}(g_*)} + \left.\frac{\partial \vec{\boldsymbol{\beta}}}{\partial f^{(j)}}\right|_{g_*} \cdot (f^{(j)} - f_*^{(j)}). \tag{4.70}$$

In principle we can solve for the beta functions $\vec{\boldsymbol{\beta}}$ from (4.69) and then compute the quantity $\left.\frac{\partial \vec{\boldsymbol{\beta}}}{\partial f^{(j)}}\right|_{g_*}$. However, since we have first to perform the inversion of the matrix $\mathbb{V}$ this task becomes impossible. In practice it is easier to start by taking derivatives of (4.69) with respect to the couplings and then evaluate the relation at $g = g_*$. Then we have

$$\left.\frac{\partial \vec{\boldsymbol{\beta}}}{\partial f^{(j)}}\right|_{g_*} = \mathbb{V}^{-1}\big|_{g_*} \cdot \left.\frac{\partial \vec{\boldsymbol{U}}}{\partial f^{(j)}}\right|_{g_*} \tag{4.71}$$

and now the inversion of the matrix is just a numerical task. Moreover we can use the equation (4.70) in order to find the linearised beta functions in the vicinity of the fixed point. However, in order to compute the eigenvalues we only need the matrix $\mathbb{M}_{ij} = \frac{\partial \beta_i}{\partial f^{(j)}}$ which is given by (4.71).

4.5.1 The computation of the matrices

Now we can use the machinery developed in the previous section to evaluate the matrix (4.71). The ingredients that we need are the ρ derivatives of the ∂_t terms and the $f^{(j)}$ derivatives of the $\vec{\boldsymbol{U}}$ term. We start with the ρ derivatives and we have for the expressions at order n in the expansion when evaluated at $\rho = 0$

$$
\begin{aligned}
V_0^{(n)} &= 12(D^S \cdot D^T)^{(n)} - 7n(D^S \cdot D^T)^{(n-1)} + n(n-1)(D^S \cdot D^T)^{(n-2)} && (4.72)\\
V_1^{(n)} &= 72(D^T)^{(n)} - 6n(D^T)^{(n-1)} - \frac{46}{5} n(n-1)(D^T)^{(n-2)} && (4.73)\\
&\quad - \frac{113}{1260} n(n-1)(n-2)(D^T)^{(n-3)} + \frac{337}{1080} n(n-1)(n-2)(n-3)(D^T)^{(n-4)} && (4.74)\\
&\quad + \frac{37}{1512} n(n-1)(n-2)(n-3)(n-4)(D^T)^{(n-5)} && (4.75)\\
V_2^{(n)} &= 324(D^T)^{(n)} - 189n(D^T)^{(n-1)} - \frac{138}{5} n(n-1)(D^T)^{(n-2)} && (4.76)\\
&\quad + \frac{81}{4} n(n-1)(n-2)(D^T)^{(n-3)} + \frac{1319}{840} n(n-1)(n-2)(n-3)(D^T)^{(n-4)} && (4.77)\\
&\quad - \frac{283}{480} n(n-1)(n-2)(n-3)(n-4)(D^T)^{(n-5)} && (4.78)\\
&\quad - \frac{181}{3360} n(n-1)(n-2)(n-3)(n-4)(n-5)(D^T)^{(n-6)} && (4.79)\\
V_3^{(n)} &= 360(D^S)^{(n)} - 390n(D^S)^{(n-1)} + 134n(n-1)(D^S)^{(n-2)} && (4.80)\\
&\quad - \frac{3011}{252} n(n-1)(n-2)(D^S)^{(n-3)} - \frac{329}{216} n(n-1)(n-2)(n-3)(D^S)^{(n-4)} && (4.81)\\
&\quad + \frac{311}{1512} n(n-1)(n-2)(n-3)(n-4)(D^S)^{(n-5)}. && (4.82)
\end{aligned}
$$

Now we have all we need in order to determine the matrix elements of the matrix $\mathbb{V}$ that appears in (4.69). By observing which terms contribute at each order of the expansion and for which beta function we can write

$$
\begin{aligned}
V_{nm} = &\binom{n}{m} V_0^{(n-m)} - c \binom{n}{m-1} V_1^{(n-m+1)} \\
&- c \binom{n}{m-2} V_2^{(n-m+2)} - c \binom{n}{m-1} V_3^{(n-m+1)} \qquad , \qquad 0 \leq m \leq n.
\end{aligned}
\tag{4.83}
$$

For $m > n$ we have that $V_{nm} = 0$. Now we can construct this matrix with these elements and evaluate it at the fixed point $g = g_*$ and then numerically invert it, which has become an easy task.

Finally, we have to take derivatives with respect to the couplings of the vector $\vec{\boldsymbol{U}}$, which is nothing more than our fixed point equation. Therefore, at order n we have to

compute the coupling derivatives of sums of two and three terms. If the sum of two terms is written $\sum_{k=0}^{n} A^{(k)} B^{(n-k)}$ then we simply use the chain rule to obtain

$$\frac{\partial}{\partial f^{(m)}} \sum_{k=0}^{n} A^{(k)} B^{(n-k)} = \sum_{k=0}^{n} A^{(k)} \frac{\partial B^{(n-k)}}{\partial f^{(m)}} + \sum_{k=0}^{n} \frac{\partial A^{(k)}}{\partial f^{(m)}} B^{(n-k)} \tag{4.84}$$

with a similar expression for the term with the sum of the three terms. So we only have to evaluate now $\frac{\partial A^{(n)}}{\partial f^{(m)}}$ for the various terms. This is identical to the ρ derivatives at order n that we found in the previous section but with replacing every $f^{(m)}$ by the Kronecker delta δ^n_m.

4.6 Results

Using the methods outlined in the two previous sections, we solved the fixed point equation and computed the critical exponents at each order of the polynomial expansion (4.35) up to a maximum order

$$N_{\max} = 35. \tag{4.85}$$

In this section we are going to present the result and to perform some quantitative analysis starting with the fixed point values.

4.6.1 Fixed points

In Table 4.2 we summarise the fixed point couplings λ_* for selected sets of approximations. Notice that the signs of the couplings follow, approximately, an eight-fold periodicity in the pattern $(++++----)$. Four consecutive couplings $\lambda_{3+4i} - \lambda_{6+4i}$ come out negative (positive) for odd (even) integer $i \geq 0$, see Table 4.2. Periodicity patterns often arise due to convergence-limiting singularities of the fixed point solution $f_*(\rho)$ in the complex ρ-plane, away from the real axis. This is well-known from scalar theories at criticality where $2n$-fold periodicities are encountered regularly [98, 103]. In what follows we are going to use the periodicity property for the analysis of our results. Moreover, the selection for the sets shown in table has been made based on this observation.

We exploit the periodicity pattern to estimate the asymptotic values of couplings $\lambda_n(N \to \infty)$ from an average over an entire cycle based on the eight highest orders in the approximation between $N_{\max} - 7$ and $N_{\max}$,

$$\langle X \rangle = \frac{1}{8} \sum_{N=N_{\max}-7}^{N_{\max}} X(N)\,, \tag{4.86}$$

N	35	31	27	23	19	15	11	7
λ_0	0.25562	0.25555	0.25560	0.25546	0.25559	0.25522	0.25577	0.25388
λ_1	−1.0272	−1.0276	−1.0276	−1.0286	−1.0281	−1.0309	−1.0289	−1.0435
λ_2	0.01567	0.01549	0.01539	0.01498	0.01490	0.01369	0.01354	0.007106
λ_3	−0.44158	−0.44687	−0.43997	−0.44946	−0.43455	−0.45726	−0.40246	−0.51261
λ_4	−0.36453	−0.36802	−0.36684	−0.37407	−0.36981	−0.38966	−0.37114	−0.48091
λ_5	−0.24057	−0.23232	−0.24584	−0.23188	−0.25927	−0.22842	−0.31678	−0.18047
λ_6	−0.02717	−0.02624	−0.02286	−0.01949	−0.01564	−0.002072	−0.003987	0.12363
λ_7	0.15186	0.13858	0.15894	0.13620	0.17702	0.12649	0.23680	
λ_8	0.23014	0.23441	0.22465	0.22904	0.21609	0.21350	0.23600	
λ_9	0.21610	0.23820	0.20917	0.24918	0.18830	0.28460	0.12756	
λ_{10}	0.08484	0.08207	0.092099	0.095052	0.095688	0.13722	−0.041490	
λ_{11}	−0.14551	−0.17774	−0.13348	−0.19444	−0.097057	−0.25527		
λ_{12}	−0.32505	−0.33244	−0.33242	−0.36205	−0.31812	−0.46476		
λ_{13}	−0.29699	−0.25544	−0.32410	−0.24239	−0.39520	−0.16735		
λ_{14}	−0.05608	−0.04049	−0.05633	−0.000217	−0.11204	0.16762		
λ_{15}	0.22483	0.16347	0.26944	0.14317	0.37336			
λ_{16}	0.36315	0.34000	0.37795	0.28611	0.50997			
λ_{17}	0.34098	0.44488	0.28138	0.50187	0.17199			
λ_{18}	0.18536	0.23941	0.15207	0.35074	−0.11901			
λ_{19}	−0.16304	−0.32036	−0.07588	−0.41733				
λ_{20}	−0.61457	−0.73133	−0.53776	−0.95176				
λ_{21}	−0.75346	−0.53875	−0.88929	−0.41230				
λ_{22}	−0.25160	−0.05746	−0.43756	0.29953				
λ_{23}	0.55701	0.22998	0.73065					
λ_{24}	0.93392	0.60948	1.3116					
λ_{25}	0.70608	1.2552	0.54266					
λ_{26}	0.35710	0.98891	−0.31179					
λ_{27}	−0.09106	−0.92872						
λ_{28}	−1.1758	−2.3752						
λ_{29}	−2.2845	−1.1315						
λ_{30}	−1.4145	0.64746						
λ_{31}	1.6410							
λ_{32}	3.5054							
λ_{33}	1.7098							
λ_{34}	−0.66883							

Table 4.2: The coordinates of the ultraviolet fixed point in a polynomial base (4.35) for selected orders in the expansion. We note the approximate eight-fold periodicity pattern in the signs of couplings. The data for $N = 7$ and $N = 11$ agree with earlier findings in [33] and [22], respectively.

where $X(N)$ stands for the N^{th} order approximation for the quantity X.

Figure 4.1 shows the first six fixed point couplings as a function of the order N in the expansion, normalised to their asymptotic value (4.86). The first two couplings λ_0 and λ_1 converge rapidly towards their asymptotic values, and settle on the percent level starting from $N \approx 10$.

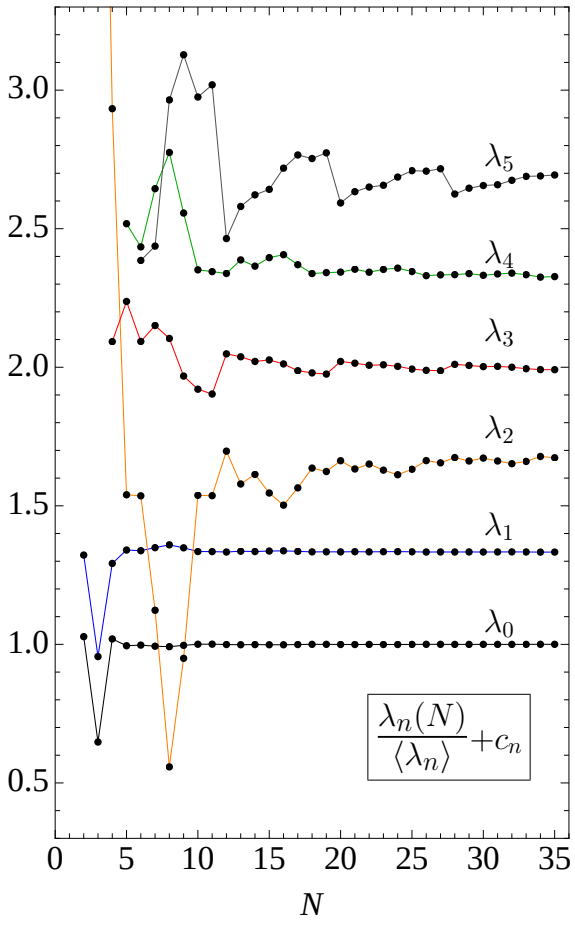

Figure 4.1: Convergence of the first six polynomial fixed point couplings λ_n with increasing order of the expansion N, (4.35). The couplings fluctuate about the asymptotic value $\langle\lambda_n\rangle$ (4.86) with decreasing amplitude and an approximate eight-fold periodicity. Note that the convergence of the R^2-coupling is slower than some of the higher-order couplings. The shift term $c_n = \frac{n}{3}$ has been added for display purposes.

As expected, the convergence is slower for the higher order couplings. An interesting exception is the R^2 coupling λ_2, which only just starts settling to its asymptotic value at the order $N \approx 20$ of the expansion, and hence much later than some of the subleading couplings. Furthermore, its value even becomes negative once, at order $N = 8$, see Table 4.3. The origin for this behaviour, we believe, is that the R^2 coupling is the sole marginal operator in the set-up, whereas all other operators have a non-trivial canonical dimension.

On the level of the RG β-function a non-vanishing canonical mass dimension leads to a term linear in the coupling, which helps stabilising the fixed point and the convergence of the coupled system. Therefore, to establish the existence of the fixed point and its stability, it becomes mandatory to extend the expansion to high orders $N \gg 8$.

Interestingly, the higher order couplings λ_3 and λ_4 converge more rapidly than λ_2 and settle close to their asymptotic value starting at $N \approx 15 - 20$. Notice also that the convergence behaviour in each coupling reflects the underlying eight-fold periodicity pattern. For the fixed point coordinates, using (4.86), we find the estimates

$$\begin{aligned} \langle \lambda_0 \rangle &= 0.25574 \quad \pm 0.015\% \\ \langle \lambda_1 \rangle &= -1.02747 \quad \pm 0.026\% \\ \langle \lambda_2 \rangle &= 0.01557 \quad \pm 0.9\% \\ \langle \lambda_3 \rangle &= -0.4454 \quad \pm 0.70\% \\ \langle \lambda_4 \rangle &= -0.3668 \quad \pm 0.51\% \\ \langle \lambda_5 \rangle &= -0.2342 \quad \pm 2.5\% \end{aligned} \tag{4.87}$$

for the first six couplings. Clearly, the couplings λ_0 and λ_1 show excellent convergence with an estimated error due to the polynomial approximation of the order of $10^{-3} - 10^{-4}$. The accuracy in the couplings λ_2, λ_3 and λ_4 is below the percent level and fully acceptable for the present study. The coupling λ_5 is the first one whose accuracy level of a few percent exceeds the one set by λ_2. Notice also that the mean value over all data differs mildly from the mean over the last cycle of eight, further supporting the stability of the result. On the other hand, had we included all data points in the error estimate, the standard deviation, in particular for λ_2 and λ_5, would grow large due to the poor fixed point values at low orders.

The results (4.87) translate straightforwardly into fixed point values for the dimensionless Newton coupling and the cosmological constant,

$$\begin{aligned} \langle g_* \rangle &= 0.97327 \quad \pm 0.027\% \\ \langle \lambda_* \rangle &= 0.12437 \quad \pm 0.041\% \ . \end{aligned} \tag{4.88}$$

Note that because λ is given by the ratio of λ_0 and λ_1 its statistical error is essentially given by the sum of theirs.

Universal quantities of interest are given by specific products of couplings. An important such quantity is the product of fixed point couplings $g \cdot \lambda = \lambda_0/(2\lambda_1^2)$. It is invariant under re-scalings of the metric field $g_{\mu\nu} \to \ell g_{\mu\nu}$, and may serve as a measure for the strength of the gravitational interactions [87]. We find the universal product

$$\langle g_* \cdot \lambda_* \rangle = 0.12105 \pm 0.07\%. \tag{4.89}$$

Furthermore, we find that $\langle g_* \cdot \lambda_* \rangle = \langle g_* \rangle \cdot \langle \lambda_* \rangle$ within the same accuracy, see (4.88), which supports the view that the cycle-averaged values have become independent of the underlying polynomial approximation.

Now we estimate the rate of convergence for the couplings with increasing order in the expansion. To that end we compute the number of relevant digits $D_n(N)$ in the coupling λ_n achieved at order N in the approximation, using the definition [98, 18]

$$10^{-D_n} \equiv \left| 1 - \frac{\lambda_n(N)}{\lambda_n(N_{\max})} \right| . \tag{4.90}$$

We could have used $\langle \lambda_n \rangle$ rather than $\lambda_n(N_{\max})$ in (4.90) to estimate the asymptotic value. Quantitatively, this makes only a small difference. The estimate for the growth rate of (4.90) is insensitive to this choice. In Figure 4.2 we display (4.90) for the first three couplings. Once more the eight-fold periodicity in the convergence pattern is clearly visible. The result also confirms that the precision in the leading fixed point couplings λ_0 and λ_1 is about 10^{-3} to 10^{-4} at the highest order in the expansion, in agreement with (4.87). The average slope ranges between $0.04 - 0.06$, meaning that the accuracy in the fixed point couplings increases by one decimal place for $N \to N + 20$.

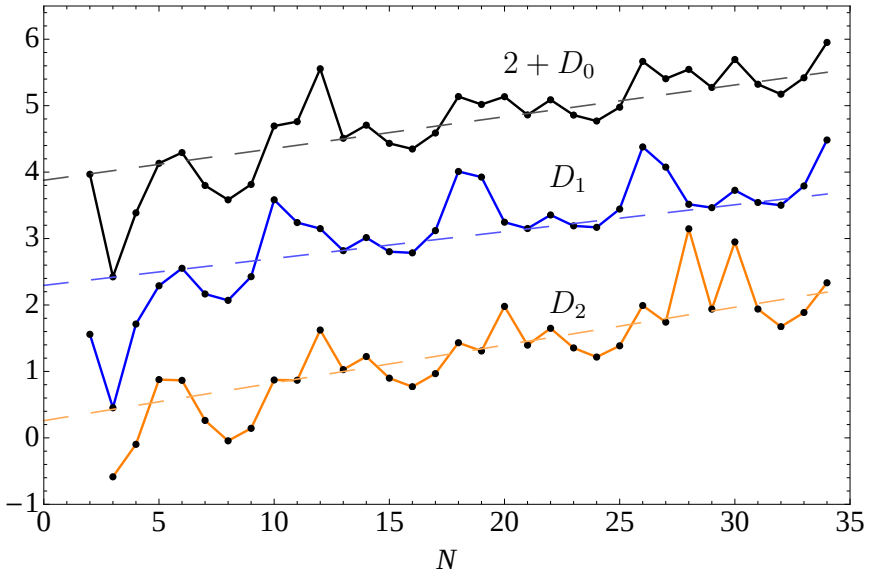

Figure 4.2: The rate of convergence of the three leading couplings λ_0, λ_1 and λ_2 as given by the number of relevant digits D_n (4.90) (from top to bottom). The mean slopes range between $0.04 - 0.06$ (dashed lines), and the data points are connected through lines to guide the eye. The curve for λ_0 is shifted upwards by two units for display purposes.

We briefly comment on additional fixed point candidates besides the one discussed above. In the search of fixed points and starting at order $N = 9$ we occasionally encounter

spurious fixed points. With 'spurious' we refer to fixed points which either only appear in few selected orders in the expansion and then disappear, or whose universal properties change drastically from order to order, such as a change in the number of negative eigenvalues. In principle, the boundary conditions (4.38), which are rational functions in the couplings, may have several real solutions λ_0 and λ_1. For example, at order $N = 35$, the vanishing of λ_{36} leads to a polynomial equation of degree 264 (167) in λ_0 (λ_1), and similarly for λ_{35}, corresponding, in principle, to a large number of potential fixed points in the complex plane. It is therefore quite remarkable that, in practice, we only find a unique and real solution which consistently persists to all orders. We conclude that the occasional spurious UV fixed points are artefacts of the polynomial expansion and we do not proceed their investigation any further.

4.6.2 Radius of convergence

The polynomial expansion (4.35) has a finite radius of convergence ρ_c, which can be estimated from the fixed point solution. Standard convergence tests fail due to the eightfold periodicity in the result, and a high-accuracy computation of ρ_c requires many orders in the expansion. As a rough approximation, we adopt the root test according to which

$$\rho_c = \lim_{n\to\infty} \rho_{c,m}(n) \quad \text{where} \quad \rho_{c,m}(n) = \left|\frac{\lambda_n}{\lambda_{n+m}}\right|^{1/m}, \tag{4.91}$$

with m held fixed, and provided the limit exists. It turns out that if m is taken to be the underlying periodicity or larger, $m \geq 8$, the ratios $\rho_{c,m}(n)$ depend only weakly on m. Since our data sets are finite, the limit $1/n \to 0$ can only be performed approximately. We estimate ρ_c from the most advanced data set ($N = 35$) by computing the smallest $\rho_c(m) \equiv \min_n[\rho_{c,m}(n)]$ for all admissible m ($8 \leq m \leq N - m$) and then taking the average over m. In this manner, the estimate will be insensitive to m. We find

$$\rho_c \approx 0.82 \pm 5\% \tag{4.92}$$

where the statistical error is due to the variation with m. The smallness of the statistical error reflects that the value (4.92) is achieved for essentially all $m \geq 8$. For illustration, we show in Figure 4.3 the fixed point solution as a function of $\rho = R/k^2$ to order $N = 31$ and $N = 35$. Both solutions visibly part each other's ways at fields of the order of (4.92), supporting our rationale.

Note that if we restrict our procedure to the first 11 fixed point couplings (by using either the $N = 11$ data, or the first 11 entries from the $N = 35$ data set), we find $\rho_c \approx 1.0 \pm 20\%$. This is consistent with the estimate $\rho_c \approx 0.99$ given in [22] based on the

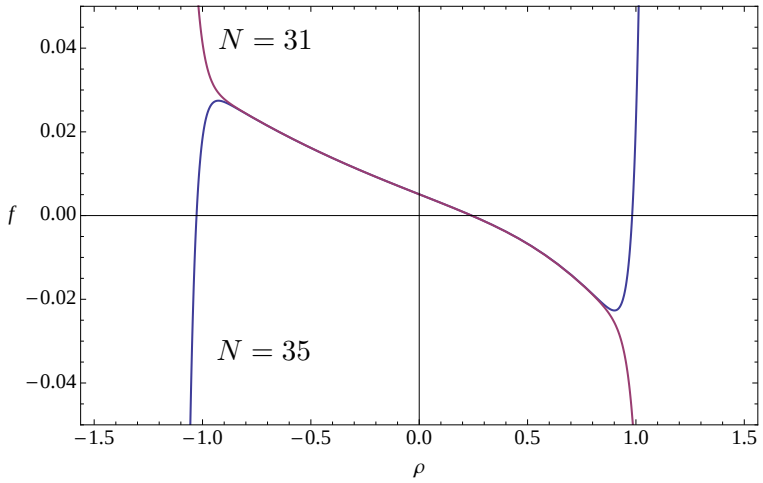

Figure 4.3: The fixed point solution f_* to order $N = 35$ (blue line) and $N = 31$ (red line) in the polynomial approximation.

same $N = 11$ data set but derived differently. The larger value for ρ_c at low orders is due to the fact that a full period has just been completed for the first time at $N = 11$ resulting in a slight over-estimation for ρ_c.

4.6.3 Anomalous dimension

We now turn to a discussion of the field-dependent anomalous dimension $\eta_{F'}$ associated to $F' \equiv dF/dR$. It is defined via the RG flow (4.15) as $\partial_t F' = \eta_{F'} F'$. In the fixed point regime, we find

$$\eta_{F'} = 2 - 2\rho\, f''(\rho)/f'(\rho)\,, \tag{4.93}$$

where $f' \equiv df/d\rho$. The fixed point solution is plotted in Fig. 4.4 for $N = 31$ (dashed line) and $N = 35$ (full line). We note that η displays a local maximum at $\rho \approx 0$. Using the same technique as before, we find that the radius of convergence $\rho_c \approx 0.65 \pm 10\%$ comes out smaller than the one for f, see (4.92). The reason for this is that the anomalous dimension involves up to two derivatives of f and is therefore more sensitive to the underlying approximation than f itself. Note that the anomalous dimension becomes small, $\eta \approx 0$, close to the radius of convergence $\rho \approx \rho_c$.

We can relate the function (4.93) to the anomalous dimension of Newton's coupling, η_N. The latter is defined through the RG flow of Newton's coupling, $\partial_t G_k = \eta_N\, G_k$. At a non-trivial fixed point for the dimensionless Newton coupling $g = G_k\, k^2$ its anomalous

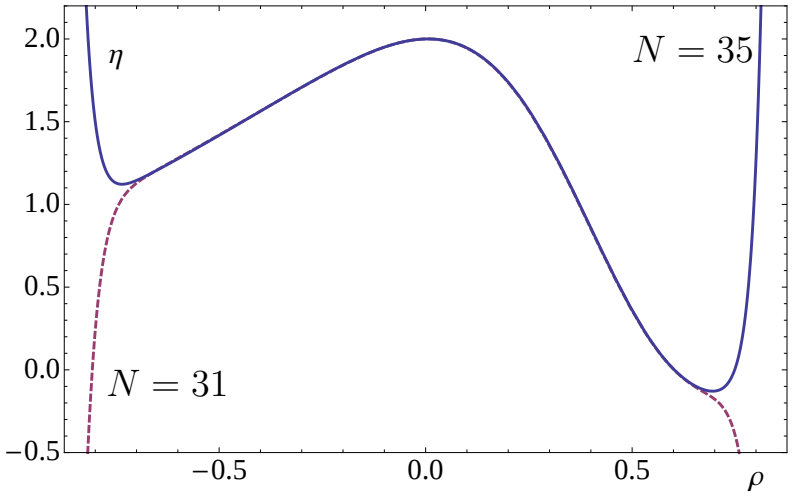

Figure 4.4: Field-dependent anomalous dimension (4.93) to order $N = 35$ (full line) and $N = 31$ (dashed line) in the polynomial approximation.

dimension takes the value

$$\eta_N = -2 \tag{4.94}$$

to ensure the vanishing of $\partial_t g = (2 + \eta_N)g$. Using the definitions (4.7), (4.9) we have that $g \propto 1/f'|_{\rho=0}$, leading to the relation

$$\eta_N = -\eta_{F'}(\rho = 0)\,. \tag{4.95}$$

In this light, it becomes natural to interpret the function $G_{\text{eff}}(\rho) = -1/(16\pi\, F'(\rho))$ as a field-dependent generalisation of Newton's coupling, which falls back onto the standard definition in the limit $\rho = 0$. Away from this point in field space, however, the effective anomalous dimension of the graviton (4.93) differs from the value (4.94) and becomes smaller in magnitude.

4.6.4 Critical exponents

In critical phenomena, fixed point coordinates are often non-universal and not measurable in any experiment. Instead, the scaling of couplings in the vicinity of a fixed point are universal. In quantum gravity, universal exponents can be read off from the eigenvalues of the stability matrix $\mathbb{M}$ defined in (1.9), which is, to order N in the approximation, a real and in general non-symmetric $N \times N$ matrix, and $\beta_i \equiv \partial_t \lambda_i$. The computation of (1.9) and its N eigenvalues ϑ_n, $(n = 0, 1, \cdots, N-1)$ is more involved than finding the fixed points, because the additional terms proportional to I_1 and I_2 in (4.15) have to be taken into account. Using the techniques developed in Section 4.5 we have computed the

eigenvalues for all N up to $N_{\max}$. Our results are summarised in Figure 4.5 and Table 4.3. A detailed discussion of the large-order behaviour of eigenvalues is deferred to Section 4.7.

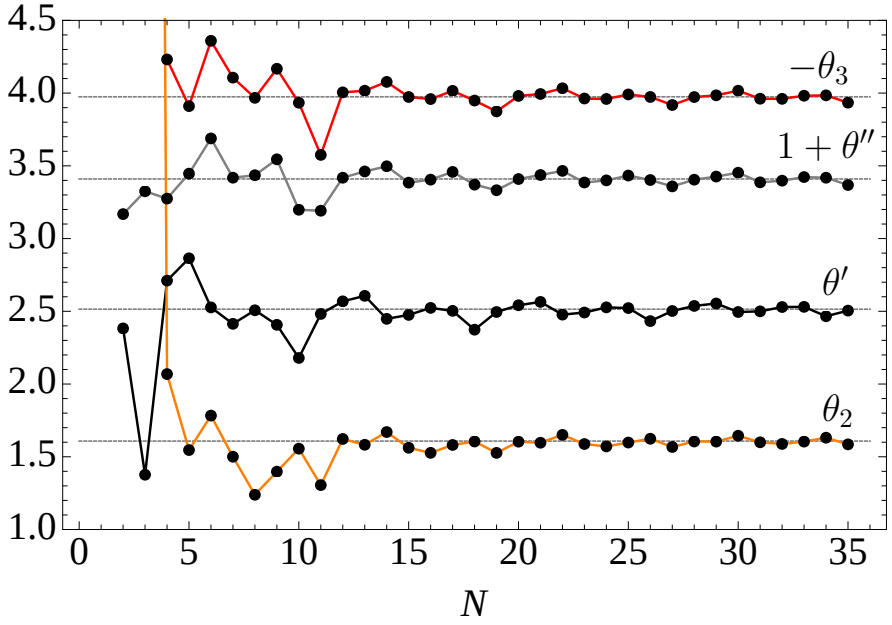

Figure 4.5: The convergence of the first four exponents $\theta = \theta' \pm i\theta''$, θ_2 and θ_3, showing θ' (blue line), $1+\theta''$ (red line), θ_2 (yellow line) and $-\theta_3$ (green) together with their mean values (straight line).

Since $\mathbb{M}$ is in general a non-symmetric matrix some of its eigenvalues may become a complex conjugate pair. At the asymptotically safe fixed point, this happens for the leading and a few sub-leading eigenvalues. It is customary to discuss universality in terms of the critical scaling exponents θ_n, to which the eigenvalues relate as $\theta_n \equiv -\vartheta_n$. The results for the first few exponents are displayed in Figure 4.5 (see Table 4.3 for the numerical values). The leading exponent is a complex conjugate pair $\theta = \theta' \pm i\theta''$. Furthermore, only the first three exponents have a positive real part, whereas all other have a negative real part. From Figure 4.5 we notice that the exponents oscillate about their asymptotic values with an eight-fold periodicity and a decreasing amplitude. We estimate their asymptotic values from an average over an entire period (4.86), leading to the exponents

$$\begin{aligned} \langle\theta'\rangle &= 2.51 \quad \pm 1.2\% \\ \langle\theta''\rangle &= 2.41 \quad \pm 1.1\% \\ \langle\theta_2\rangle &= 1.61 \quad \pm 1.3\% \\ \langle\theta_3\rangle &= -3.97 \quad \pm 0.6\%\,. \end{aligned} \tag{4.96}$$

Here, the accuracy in the result has reached the percent level for the first two real and the first pair of complex conjugate eigenvalues. The error estimate (4.96) allows us to conclude that the ultraviolet fixed point has three relevant directions. The asymptotic estimates $\langle\theta'\rangle$, $\langle\theta''\rangle$ and $\langle\theta_3\rangle$ depend only mildly on whether the average is taken over all approximations, or only the highest ones, see Table 4.3. An exception to this is the exponent θ_2. The slow convergence of the underlying fixed point λ_2 has lead to a very large eigenvalue at the order $N = 3$. Although the eigenvalue rapidly decreases by a factor of nearly 20 with increasing N, its presence is responsible for the overall mean value to deviate by 40% from $\langle\theta_2\rangle$, (4.96), see Table 4.3. We therefore conclude that the large eigenvalue $\theta_2\,(N = 3)$ is unreliable and an artefact of the approximation $N = 3$.

4.6.5 Stability

Thus far we have identified fixed points and their eigenvalues by increasing the order of expansion one by one, achieving a coherent picture for a non-trivial UV fixed point. The stability in the fixed point coordinates with increasing order confirms that we have identified one and the same underlying fixed point at each order in the expansion. To clarify the role of higher-order couplings we perform the fixed point search at order N by using a one-parameter family of boundary conditions which are informed by the non-perturbative fixed point values (4.87), namely

$$\begin{aligned} \lambda_N &= \alpha \cdot \lambda_N^{\rm np} \\ \lambda_{N+1} &= \alpha \cdot \lambda_{N+1}^{\rm np}\,. \end{aligned} \tag{4.97}$$

Here, the numbers $\lambda^{\rm np}$ stand for the non-perturbative values of the higher order couplings which are not part of the RG dynamics at approximation order N. We thus use the asymptotic estimates (4.87) as input. The free parameter α is then used to interpolate between the boundary condition (4.97) ($\alpha = 0$) adopted initially to detect the fixed point, and the improved boundary condition where the higher order couplings are identified with the by-now known non-perturbative result ($\alpha = 1$). For notational simplicity, we refer to the approximation at order N with (4.97) as the 'N_α-approximation'. In this convention our results in Table 4.2 correspond to $N \equiv N_{\alpha=0}$.

From the point of view of the RG flow, the boundary condition (4.97) with $\alpha = 1$ means that we splice non-perturbative information originating from higher orders back into a smaller sub-system of relevant couplings. The boundary condition acts like a

'non-perturbative background' generated from irrelevant and non-dynamical higher-order couplings. Evidently, by virtue of the exact recursive relations amongst the fixed point couplings, we find that the fixed point coordinates in the approximation $N_{\alpha=1}$ are given by the asymptotic values (4.87). Hence, the primary effect of the non-perturbative boundary condition is to re-align the fixed point coordinates with those achieved asymptotically.

A secondary effect is the impact of the non-dynamical higher order couplings on the scaling exponents. We illustrate the quantitative effect of the latter for the case with three and four independent couplings, beginning with $N_{\alpha=0} = 3$ where the exponent θ_2 deviates substantially from the asymptotic value. Using the improved boundary condition as described above, we find for $N_{\alpha=1} = 3$ the scaling exponents

$$\begin{aligned} \theta' &= 3.0423 \\ \theta'' &= 2.0723 \\ \theta_2 &= 1.3893\,. \end{aligned} \tag{4.98}$$

This should be compared with the result for $N_{\alpha=0} = 3$, see Table 4.2. Most notably, the exponent θ_2 is vastly different from its value at $N_0 = 3$ and all three values (4.98) are now substantially closer to the asymptotic ones (4.96). Quantitatively, at order $N_0 = 3$ the exponents (θ', θ_2) differ from the asymptotic ones (4.96) by about $(50\%, 1700\%)$. This is reduced to $(15\%, 15\%)$ at order $N_{\alpha=1} = 3$, (4.98). The universal phase θ'' stays within 5% throughout. The remaining difference between (4.98) and (4.96) is due to the fact that the RG dynamics of higher order couplings is not taken into account in the former. Therefore, about 15% of the scaling exponents' values is attributed to the dynamics of all higher order interactions. Conversely, about 85% of their values is due to the dynamics of the three lowest, in conjunction with the non-dynamical higher order couplings.

Turning to the approximation $N_{\alpha=1} = 4$, we find

$$\begin{aligned} \theta' &= 2.9010 \\ \theta'' &= 2.3042 \\ \theta_2 &= 1.8336 \\ \theta_3 &= -2.9824\,. \end{aligned} \tag{4.99}$$

It is very encouraging that the dynamical effect of the higher-order interactions only leads to a comparatively small quantitative shift, without affecting the qualitative result. The result (4.98) also establishes that the fixed point of the system is already carried by a low-order approximation. This pattern persists to higher N.

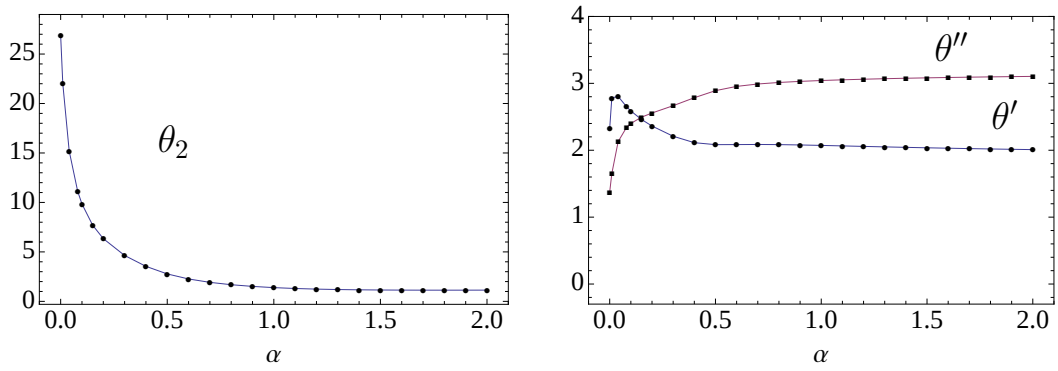

Figure 4.6: Stability of the fixed point for R^2 gravity, shown in terms of the critical exponents $\theta_2(\alpha)$ (left panel) and $\theta'(\alpha)$, $\theta''(\alpha)$ (right panel) as functions of α. The curves smoothly interpolate between Table 4.4 ($\alpha = 0$) and (4.98) ($\alpha = 1$). The dependence on α becomes very weak already around $\alpha \approx 1$.

4.6.6 Continuity

At low order in the approximation order N, in particular at $N = 3$, the coordinates and scaling exponents deviate more strongly from their asymptotic value. This raises questions as to whether these solutions are spurious rather than images of the physical fixed point, and whether there are ways of improving the low-order results. To answer this question, we assess the continuity of our results subject to the boundary condition. We vary α over some range, $0 \leq \alpha \leq 2$ to understand how strongly the scaling exponents are affected by the boundary condition. Our results to order $N = 3$ in the approximation are given in Figure 4.6. We note that all three exponents vary strongly with α close to the boundary condition (4.38), $\alpha < 1/2$. Furthermore, the result establishes that the fixed point at order $N_{\alpha=0} = 3$ is continuously connected with the result $N_{\alpha=1} = 3$. Most importantly, we also find that the relative variations with α are small,

$$\frac{\partial \ln \theta'}{\partial \ln \alpha} \approx -0.0339\,, \qquad \frac{\partial \ln \theta''}{\partial \ln \alpha} \approx 0.0383\,, \qquad \frac{\partial \ln \theta_2}{\partial \ln \alpha} \approx -0.761\,, \tag{4.100}$$

once α is of order unity. We therefore conclude that imposing non-perturbative boundary conditions, provided they are available, improves the dynamical result at low orders. The corresponding results for $N = 4$ are shown in Figure 4.7. We note that the fixed point coordinates depend weakly on α. In addition, the universal eigenvalues show a weak and smooth dependence on α, and the value $\alpha = 1$ is not distinguished. We conclude that the fixed point is stable under variations of the boundary condition imposed on the higher order couplings.

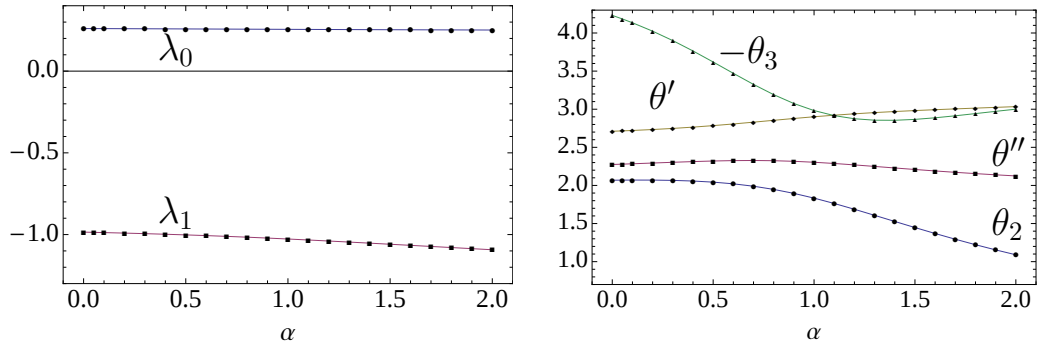

Figure 4.7: Stability of the fixed point for R^3 gravity, showing the coordinates (left panel) and the exponents (right panel) as functions of α. The result smoothly interpolates between the data in Table 4.4 ($\alpha = 0$) and (4.99) ($\alpha = 1$). Note that the dependence on α becomes very weak already around $\alpha \approx 1$.

4.6.7 De Sitter solutions

We finally turn to the possibility of de Sitter solutions to the $F(R)$ equations of motion, which is of relevance for cosmological scenarios with inflation. De Sitter solutions correspond to values of the dimensionless scalar curvature $\rho = \rho_0$ which satisfy

$$\rho f'(\rho) - 2f(\rho)\big|_{\rho=\rho_0} = 0\,. \tag{4.101}$$

We can look for solutions to (4.101) at each order N in the approximation by plotting the LHS of the equation and looking for zeros. Interestingly, solutions to (4.101) can be found at some orders in the approximation. These may be considered as physical provided they occur within the radius of convergence of the expansion, and persist to high orders in the expansion.

We can use the same technique as before to calculate the radius of convergence from the LHS of (4.101). However since ρ^2 is a zero mode of (4.101) there will be no terms proportional to ρ^2 and therefore we take $n \geq 3$ when determining $\rho_c(m) \equiv \min_n[\rho_{c,m}(n)]$ and average m over values $8 \leq m \leq 31$. Using this method we obtain $\rho_c \approx 0.77 \pm 5\%$ which is less than the value obtained from $f(\rho)$. The reason for this is that the equation of motion contains a derivative of $f(\rho)$ and is therefore more sensitive to the approximation. We find that de Sitter solutions only occur within the radius of convergence at low orders in the approximation, without persisting to higher orders. For example at orders $N = 10$ and $N = 11$ de Sitter solutions were found previously at $\rho_0 \approx 0.758$ and $\rho_0 \approx 0.769$ [22], but at order $N = 12$ no de Sitter solution is found within the radius of convergence. We

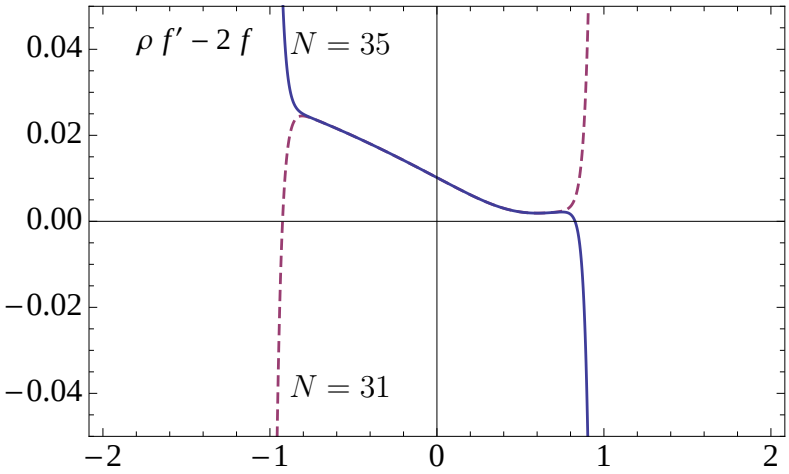

Figure 4.8: The equation of motion (4.101) to order $N = 35$ (full line) and $N = 31$ (dashed line) in the polynomial approximation.

conclude that there are no de Sitter solutions of the fixed point action $f^*(\rho)$ within the radius of convergence of a polynomial approximation.

It may be possible that de Sitter solutions exist outside the radius ρ_c but within the region for which a numerical (non-polynomial) solution exists. However, we conclude that a de Sitter solution in the fixed point regime at small R/k^2 is absent. This implies that a de Sitter phase with inflationary expansion during the fixed point regime of $f(R)$ gravity may require large curvature.

4.7 Canonical power counting

In a theory with a gaussian (non-interacting) UV fixed point, such as QCD, one can use the canonical power counting method to determine if an operator is relevant, marginal or irrelevant just by reading its canonical mass dimension. However, when a theory exhibits a non-trivial (interacting) UV fixed point, there is no a-priori guiding principle in order to determine what operators are relevant, marginal or irrelevant. One would expect that the interactions at the UV fixed point could alter the ordering of the operators and as discussed in Chapter 1 this could spoil the predictive power of the theory and consequently the asymptotic safety scenario for gravity. In this section we are going to use the results of our calculation in order to examine the spectrum of the operators.

We start by recalling the argument by Weinberg [148] presented in Chapter 1. Suppose

that we have an effective average action of the form

$$\Gamma_k = \sum_i \int d^4x \, \bar{\lambda}_i \, \mathcal{O}_i \tag{4.102}$$

in terms of the operators $\mathcal{O}_i$ and of the dimensionfull couplings $\bar{\lambda}_i$. Then we switch to dimensionless couplings λ_i with mass dimension $[d_i]$ and the corresponding mass dimension of the operators being $[\mathcal{O}_i] = 4-2n$, where $2n$ denotes the number of derivatives contained in $\mathcal{O}_i$. The form of the beta functions for the dimensionless couplings then becomes

$$\beta_i = -d_i \, \lambda_i + \text{quantum corrections}. \tag{4.103}$$

If the quantum corrections are absent, as would be in a gaussian fixed point (the case of QCD), then the eigenvalues of the stability matrix $\mathbb{M}$ are simply given by the canonical mass dimensions of the couplings

$$\vartheta_{G,n} = 2n - 4. \tag{4.104}$$

In $4d$ gravity, only the cosmological constant and Newton's coupling are relevant which follows directly from dimensional analysis. Terms involving four derivatives such as R^2, $\Box R$, $R_{\mu\nu}R^{\mu\nu}$ or $R_{\mu\nu\rho\sigma}R^{\mu\nu\rho\sigma}$ are marginal, and those involving more than four derivatives such as R^n $(n \geq 2)$ or the seminal Goroff-Sagnotti term $R_{\mu\nu}{}^{\rho\sigma}R_{\rho\sigma}{}^{\lambda\tau}R_{\lambda\tau}{}^{\mu\nu}$ are perturbatively irrelevant and their Gaussian eigenvalues (4.106) increase strongly with the number of derivatives.

Including quantum corrections, the eigenvalue spectrum at a non-trivial fixed point is modified. It is conceivable that some of the eigenvalues (4.106) may change sign due to interactions, which would be in accord with the asymptotic safety scenario provided that the set of negative eigenvalues remains finite. On the other hand, a fixed point theory would lose its predictive power if the eigenvalues of infinitely many couplings changed their sign due to quantum corrections. This would require substantial corrections to infinitely many eigenvalues, nearly all of which need to be very large and with the opposite sign.

We can now proceed to analyse our results from $f(R)$ gravity and to make quantitative observations regarding the departure from gaussianity. We start with the two sets of universal eigenvalues that we intend to compare. First, at order N of the approximation we have N universal eigenvalues corresponding to each coupling

$$\{\vartheta_n(N), \qquad 0 \leq n \leq N-1\}\,. \tag{4.105}$$

The second set of eigenvalues corresponds to the gaussian values that we would have provided that $f(R)$ gravity exhibits a non-interacting fixed point. These would be

$$\{\vartheta_{G,n}(N) = 2n-4, \qquad 0 \leq n \leq N-1\}\,. \tag{4.106}$$

These eigenvalues are ordered by the number n of derivatives at each operator. Our task is to find an ordering principle for the non-gaussian eigenvalues ϑ_n in order to compare the two sets.

In our study for the critical exponents we find, occasionally, pairs of complex conjugate eigenvalues. These complex exponents have been found in a number of studies and they are coming from the fact that the stability matrix $\mathbb{M}$, defined in (1.9), is in general real but not symmetric. Complex eigenvalues are an indication for a degeneracy in the scaling behaviour of the system. The degeneracy is induced by interactions, leading to large off-diagonal terms in the stability matrix. As a consequence, the scaling of operators becomes entangled and can no longer be distinguished, leading to complex exponents. It is possible that these degeneracies are lifted by the inclusion of other terms, that the $f(R)$ approximation neglects, such as Weyl interactions or ghost interactions [16].

In any case, what determines if an operator is relevant, marginal, or irrelevant is the real part of the eigenvalue, as can be deduced from equation (1.10). Therefore we order the non-gaussian eigenvalues (4.105) according to the size of their real part

$$\mathrm{Re}\,\vartheta_n(N) < \mathrm{Re}\,\vartheta_{n+1}(N)\,. \tag{4.107}$$

When the largest eigenvalue at fixed approximation order is a complex conjugate pair, it is numerically more unstable, while when it is real its value is much more reliable. For this, in Figure 4.9 we plot the largest real eigenvalue at each order of the approximation, which we denote as

$$\vartheta_{\max}(N) = \max_n \vartheta_n(N)\,. \tag{4.108}$$

The view taken here is that the largest real eigenvalue ϑ at order N is the leading order approximation to the full eigenvalue ϑ_n, where $n = N-1$. Increasing the order from $N-1$ to N, the set of eigenvalues (4.105) of the new fixed point solution will contain a new largest real eigenvalue $\vartheta_{\max}(N)$. It arises mainly through the addition of the invariant $\int \sqrt{\det g_{\mu\nu}} R^{N-1}$. We wish to compare this eigenvalue with the largest eigenvalue within (4.106) in the absence of fluctuations, at the same order N,

$$\vartheta_{\mathrm{G},\max}(N) = 2(N-1) - 4\,. \tag{4.109}$$

In Fig. 4.9 we indicate (4.109) by the full line. For low values of N the largest real eigenvalue $\vartheta_{\max}(N)$ differs from its classical counterpart $\vartheta_{\mathrm{G},\max}(N)$. In particular the perturbatively marginal operator $\propto R^2$ becomes a relevant operator non-perturbatively. With increasing order N we approximately find

$$\frac{\vartheta_{\max}(N)}{\vartheta_{\mathrm{G},\max}(N)} \to 1 \quad \text{for} \quad 1/N \to 0\,. \tag{4.110}$$

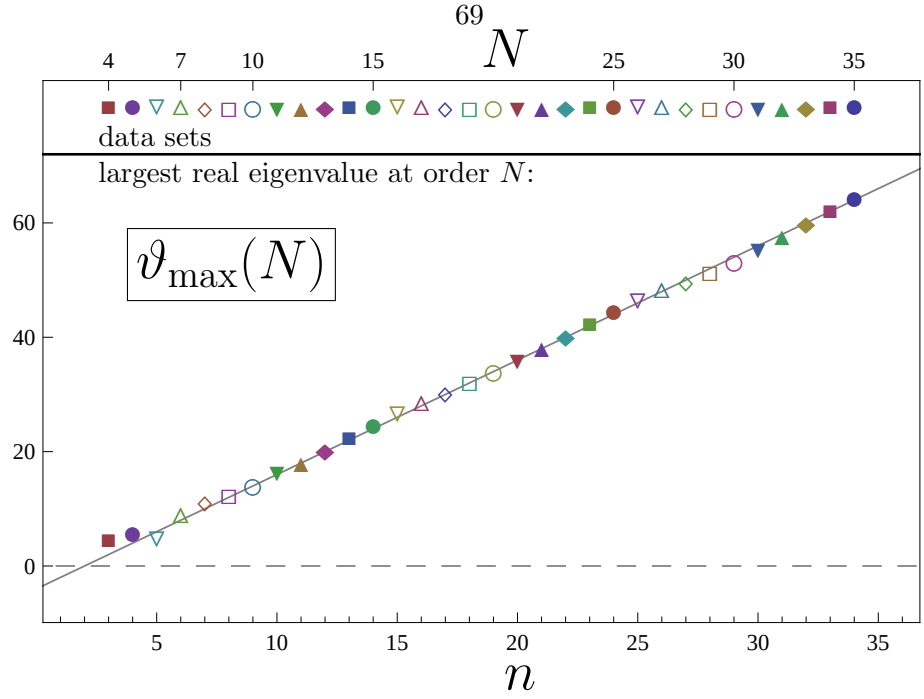

Figure 4.9: The largest real eigenvalue $\vartheta_{\max}(N)$ to order $N \geq 4$ in the expansion in comparison with the corresponding Gaussian exponent $\vartheta_{\mathrm{G,max}}(N) = 2(N-1)-4$ in the absence of fluctuations (full line). The lower panel shows our data points for all approximation orders $4 \leq N \leq 35$, and the lower axis shows $n = N-1$. The upper panel relates the symbols used in the lower panel to the approximation order N.

The significance of the result (4.110) is as follows. The addition of the invariant $\int \sqrt{g} R^N$ leads to the appearance of a new largest real eigenvalue $\vartheta_{\max}(N)$. The newly added interaction term also feeds into the lower order couplings and eigenvalues, and vice versa. The coupled system achieves a fixed point with $\vartheta_{\max}(N) \approx \vartheta_{\mathrm{G}}(N)$ for all N (provided N is not too small), stating that the UV scaling of invariants with a large canonical mass dimension becomes mainly Gaussian, even in the vicinity of an interacting fixed point.

It remains to establish the stability of this pattern under the inclusion of further interactions. This is assessed through a term-by-term comparison of the asymptotically safe set of eigenvalues (4.105) retaining the complex conjugate pairs of eigenvalues, and the Gaussian set (4.106), to sufficiently high order N in the approximation, see Table 4.4. The data in Fig. 4.10 is complementary to Fig. 4.9 in that it shows how the eigenvalue distribution has evolved under the inclusion of further invariants. The result states that the eigenvalue $\vartheta_{\max}(n)$, the n^{th} largest real eigenvalue at the order $N = n+1$ in the expansion (4.35), is already a good approximation to the full n^{th} eigenvalue $\vartheta_n(N)$ at a higher order in the expansion $N > n+1$. The latter is fuelled by $(N-n-1)$ additional operators in the effective action. Collecting all data from the values of the critical exponents into

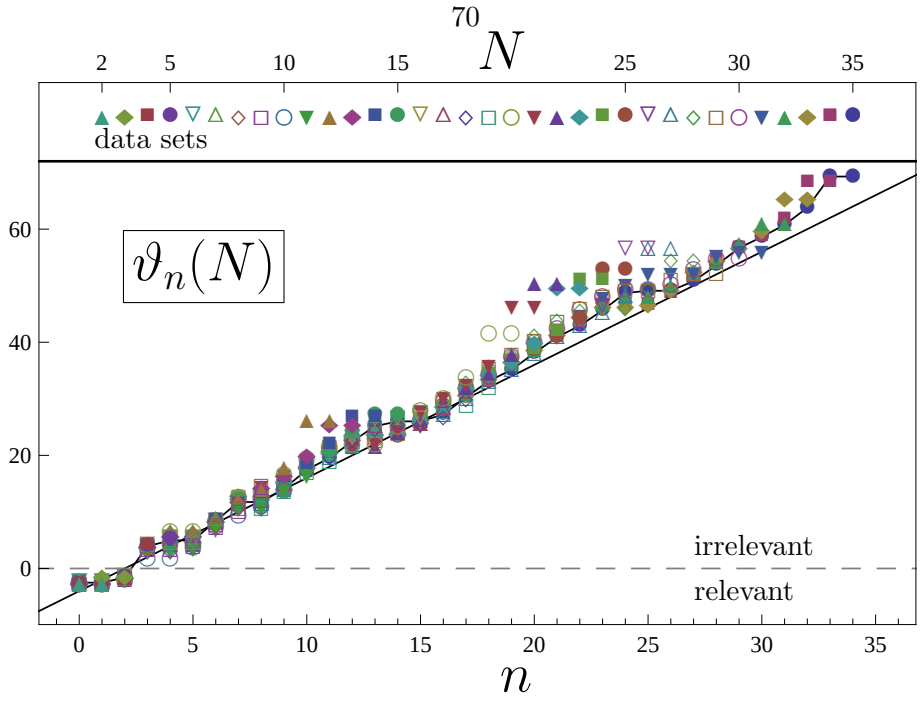

Figure 4.10: The overlay of all data sets for the universal scaling exponents $\vartheta_n(N)$ for $2 \leq N \leq 35$. The straight full line denotes Gaussian exponents. The exponents at $N = 35$ are connected by a line, to guide the eye. The upper panel relates the symbols used in the lower panel to the approximation order N.

Figure 4.10, we find that the eigenvalues ϑ_n vary by about 20% due to the inclusion of higher order invariants with $N > n + 1$. Furthermore, Figure 4.10 also confirms the good numerical convergence of exponents for all n. As already noted earlier, the largest deviations from the best estimate ($N = 35$) arise provided the largest eigenvalues are a complex conjugate pair. A quantitative estimate for the deviation from Gaussian behaviour is given in Fig. 4.11, where the relative deviation $|\vartheta_n - \vartheta_{G,n}|/\vartheta_{G,n}$ is computed. Asymptotically, our results suggest that

$$\frac{\mathrm{Re}\,\vartheta_n(N)}{\vartheta_{\mathrm{G},n}} \to 1 \quad \text{for} \quad n \to \infty \tag{4.111}$$

for approximations including up to $N = 35$. Clearly, the large eigenvalues only differ mildly from the Gaussian ones.

To conclude, the qualitative, and largely even quantitative, similarity of Figure 4.9 and Figure 4.10 establishes the stability of the results (4.110) and (4.111) under increasing orders in the polynomial expansion. In this light, the main effect of asymptotically safe interactions is to induce a shift away from Gaussian eigenvalues

$$\vartheta_{\mathrm{G},n} \to \vartheta_n = \vartheta_{\mathrm{G},n} + \Delta_n\,, \tag{4.112}$$

thereby generating in the UV precisely one further relevant eigenvalue in the spectrum by

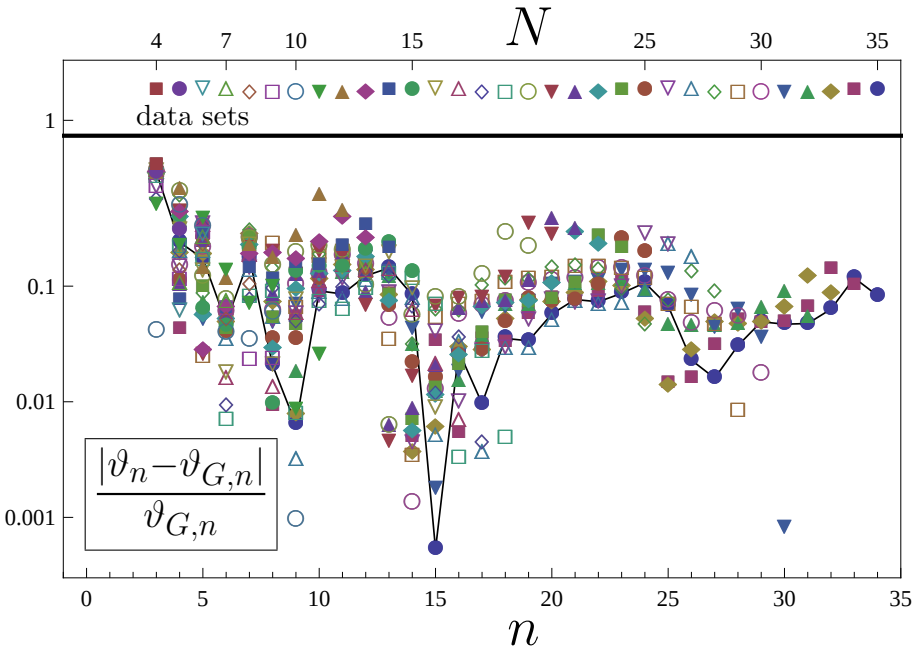

Figure 4.11: The relative variation of the non-perturbative scaling exponents $\vartheta_n(N)$ in comparison with the Gaussian ones $\vartheta_{G,n}$. The lower panel shows the data points for all approximation orders $4 \leq N \leq 35$. The thin line connects the data in the highest order approximation ($N = 35$) to guide the eye. The upper panel relates the symbols used in the lower panel to the approximation order N.

turning a marginal eigenvalue into a relevant one, i.e. $\vartheta_2 = \Delta_2 < 0$. Also, the interaction-induced shifts Δ_n come out bounded, with $\Delta_n/\vartheta_n \sim \Delta_n/n \to 0$ for $1/n \to 0$. The eigenvalue distribution approaches Gaussian scaling with increasing canonical dimension, despite the fact that the underlying theory displays an interacting fixed point. Note also that the non-perturbative shifts Δ_n are mostly positive once $n > 5$, meaning that the asymptotically safe interactions generate scaling operators which are more irrelevant than their perturbative counterparts. Interestingly, this structure is more than what is needed to ensure an asymptotic safety scenario. It is then conceivable that asymptotic safety persists under the inclusion of further curvature invariants beyond those studied here.

4.8 Summary

In this chapter we investigated the properties of $F(R)$ quantum gravity using renormalisation group techniques with the aim to test the asymptotic safety conjecture. We adopted a bootstrap approach and we systematically found a self-consistent fixed point and three

negative eigenvalues for every order in the polynomial expansion up to $N_{\max} = 35$. We also investigated the ordering principle for critical exponents based on the observation that curvature invariants become increasingly irrelevant with increasing mass dimension.

In the results that we presented, fixed point values showed a remarkable convergence towards their asymptotic values with particularly small statistical errors, especially for the case of λ_0 and λ_1. A notable exception of this pattern concerns the coupling λ_2 of the marginal operator R^2. This coupling has much larger statistical fluctuations and much smaller convergence rate, associated with the fact that it is the only marginal operator of the theory. For all the quantities that were examined we observed for the first time an 8-fold periodicity of the results and speculated that this is coming due to singularities in the complex plane of the polynomial expansion. We also estimated the radius of convergence for the function $f(\rho)$ and concluded that there are no de-Sitter solutions within. Moreover, we examined the dependence of our results to the specific boundary conditions that we choose in order to solve the fixed point equation and found that these modifications are unimportant. This suggests that the inclusion of higher order operators and consequently the modification of the boundary conditions, have little effect on low order quantities.

Next we turned our attention to the evaluation of the critical exponents. In support of the asymptotic safety scenario, we consistently find in every order of the approximation three negative eigenvalues. The stability properties of all the eigenvalues were examined with the three negative ones showing very good rate of convergence. Here, we observe again the 8-fold periodicity in the quantities that we studied. Taking advantage of the large data set that the calculation up to $N_{\max}$ provides us, we sorted all the eigenvalues at every order of the approximation according to the value of their real part. Then we made the important observation that the highest real eigenvalue at every N takes a value extremely close to the gaussian line and that after including the contributions from all the higher operators they stabilise very close to that line. This result provides strong evidence in favour of the asymptotic safety conjecture by Weinberg [148] since it shows that the fluctuations induced by quantum interactions are not altering dramatically the canonical scaling of the operators and consequently they do not show evidence that infinitely many critical exponents can turn negative in order to spoil the predictive power of the theory.

N	g_*	λ_*	$g_* \times \lambda_*$	$10 \times \lambda_2$	θ'	θ''	θ_2	θ_3
2	0.98417	0.12927	0.12722		2.3824	2.1682		
3	1.5633	0.12936	0.20222	0.7612	1.3765	2.3250	26.862	
4	1.0152	0.13227	0.13429	0.3528	2.7108	2.2747	2.0684	−4.2313
5	0.96644	0.12289	0.11876	0.1359	2.8643	2.4463	1.5462	−3.9106
6	0.96864	0.12346	0.11959	0.1353	2.5267	2.6884	1.7830	−4.3594
7	0.95832	0.12165	0.11658	0.07105	2.4139	2.4184	1.5003	−4.1063
8	0.94876	0.12023	0.11407	−0.01693	2.5070	2.4354	1.2387	−3.9674
9	0.95887	0.12210	0.11707	0.04406	2.4071	2.5448	1.3975	−4.1673
10	0.97160	0.12421	0.12069	0.1356	2.1792	2.1981	1.5558	−3.9338
11	0.97187	0.12429	0.12079	0.1354	2.4818	2.1913	1.3053	−3.5750
12	0.97329	0.12431	0.12099	0.1604	2.5684	2.4183	1.6224	−4.0050
13	0.97056	0.12386	0.12021	0.1420	2.6062	2.4614	1.5823	−4.0163
14	0.97165	0.12407	0.12055	0.1474	2.4482	2.4970	1.6699	−4.0770
15	0.96998	0.12378	0.12006	0.1369	2.4751	2.3844	1.5618	−3.9733
16	0.96921	0.12367	0.11987	0.1301	2.5234	2.4051	1.5269	−3.9590
17	0.97106	0.12402	0.12043	0.1398	2.5030	2.4582	1.5811	−4.0154
18	0.97285	0.12433	0.12096	0.1509	2.3736	2.3706	1.6051	−3.9487
19	0.97263	0.12430	0.12090	0.1490	2.4952	2.3323	1.5266	−3.8741
20	0.97285	0.12427	0.12090	0.1551	2.5415	2.4093	1.6038	−3.9805
21	0.97222	0.12417	0.12073	0.1504	2.5646	2.4370	1.5965	−3.9938
22	0.97277	0.12428	0.12089	0.1532	2.4772	2.4653	1.6506	−4.0332
23	0.97222	0.12418	0.12073	0.1498	2.4916	2.3853	1.5876	−3.9629
24	0.97191	0.12414	0.12065	0.1472	2.5271	2.3999	1.5711	−3.9596
25	0.97254	0.12426	0.12084	0.1503	2.5222	2.4334	1.5977	−3.9908
26	0.97335	0.12440	0.12109	0.1551	2.4328	2.4025	1.6237	−3.9734
27	0.97318	0.12437	0.12104	0.1539	2.5021	2.3587	1.5673	−3.9182
28	0.97329	0.12436	0.12104	0.1568	2.5370	2.4047	1.6050	−3.9728
29	0.97305	0.12432	0.12097	0.1549	2.5537	2.4262	1.6044	−3.9849
30	0.97337	0.12438	0.12107	0.1565	2.4951	2.4527	1.6446	−4.0165
31	0.97310	0.12434	0.12099	0.1549	2.4997	2.3865	1.5995	−3.9614
32	0.97291	0.12431	0.12094	0.1534	2.5294	2.3980	1.5882	−3.9606
33	0.97319	0.12437	0.12103	0.1547	2.5306	2.4228	1.6042	−3.9819
34	0.97367	0.12445	0.12117	0.1574	2.4660	2.4183	1.6311	−3.9846
35	0.97356	0.12443	0.12114	0.1567	2.5047	2.3682	1.5853	−3.9342
mean (all)	0.98958	0.12444	0.12320	0.1580	2.4711	2.3996	2.3513	−3.9915
mean (cycle)	0.97327	0.12437	0.12105	0.1557	2.5145	2.4097	1.6078	−3.9746
st. dev. (%)	0.02668	0.04025	0.06673	0.89727	1.122	1.085	1.265	0.603

Table 4.3: The fixed point values for the dimensionless Newton coupling g_*, the dimensionless cosmological constant λ_*, the R^2 coupling λ_2, the universal product $\lambda \cdot g$, and the first four exponents to various orders in the expansion, including their mean values and standard deviations.

		asymptotically safe fixed point					
eigenvalues	Gauss	$N = 35$	31	23	15	11	7
ϑ_0	-4	-2.5047	-2.4997	-2.4916	-2.4751	-2.4818	-2.4139
ϑ_1	-2	-2.5047	-2.4997	-2.4916	-2.4751	-2.4818	-2.4139
ϑ_2	0	-1.5853	-1.5995	-1.5876	-1.5618	-1.3053	-1.5003
ϑ_3	2	3.9342	3.9614	3.9629	3.9733	3.0677	4.1063
ϑ_4	4	4.9587	5.6742	5.6517	5.6176	3.0677	4.4184
ϑ_5	6	4.9587	5.6742	5.6517	5.6176	3.5750	4.4184
ϑ_6	8	8.3881	8.4783	8.4347	8.3587	6.8647	8.5827
ϑ_7	10	11.752	12.605	12.366	12.114	10.745	
ϑ_8	12	11.752	12.605	12.366	12.114	10.745	
ϑ_9	14	14.089	15.014	15.384	15.867	13.874	
ϑ_{10}	16	17.456	17.959	18.127	18.336	16.434	
ϑ_{11}	18	19.540	20.428	20.510	20.616		
ϑ_{12}	20	22.457	23.713	23.686	24.137		
ϑ_{13}	22	25.158	25.087	23.686	27.196		
ϑ_{14}	24	26.014	25.087	23.862	27.196		
ϑ_{15}	26	26.014	26.048	26.311			
ϑ_{16}	28	27.235	28.534	28.734			
ϑ_{17}	30	30.289	31.848	32.045			
ϑ_{18}	32	33.131	34.205	34.361			
ϑ_{19}	34	35.145	36.606	36.629			
ϑ_{20}	36	38.069	39.876	40.008			
ϑ_{21}	38	40.914	42.258	49.675			
ϑ_{22}	40	42.928	44.707	49.675			
ϑ_{23}	42	45.640	48.011				
ϑ_{24}	44	48.708	50.248				
ϑ_{25}	46	49.101	52.159				
ϑ_{26}	48	49.101	52.159				
ϑ_{27}	50	50.800	52.291				
ϑ_{28}	52	53.591	55.422				
ϑ_{29}	54	56.658	56.048				
ϑ_{30}	56	58.625	56.048				
ϑ_{31}	58	60.755					
ϑ_{32}	60	63.796					
ϑ_{33}	62	69.299					
ϑ_{34}	64	69.299					

Table 4.4: The large-order behaviour of asymptotically safe eigenvalues for a selection of orders N in the polynomial expansion, in comparison with the Gaussian eigenvalues. If the eigenvalues are a complex conjugate pair, only the real part is given.

Chapter 5

The $f(R^{\mu\nu}R_{\mu\nu})$ approximation

5.1 Introduction

The investigation of the $f(R)$ approximation has revealed a very encouraging and stable picture in support of asymptotic safety scenario. A polynomial expansion in powers of R was performed and the requirements for asymptotic safety were checked to hold true for every order in the approximation up to $N_{\max} = 35$. An intriguing open question is how this picture is affected by the inclusion of more complicated tensor structures, such as the Ricci tensor $R_{\mu\nu}$.

Previous research in this direction was concentrated on the inclusion of a single Weyl squared term [16, 17] where a UV fixed point and three real negative eigenvalues were reported. This is a special case in the sense that properties of Euler's topologically invariant can be used in order to factor the second variation in terms of Lichnerowicz operators. This allows for the use of a generic compact Einstein background which permits the differentiation between the Ricci scalar and the Riemann tensor in the flow equation. When one tries to go beyond this approximation these properties do not hold true and it is required that the background metric is chosen to be a sphere. However, dynamics of more complicated tensor structures can be taken into account through the second variation even when we project on the maximally symmetric background.

In this chapter we investigate the renormalisation group flow when we consider the inclusion in the gravitational approximation of terms with powers of the Ricci curvature squared

$$\sim R^{\mu\nu}R_{\mu\nu}\,. \tag{5.1}$$

Ricci curvature tensor encodes more dynamics than Ricci scalar due to its non-trivial index structure. With this inclusion we expect to capture in the renormalisation group equation

the effects that these dynamics have. Since we project on the sphere we have to make sure that for each mass dimension we have only one term. With increasing mass dimension there is a growing number of candidate terms. For example using Ricci curvature tensor and Ricci scalar with total mass dimension $[d] = 6$ we can form the invariants $R_{\mu\nu}R^{\mu}_{\alpha}R^{\alpha\nu}$ and $R\,R_{\mu\nu}R^{\mu\nu}$. Among the various possibilities we choose those terms that are pure powers of Ricci curvature squared and those that are coupled with a single power of the Ricci scalar. Therefore, we are interested in an expansion of the form

$$\bar{\Gamma}_k[g] = \int d^dx\sqrt{g}\left\{\ \lambda_0 + \lambda_1 R + \lambda_2 R^{\mu\nu}R_{\mu\nu} + \lambda_3 R\,R^{\mu\nu}R_{\mu\nu} + \lambda_4 R_{\mu\nu}R^{\mu\nu}R_{\alpha\beta}R^{\alpha\beta} + \dots\right\} \tag{5.2}$$

With this ansatz we capture the leading order contributions of the Ricci tensor as these are encoded in the second variation. It turns out that it is more efficient for our calculation to consider two general functions of Ricci curvature squared with one of them coupled to the Ricci scalar

$$\bar{\Gamma}_k[g] = \int d^dx\sqrt{g}\left\{F_k(R_{\mu\nu}R^{\mu\nu}) + R\,Z_k(R_{\mu\nu}R^{\mu\nu})\right\}. \tag{5.3}$$

The result is a renormalisation group flow for the two functions F_k and Z_k in a closed form similarly to the case of $f(R)$. To analyse the UV properties of this system we perform a series expansion in powers of R. We find that a self-consistent UV fixed point exists for every step of the approximation up to order $N_{\max} = 7$. Moreover the critical exponents are computed up to the same order and it is found that the number of attractive directions is always three. These findings are in qualitative agreement with the previous analysis of $f(R)$ quantum gravity and provide evidence that the inclusion of more complicated tensor structures do not have the tendency to invalidate the requirements of asymptotic safety.

The rest of this chapter is organised as follows. In Section 5.2 we compute the Hessians for our gravitational ansatz and we derive the Hessians for the effective average action taking into account the contributions of the gauge fixing action, the ghost fields and the auxiliary fields as were calculated in Chapter 3. In Section 5.3 we compute the flow equation for the effective average action using the general techniques and the algorithm of Chapter 3. In Section 5.4 we present our results for the fixed points and the critical exponents for the first 6 orders of the approximation and in Section 5.5 we sum up with our conclusions.

5.2 Deriving the Hessians

Here we are going to use exactly the same methods as before in order to derive the Hessians for all the fields that contribute to our ansatz. As explained in 2.3.2 the effective average action takes the form

$$\Gamma_k[g,\bar{g},c,\bar{c}] = \bar{\Gamma}_k[g] + S_{\rm gf}[h;\bar{g}] + S_{\rm gh}[h,c,\bar{c};\bar{g}]. \tag{5.4}$$

For the gauge fixing part and the ghost part there are no modifications compared to the case of $f(R)$. The corresponding Hessians were computed in Chapter 3 and are given in 3.2.2 for the gauge fixing and in 3.2.3 for the ghost part. The missing element is the computation of the second variation for the gravitational part.

5.2.1 The gravity part

Following the discussion in 5.1 we will choose our approximation ansatz for the gravitational effective average action to be formed by two functions of the Ricci squared term, with one of them multiplied by the Ricci scalar for mass dimension consistency. Then we have

$$\bar{\Gamma}_k[g] = \int \sqrt{g}\left(F_k(R_{\mu\nu}R^{\mu\nu}) + R\, Z_k(R_{\mu\nu}R^{\mu\nu})\right), \tag{5.5}$$

where we have defined our two functions $F_k(R_{\mu\nu}R^{\mu\nu})$ and $Z_k(R_{\mu\nu}R^{\mu\nu})$. As was argued in 5.1 this is a good leading order approximation for the addition to the effective average action of more complicated tensor structures with non-trivial dynamics. In order to compute the Hessians and evaluate the flow equation we need to know $\Gamma_k^{(2)}$ as it is defined in (2.27). We proceed the same way as with the $f(R)$ and we make an expansion the gravitational part $\bar{\Gamma}_k[g]$ as

$$\bar{\Gamma}_k[\bar{g}+\bar{h};\bar{g}] = \bar{\Gamma}_k[\bar{g};\bar{g}] + \mathcal{O}(h) + \frac{1}{2}\bar{\Gamma}_k^{\rm quad}[\bar{g}+\bar{h};\bar{g}] + \mathcal{O}(h^3). \tag{5.6}$$

and then applying (2.27) in order to extract the quadratic part. Then the quadratic part takes the form

$$\begin{aligned}\bar{\Gamma}_k^{\rm quad} = \int & \delta^{(2)}(\sqrt{g})\left[F_k + R\, Z_k\right] + 2\delta(\sqrt{g})\delta(R_{\mu\nu}R^{\mu\nu})\left[F_k' + R\, Z_k'\right] \\ & + \sqrt{g}\left[\delta(R_{\mu\nu}R^{\mu\nu})\right]^2\left[F_k'' + R\, Z_k''\right] + \sqrt{g}\delta^{(2)}(R_{\mu\nu}R^{\mu\nu})\left[F_k' + R\, Z_k'\right] \\ & + \sqrt{g}\delta^{(2)}(R)\, Z_k + 2\delta(\sqrt{g})\delta(R)\, Z_k + 2\sqrt{g}\delta(R)\delta(R_{\mu\nu}R^{\mu\nu})Z_k',\end{aligned} \tag{5.7}$$

where all the geometric quantities of the above equation are constructed from the background metric. Moreover it is understood from now on that $F_k \to F_k(R_{\mu\nu}R^{\mu\nu})$ as well as

$Z_k \to Z_k(R_{\mu\nu}R^{\mu\nu})$ and that the primes denote derivatives with respect to the argument. Using the expressions in the Appendix A we find that the quadratic part takes the form

$$
\begin{aligned}
\bar{\Gamma}_k^{\rm quad} = \int \sqrt{g}\, h_{\mu\nu} \Bigg\{ & \frac{1}{2}(F_k' + R\, Z_k')\nabla^4 + \left[\frac{d-3}{d-1}\frac{R}{d}(F_k' + R\, Z_k') + \frac{1}{2}Z_k\right]\nabla^2 \\
& + 2\frac{d^2-3d+3}{(d-1)^2}\frac{R^2}{d^2}(F_k' + R\, Z_k') - \frac{1}{2}F_k \Bigg\} h^{\mu\nu} \\
+ \sqrt{g}\, h \Bigg\{ & \left[\frac{1}{2}(F_k' + R\, Z_k') + 4\frac{R}{d}\left(\frac{R}{d}F_k'' + Z_k' + \frac{R^2}{d}Z_k''\right)\right]\nabla^4 \\
& + \left[-\frac{d-5}{2(d-1)}\frac{R}{d}(F_k' + R\, Z_k')\nabla^2 + 8\frac{R^2}{d^2}\left(\frac{R}{d}F_k'' + Z_k' + \frac{R^2}{d}Z_k''\right) - \frac{1}{2}Z_k\right]\nabla^2 \\
& - 2\frac{(d-2)^2}{(d-1)^2}\frac{R^2}{d^2}(F_k' + R\, Z_k') + 4\frac{R^3}{d^3}\left(\frac{R}{d}F_k'' + Z_k' + \frac{R^2}{d}Z_k''\right) \\
& + \frac{1}{4}(F_k + R\, Z_k) - \frac{d-2}{d-1}\frac{R}{d}\, Z_k \Bigg\} h \\
+ \sqrt{g}(\nabla^\mu\nabla^\nu h_{\mu\nu}) \Bigg\{ & \left[-(F_k' + R\, Z_k') - 8\frac{R}{d}\left(\frac{R}{d}F_k'' + Z_k' + \frac{R^2}{d}Z_k''\right)\right]\nabla^2 \\
& + 2\frac{R}{d}(F_k' + R\, Z_k') - 8\frac{R^2}{d^2}\left(\frac{R}{d}F_k'' + Z_k' + \frac{R^2}{d}Z_k''\right) + Z_k \Bigg\} h \\
+ \sqrt{g}(\nabla_\alpha h^{\alpha\beta}) & \left\{[F_k' + R\, Z_k']\nabla^2 + 3\frac{R}{d}(F_k' + R\, Z_k') + Z_k\right\}(\nabla^\mu h_{\mu\beta}) \\
+ (\nabla^\mu\nabla^\nu h_{\mu\nu}) & \left\{F_k' + R\, Z_k' + 4\frac{R}{d}\left(\frac{R}{d}F_k'' + Z_k' + \frac{R^2}{d}Z_k''\right)\right\}(\nabla^\alpha\nabla^\beta h_{\alpha\beta}).
\end{aligned}
\tag{5.8}
$$

As was the case also in the $f(R)$ approximation we use the metric field decomposition as defined in Section 3.2.1 and we find the Hessians in terms of each component field. These are given in Appendix A. Since the decomposition we perform is the same with the one for the $f(R)$ the auxiliary fields and their second variations are the same as before. These can be found in Section 3.2.4. In Table 5.1 we summarise the contribution from each individual component field after adding the contributions from the gauge fixing part, the ghost part and the auxiliary fields.

5.3 The flow equation

Having evaluated the second variation for our ansatz we are ready to continue and use the machinery developed in Chapter 3 and to compute the flow equation. As always we need to introduce dimensionless variables for the two functions that make up the effective average action. Note that after taking the second variation and before we compute the trace we evaluate all the expressions at the background metric, which we take to be a

$\phi_i\phi_j$	The matrix element of $\left(\Gamma_k^{(2)}\right)^{\phi_i\phi_j}$
$h^{T\mu\nu}h^T_{\mu\nu}$	$\frac{1}{2}(F'_k+R\,Z'_k)\Box^2+\left[\frac{1}{2}Z_k+\frac{R}{d}\frac{d-3}{d-1}(F'_k+R\,Z'_k)\right]\Box$ $+2\frac{R^2}{d^2}\frac{d^2-3d+3}{(d-1)^2}(F'_k+R\,Z'_k)-\frac{1}{2}(F_k+R\,Z_k)+\frac{d-2}{d(d-1)}R\,Z_k$
$\xi^\mu\xi_\mu$	$\frac{1}{\alpha}\Box^2+\left[\frac{2}{\alpha}\frac{R}{d}-4\frac{R^2}{d^2}(F'_k+R\,Z'_k)+F_k+R\,Z_k-2\frac{R}{d}Z_k\right]\Box$ $+\frac{1}{\alpha}\frac{R^2}{d^2}-4\frac{R^3}{d^3}(F'_k+R\,Z'_k)+\frac{R}{d}(F_k+R\,Z_k)-2\frac{R^2}{d^2}Z_k$
$\sigma\sigma$	$\left[\frac{1}{2}\frac{d-1}{d}(F'_k+R\,Z'_k)+4\frac{R}{d}\left(\frac{d-1}{d}\right)^2\left(Z'_k+\frac{R^2}{d}Z''_k+\frac{R}{d}F''_k\right)\right]\Box^4$ $+\left[-\frac{1}{\alpha}\left(\frac{d-1}{d}\right)^2-\frac{R}{d}\frac{d^2-10d+8}{2d^2}(F'_k+R\,Z'_k)+8\frac{R^2}{d^2}\frac{d-1}{d}\left(Z'_k+\frac{R^2}{d}Z''_k+\frac{R}{d}F''_k\right)-\frac{(d-1)(d-2)}{2d^2}Z_k\right]\Box^3$ $+\left[-\frac{2(d-1)}{\alpha}\frac{R}{d^2}+\frac{R^2}{d^2}\frac{d+2}{d}(F'_k+R\,Z'_k)+4\frac{R^3}{d^3}\left(Z'_k+\frac{R^2}{d}Z''_k+\frac{R}{d}F''_k\right)-\frac{1}{2}\frac{d-1}{d}(F_k+R\,Z_k)+\frac{1}{2}\frac{R}{d}Z_k\right]\Box^2$ $+\left[-\frac{1}{\alpha}\frac{R^2}{d^2}+2\frac{R^3}{d^3}(F'_k+R\,Z'_k)-\frac{1}{2}\frac{R}{d}(F_k+R\,Z_k)+\frac{R^2}{d^2}Z_k\right]\Box$
hh	$\left[\frac{d-1}{2d}(F'_k+R\,Z'_k)+4\frac{R}{d}\left(\frac{d-1}{d}\right)^2\left(Z'_k+\frac{R^2}{d}Z''_k+\frac{R}{d}F''_k\right)\right]\Box^2$ $+\left[-\frac{\rho^2}{\alpha}\frac{1}{d^2}-\frac{R}{d}\frac{d^2-10d+8}{2d^2}(F'_k+R\,Z'_k)+8\frac{R^2}{d^2}\frac{d-1}{d}\left(Z'_k+\frac{R^2}{d}Z''_k+\frac{R}{d}F''_k\right)-\frac{(d-1)(d-2)}{2d^2}Z_k\right]\Box$ $-2\frac{R^2}{d^2}\frac{d-3}{d}(F'_k+R\,Z'_k)+4\frac{R^3}{d^3}\left(Z'_k+\frac{R^2}{d}Z''_k+\frac{R}{d}F''_k\right)+\frac{d-2}{4d}(F_k+R\,Z_k)-\frac{R}{d}\frac{d-2}{d}Z_k$
$h\sigma$	$\left[-\frac{d-1}{d}(F'_k+R\,Z'_k)-8\frac{(d-1)^2}{d^3}R\left(Z'_k+\frac{R^2}{d}Z''_k+\frac{R}{d}F''_k\right)\right]\Box^3$ $+\left[\frac{\rho}{\alpha}\frac{2(d-1)}{d}+\frac{R}{d}\frac{d^2-10d+8}{d^2}(F'_k+R\,Z'_k)-16\frac{R^2}{d^2}\frac{d-1}{d}\left(Z'_k+\frac{R^2}{d}Z''_k+\frac{R}{d}F''_k\right)+\frac{(d-1)(d-2)}{d^2}Z_k\right]\Box^2$ $+\left[\frac{\rho}{\alpha}\frac{2R}{d^2}+2\frac{R^2}{d^2}\frac{d-4}{d}(F'_k+R\,Z'_k)-8\frac{R^3}{d^3}\left(Z'_k+\frac{R^2}{d}Z''_k+\frac{R}{d}F''_k\right)+\frac{R}{d}\frac{d-2}{d}Z_k\right]\Box$
$\bar{C}^T_\mu C^{T\mu}$	$-\sqrt{2}\Box-\sqrt{2}\frac{R}{d}$
$\bar{\eta}\eta$	$\frac{2\sqrt{2}}{d}\left[d-\rho-1\right]\Box^2+\frac{2\sqrt{2}}{d}R\Box$
$\bar{\lambda}\lambda$	$\left[1-\frac{1}{d}\right]\Box^2+\frac{R}{d}\Box$
$\omega\omega$	$\left[1-\frac{1}{d}\right]\Box^2+\frac{R}{d}\Box$
$\bar{c}^T_\mu c^{T\mu}$	$\Box+\frac{R}{d}$
$\zeta^T_\mu\zeta^{T\mu}$	$\Box+\frac{R}{d}$
$\bar{s}s$	$-\Box$

Table 5.1: Summary of the decomposed second variation

sphere. This has already been done in (5.1). Thus the arguments of our functions become $\frac{R^2}{d}$. Then we define

$$f_k\left(\frac{R^2}{k^4d}\right)=k^{-d}F_k\left(\frac{R^2}{d}\right)\qquad;\qquad z_k\left(\frac{R^2}{k^4d}\right)=k^{-d+2}Z_k\left(\frac{R^2}{d}\right)\tag{5.9}$$

and the dimensionless Ricci scalar curvature by $\rho=\frac{R}{k^2}$. The missing element is the scale derivatives of the functions F and Z. Then we have

$$\partial_t F_k^{(n)}=k^{d-4n}\left((d-4\,n)f_k^{(n)}-4\frac{\rho^2}{d}f_k^{(n+1)}+\partial_t f_k^{(n)}\right)\tag{5.10}$$

and similarly for the Z function

$$\partial_t Z_k^{(n)}=k^{d-4n-2}\left((d-4\,n-2)z_k^{(n)}-4\frac{\rho^2}{d}z_k^{(n+1)}+\partial_t z_k^{(n)}\right).\tag{5.11}$$

As mentioned, after projecting to the sphere the arguments become $\frac{R^2}{d}$. It is assumed that from now on when we write F we mean $F\left(\frac{R^2}{d}\right)$ and similarly for Z. For the dimensionless

functions f and z the arguments become $\frac{\rho^2}{d}$. Moreover, we remind that the primes denote derivatives with respect to the argument as always. Gathering together all the above we can compute the L.H.S. of the flow equation for the effective average action given by (5.4). Then we have

$$\partial_t \bar{\Gamma}_k = \frac{384\pi^2}{\rho^2}\left[4f_k + 2\rho\, z_k - \rho^2\left(f_k' + \rho\, z_k'\right) + \partial_t f_k + \rho\,\partial_t z_k\right]. \tag{5.12}$$

The R.H.S. of the equation is given by the sum of the traces for the individual components after using the algorithm described in 3.3 and subtracting the appropriate exclusion modes. Then, in terms of the components we have

$$\begin{aligned}\partial_t\bar{\Gamma}[\bar{g},\bar{g}] =& \frac{1}{2}\mathrm{Tr}_{(2T)}\left[\frac{\partial_t\mathcal{R}_k^{h^Th^T}}{\bar{\Gamma}^{(2)}_{h^Th^T}}\right] + \frac{1}{2}\mathrm{Tr}'_{(1T)}\left[\frac{\partial_t\mathcal{R}_k^{\xi\xi}}{\bar{\Gamma}^{(2)}_{\xi\xi}}\right] + \frac{1}{2}\mathrm{Tr}''_{(0)}\left[\frac{\partial_t\mathcal{R}_k^{\sigma\sigma}}{\bar{\Gamma}^{(2)}_{\sigma\sigma}}\right] + \frac{1}{2}\mathrm{Tr}_{(0)}\left[\frac{\partial_t\mathcal{R}_k^{hh}}{\bar{\Gamma}^{(2)}_{hh}}\right] \\ &+ \mathrm{Tr}''_{(0)}\left[\frac{\partial_t\mathcal{R}_k^{\sigma h}}{\bar{\Gamma}^{(2)}_{\sigma h}}\right] - \mathrm{Tr}'_{(1T)}\left[\frac{\partial_t\mathcal{R}_k^{\bar{C}^TC^T}}{\bar{\Gamma}^{(2)}_{\bar{C}^TC^T}}\right] - \mathrm{Tr}''_{(0)}\left[\frac{\partial_t\mathcal{R}_k^{\bar{\eta}\eta}}{\bar{\Gamma}^{(2)}_{\bar{\eta}\eta}}\right] - \mathrm{Tr}''_{(0)}\left[\frac{\partial_t\mathcal{R}_k^{\bar{\lambda}\lambda}}{\bar{\Gamma}^{(2)}_{\bar{\lambda}\lambda}}\right] \\ &+ \frac{1}{2}\mathrm{Tr}''_{(0)}\left[\frac{\partial_t\mathcal{R}_k^{\omega\omega}}{\bar{\Gamma}^{(2)}_{\omega\omega}}\right] - \mathrm{Tr}'_{(1T)}\left[\frac{\partial_t\mathcal{R}_k^{\bar{c}^Tc^T}}{\bar{\Gamma}^{(2)}_{\bar{c}^Tc^T}}\right] + \frac{1}{2}\mathrm{Tr}'_{(1T)}\left[\frac{\partial_t\mathcal{R}_k^{\zeta^T\zeta^T}}{\bar{\Gamma}^{(2)}_{\zeta^T\zeta^T}}\right] + \mathrm{Tr}''_{(0)}\left[\frac{\partial_t\mathcal{R}_k^{\bar{s}s}}{\bar{\Gamma}^{(2)}_{\bar{s}s}}\right]\end{aligned} \tag{5.13}$$

where the Hessians for each field component are give in the table 5.1, the primes at the traces denote the number of lowest modes to be excluded as described in Section 3.3 and the traces are to be computed using the algorithm for the Q's and the relevant $\mathbf{b}_n$ coefficients listed in Appendix B. Moreover, the auxiliary fields have inherited the primes from the fields which they originate.

Following the approach that we adopted for the $f(R)$ approximation we concentrate to the four dimensional case ($d = 4$) and we fix the gauge by setting

$$\rho = 0 \qquad ; \qquad \alpha \to 0. \tag{5.14}$$

This choice of gauge results in two simplifications of the flow equation. Since we take the limit $\alpha \to 0$ the gauge fixing terms are tending to ∞. However, since terms proportional to $\frac{1}{\alpha}$ are also included in the regulator, when we take the limit $\alpha \to 0$ at the level of the FRGE only the terms proportional to $\frac{1}{\alpha}$ survive.

As a result the non-diagonal term σh vanishes since it has no dependence on α (for $\rho = 0$) while the denominator involves the components hh and $\sigma\sigma$ and it tends to ∞. The second simplification which occurs is that the gravity and the gauge degrees of freedom and the gravity degrees of freedom totally decouple. The gravity d.o.f. are encoded in h^Th^T and hh, while the gauge d.o.f. are in $\xi\xi$ and $\sigma\sigma$.

After the trace computation we get for the flow equation

$$384\pi^2\left[4f+2\rho\, z-\rho^2\left(f'+\rho\, z'\right)+\partial_t f+\rho\,\partial_t z\right]=I[f,z](\rho) \tag{5.15}$$

where the RHS encodes the contributions from fluctuations and it splits in several parts as

$$\begin{aligned} I[f,z](\rho) =& I_0[f,z](\rho)+\partial_t z\, I_1[f,z](\rho)+\partial_t f'\, I_2[f,z](\rho)+\partial_t z'\, I_3[f,z](\rho) \\ &+\partial_t f''\, I_4[f,z](\rho)+\partial_t z''\, I_5[f,z](\rho) \end{aligned} \tag{5.16}$$

The flow terms appearing (5.16) arise through the Wilsonian momentum cutoff $\partial_t R_k$, which we have chosen to depend on the background field. All the terms $I_0[f,z],...,I_5[f,z]$ arise from tracing over the fluctuations of the metric field for which we have adopted the transverse traceless decomposition. The term $I_0[f,z]$ also receives f,z-independent contributions from the ghosts and from the Jacobians originating from the split of the metric fluctuations into tensor, vector and scalar parts. To indicate the origin of the various contributions in the expressions below, we use superscipts T, V , and S to refer to the transverse traceless tensorial, vectorial, and scalar origin respectively. Then we have for the various components $I_i[f,z](\rho)$

$$\begin{aligned} I_0[f,z] =& \frac{P_c^V}{D_c^V}+\frac{P_c^S}{D_c^S}+\frac{P_0^{Tz0}z+P_0^{Tf1}f'+P_0^{Tz1}z'+P_0^{T2}(f''+\rho z'')}{D^T} \\ &+\frac{P_0^{Sz0}z+P_0^{Sf1}f'+P_0^{Sz1}z'+P_0^{Sf2}f''+P_0^{Sz2}z''+P_0^{S3}(f^{(3)}+\rho z^{(3)})}{D^S} \end{aligned} \tag{5.17}$$

$$I_1[f,z] = \frac{P_1^T}{D^T}+\frac{P_1^S}{D^S} \tag{5.18}$$

$$I_2[f,z] = \frac{P_2^T}{D^T}+\frac{P_2^S}{D^S} \tag{5.19}$$

$$I_3[f,z] = \frac{P_3^T}{D^T}+\frac{P_3^S}{D^S} \tag{5.20}$$

$$I_4[f,z] = \frac{P_4^S}{D^S} \tag{5.21}$$

$$I_5[f,z] = \frac{P_5^S}{D^S} \tag{5.22}$$

with the denominators appearing in the above equations given by

$$D^T = 36f+(24\rho+36)z-(7\rho^2-6\rho+36)(f'+\rho\, z') \tag{5.23}$$

$$\begin{aligned} D^S =& 8f+12z+(-2\rho^2-8\rho+24)f'+(2\rho^3-32\rho^2+60\rho)z' \\ &+\rho^2(\rho-3)^2(f''+\rho\, z'') \end{aligned} \tag{5.24}$$

$$D_c^V = 4-\rho \tag{5.25}$$

$$D_c^S = 3-\rho \tag{5.26}$$

and the polynomials given in Table 5.2.

P_c^V	$\frac{607}{15}\rho^2 - 24\rho - 144$	P_c^S	$\frac{511}{30}\rho^2 - 12\rho - 36$
P_0^{Tz0}	$\frac{311}{63}\rho^3 - 4\rho^2 - 1080\rho + 2880$	P_0^{Tf1}	$-\frac{\rho^3}{3} - 116\rho^2 + 1800\rho - 4320$
P_0^{Tz1}	$\frac{129134}{189}\rho^5 + \rho^4 + 122\rho^3 + 840\rho^2 - 3240\rho$	P_0^{T2}	$+\frac{259201}{756}\rho^6 + \frac{\rho^5}{6} + 29\rho^4 - 300\rho^3 + 540\rho^2$
P_0^{Sz0}	$+\frac{37}{189}\rho^3 + \frac{116}{15}\rho^2 + 72\rho + 192$	P_0^{Sf1}	$-\frac{116}{45}\rho^3 - \frac{248}{15}\rho^2 + 96\rho + 576$
P_0^{Sz1}	$\frac{1111}{2268}\rho^5 - \frac{29}{15}\rho^4 - \frac{170}{3}\rho^3 + 40\rho^2 + 1080\rho$	P_0^{Sf2}	$+\frac{1333}{4536}\rho^6 + \frac{29}{9}\rho^5 + \frac{62}{15}\rho^4 - 16\rho^3 + 36\rho^2$
P_0^{Sz2}	$+\frac{27991}{45360}\rho^7 + \frac{406}{45}\rho^6 + \frac{943}{30}\rho^5 - 16\rho^4 - 126\rho^3$	P_0^{S3}	$+\frac{181}{3360}\rho^8 + \frac{29}{30}\rho^7 + \frac{91}{20}\rho^6 - 27\rho^4$
P_1^T	$+\frac{311}{126}\rho^3 - \rho^2 - 180\rho + 360$	P_1^S	$+\frac{37}{378}\rho^3 + \frac{29}{15}\rho^2 + 12\rho + 24$
P_2^T	$-\frac{259201}{756}\rho^4 - \frac{\rho^3}{6} - 29\rho^2 + 300\rho - 540$	P_2^S	$-\frac{127}{1620}\rho^4 - \frac{58}{45}\rho^3 - \frac{62}{15}\rho^2 + 16\rho + 72$
P_3^T	$-\frac{259201}{756}\rho^5 - \frac{\rho^4}{6} - 29\rho^3 + 300\rho^2 - 540\rho$	P_3^S	$-\frac{1333}{4536}\rho^5 - \frac{232}{45}\rho^4 - \frac{67}{3}\rho^3 + 16\rho^2 + 180\rho$
P_4^S	$-\frac{181}{3360}\rho^6 - \frac{29}{30}\rho^5 - \frac{91}{20}\rho^4 + 27\rho^2$	P_5^S	$-\frac{181}{3360}\rho^7 - \frac{29}{30}\rho^6 - \frac{91}{20}\rho^5 + 27\rho^3$

Table 5.2: The polynomials appearing in the flow equation

5.4 Results

Having computed the flow equation for the gravitational anstatz (5.4) we can proceed and examine if the requirements for the asymptotic safety scenario still hold after taking into account the non-trivial dynamics of the Ricci tensor. As before we solve the fixed point equation

$$384\pi^2\left[4f + 2\rho\, z - \rho^2\left(f' + \rho\, z'\right) + \partial_t f + \rho\,\partial_t z\right] = I_0[f, z](\rho) \tag{5.27}$$

by making an expansion in the dimensionless curvature ρ. We label the order N of the approximation by the number of couplings that contribute to it. Then we find that at each order of the approximation form $N = 2$ to $N = 7$ there exists a UV fixed point in accordance with the asymptotic safety scenario. The values of the fixed point can be read in Table 5.3.

The next task is to compute the critical exponents for the fixed point values that we found. Again, at each order of the approximation from $N = 2$ to $N = 7$ we find that there are always 3 attractive directions, or 3 negative eigenvalues, exactly as was the case for the $f(R)$ approximation up to order $N = 35$. The values of the critical exponents can be read in Table 5.4. These results are encouraging and indicate that the number of negative eigenvalues is not affected by the inclusion of more complicated tensor structures.

N	$f(0)$	$z(0)$	$f'(0)$	$z'(0)$	$f''(0)$	$z''(0)$	$f^{(3)}$
2	0.005226	-0.020214	-	-	-	-	-
3	0.004633	-0.01356	0.00459	-	-	-	-
4	0.006347	-0.016722	0.0037125	-0.011622	-	-	-
5	0.006459	-0.016536	0.0038054	-0.012477	-0.008709	-	-
6	0.006476	-0.016508	0.0038208	-0.012585	-0.010126	-0.001842	-
7	0.006507	-0.016456	0.0038510	-0.012782	-0.012926	-0.006633	-0.046311

Table 5.3: Summary of the fixed point values

N	$Re(\theta_1)$	$Im(\theta_1)$	θ_3	$Re(\theta_4)$	$Im(\theta_4)$	θ_6	θ_7
2	2.38163	2.16904	-	-	-	-	-
3	1.62684	2.57034	21.2325	-	-	-	-
4	2.45042	2.4209	1.10754	-8.27329	-	-	-
5	2.41456	2.28641	0.996519	-5.32054	-3.81429	-	-
6	2.40478	2.27198	0.985012	-5.1241	-3.8021	-12.4043	-
7	2.39379	2.21574	0.946169	-5.12187	-3.83211	-13.7131	-20.0635

Table 5.4: Summary of the critical exponents

With the above results in hand we can make a few comments for the fixed points and the critical exponents of the low order approximations of the ansatz (5.4). First, we observe that there is a reasonably good stability from $N = 3$ and onwards. In the lowest order $N = 2$ we recover the results for the Einstein-Hilbert truncation and the second order $N = 3$ is the most unstable as was expected by naive power counting arguments and as was found also in the $f(R)$ approximation. Starting from order $N = 3$ we also find spurious fixed point which either disappear in the next order or they do not have consistently the correct number of relevant directions.

In our search we went up to the seventh order in the expansion. We note that for the gravitational approximation given by (5.4) it is much more demanding to extend our search to higher orders as we did with the $f(R)$ approximation. The main obstacle for this becomes clear with the observation that in the flow equation (5.15) the highest coefficient in a ρ expansion is quadratic and not linear as in the case of $f(R)$. This means that we can still solve for the highest coefficient and set up a recursive relation but now the result are the roots of a quadratic equation which in general involves square roots of complicated quantities and become very cumbersome to solve using computer algorithms

as those we developed before. The reason for the highest coupling being quadratic is the fact that the contribution from the transverse traceless part $h^{T\mu\nu}$ contains the highest coupling, something which was not the case in the $f(R)$. In turn, the appearance of the highest coupling in the contribution of $h^{T\mu\nu}$ originates from the fact that its second variation contain a term with $\Box^2$ which was absent for the $f(R)$. However, a more careful examination of the flow equation is currently being carried out and extension of the current results to higher orders is left for future work.

5.5 Conclusions

In this Chapter we investigated the effects to the asymptotic safety scenario that come from the inclusion of more complicated tensor structures as the Ricci tensor $R_{\mu\nu}$. We motivated an extension of the gravitational ansatz that includes powers of the Ricci tensor squared and we defined two functions with one of them being multiplied by the Ricci scalar for mass dimension consistency. The flow equation was derived and the fixed point structure was examined.

In order to make the evaluation of the functional trace possible, we chose our background to be a sphere. The effects of the Ricci tensor are taken into account through the non-trivial dynamics coming from the second variation. We evaluated the second variation and we used the trace computation algorithm that we developed in Chapter 3. The resulting flow equation is stated and examined in Section 5.3. This is considerably more involved than the case of $f(R)$ and has the disadvantage that it is not linear in the highest coefficient but quadratic. Therefore, the application of recursive techniques was not possible.

With the flow equation at hand we moved on to examine the fixed points and the critical exponents of our system using the conventional techniques. We find that for every order from $N = 2$ to $N = 7$ there exist a self-consistent UV fixed point with always 3 relevant directions. These are very encouraging results since they indicate that the underlying structure of the asymptotic safety scenario and the fact that we always find the same number of negative eigenvalues do not break down when we consider more complicated tensor structures. Moreover, we find that our results look very stable even at low orders in the approximation studied here.

Chapter 6

Black Holes

6.1 Introduction

Black holes are classical solutions of the Einstein's field equations with many interesting properties and have been a central field of research since their discovery by Schwarzschild [139]. Their most striking feature is the existence of a 2-dimensional surface, the event horizon, which separates two causally disconnected regions. In order for black holes to describe physically realistic situations these solutions must be extended to rotating space-times. It took almost 40 years until such a generalisation was discovered by Kerr in 1963 [88]. Solutions in higher dimensions were found in the spherical symmetric case by Tangherlini [144] and in the spinning case by Myers and Perry [113].

Higher dimensional black holes have been proved much richer than their four dimensional counterparts and have kicked off a very active field of research. While, it was immediately observed that rotating black holes in $d \geq 6$ dimensions can have arbitrary large rotation, it was recently suggested [48] that these solutions are unstable leading to an extensive investigation of ultra-spinning instabilities [38, 40] and black hole phase transitions [72, 39, 111, 47]. Another remarkable feature of higher dimensional solutions is the discovery of black objects with non-spherical event horizons [49], which is a direct violation of uniqueness theorems for $d > 4$.

While the description of black holes within general relativity is valid up to the semi-classical level, it is expected to break down when we approach the Planck scale and quantum gravity effects become important. The perturbative non-renormalisability of gravity [143] brings obstacles to the inclusion of perturbative quantum effects. However, since the pioneering work of Weinberg [148] the possibility that gravity is non-perturbatively renormalisable has arisen and numerous evidence has been since provided

in four dimensions [130, 141, 118], higher dimensions [99, 100, 55], as well as higher derivative terms [91, 32, 33, 34, 105, 16, 52] and under the inclusion of matter fields [122, 121, 57, 74, 159]. This picture provides a UV completion of gravity and is based on the existence of a non-trivial fixed point together with a flow under the renormalisation group which connects the classical regime with the high energy regime. Previous applications to black holes include the case of four dimensional Schwarzschild [23], four dimensional Kerr [133, 134], higher dimensional spherical symmetric black holes [54] as well as black holes coming from higher derivative gravity [26] or from the inclusion of boundary terms [14] and the cosmological constant [89].

In this chapter we investigate quantum corrections for higher dimensional rotating black holes coming from the running of the Newton's constant as dictated by the asymptotic safety scenario. We assume that the leading quantum corrections come from the replacement of the gravitational coupling with the momentum dependent coupling after an appropriate identification of the momentum and position scales. In this context we examine the modifications of the horizons and we find qualitative differences for spacetime dimensions $d \geq 5$. A significant feature of these modifications is the existence of a critical mass M_c below which there are no black hole solutions. As a consequence the phase space of ultra-spinning black holes is greatly reduced. Qualitative differences are found also for the temperature and the specific heat associated with the quantum corrected black holes again due to the existence of M_c. Moreover, the fact that the quantum corrected metric is not a solution of the Einstein's equations implies the existence of an effective energy momentum tensor whose positivity properties are violated and thus allowing for the curvature singularities to be softened or even absent. Finally, modifications of the laws of black hole mechanics are discussed.

We organise the rest of this chapter as follows. In Section 6.2 we review classical higher dimensional spinning black holes and we introduce our setup for the inclusion of quantum corrections. In Section 6.3 we investigate how the horizon structure is changed in our case and we distinguish between the three qualitatively different cases with $d = 4$, $d = 5$ and $d \geq 6$. In Section 6.4 we are concerned with the thermodynamical properties of our corrected black holes and we examine the form of temperature and specific heat. In Section 6.5 we compute the effective energy-momentum tensor, we examine the fate of the curvature singularities and we evaluate the Komar mass and angular momentum of the spacetime. Finally, in Section 6.6 we summarise with our conclusions.

6.2 Generalities

In this section we review the classical higher dimensional rotating black hole solutions and we establish our notation. Furthermore, we present some considerations about quantum corrections and we define the setup we will use in this chapter.

6.2.1 Myers-Perry black holes

The first extension of solutions to Einstein's equations in higher dimensions was made by Tangherlini in 1963, who generalised the spherically symmetric solutions, leading to the Schwarzschild-Tangherlini metric [144]. It was not until 1986 that spinning black holes in higher dimensions were found by Myers and Perry [113]. Unlike the four dimensional case, spinning black holes in higher dimensions can rotate in more than one independent plane. For a complete review see [50]. For simplicity, here we are going to examine only the case of rotation in a single plane. This spacetime is described by the metric

$$\begin{aligned} ds^2 = &- dt^2 + G_N \frac{M}{r^{d-5}\Sigma}(dt - a\sin^2\theta\, d\phi)^2 + \frac{\Sigma}{\Delta}dr^2 \\ &+ \Sigma\, d\theta^2 + (r^2 + a^2)\sin^2\theta\, d\phi^2 + r^2\cos^2\theta\, d\Omega_{d-4}^2, \end{aligned} \tag{6.1}$$

where Σ and Δ are defined by

$$\begin{aligned} \Sigma &= r^2 + a^2\cos^2\theta \\ \frac{\Delta}{r^2} &= 1 + \frac{a^2}{r^2} - G_N\frac{M}{r^{d-3}} \end{aligned} \tag{6.2}$$

and d is the number of spacetime dimensions, G_N the Newton's coupling constant, $d\Omega_{d-4}^2$ the line element on the unit $d-4$ sphere, while the reduced mass M and the parameter a are related to the physical mass $M_{\rm phys}$ and angular momentum J by

$$M = \frac{8\,\Gamma(\frac{1}{2}(d-1))}{(d-2)\pi^{(d-3)/2}}\, M_{\rm phys} \tag{6.3}$$

$$a = \frac{d-2}{2}\frac{J}{M_{\rm phys}}\,. \tag{6.4}$$

The limit $d = 4$ of this spacetime is the well known Kerr solution. The horizons of Myers-Perry solutions are found from the coordinate singularities $g^{rr} = 0$, or $\Delta = 0$. We observe from (6.2) that $d = 5$ is distinguished: The centrifugal force does not depend on the dimensionality of spacetime. On the other hand, the gravitational force is dimension-dependent and dominates for $d > 5$ for small r, making (6.2) negative. This leads to event horizons for spacetimes with arbitrary large angular momentum, the so-called *ultra-spinning* black holes. It is interesting to note that ultra-spinning regions can also exist when we have rotation in many planes [50], [113].

The above considerations make it interesting to study separately the properties of the three qualitatively different cases of $d = 4$, $d = 5$ and $d \geq 6$. We begin with the four dimensional case where the line element (6.1) reduces to that of the Kerr solution. The expression $\Delta(r)$ which gives the horizons is a quadratic polynomial with two solutions

$$r_{\pm} = \frac{1}{2}\left[G_N M \pm \sqrt{(G_N M)^2 - 4a^2}\right], \tag{6.5}$$

where r_+ corresponds to the event horizon and r_- to the inner (Cauchy) horizon. It is evident from (6.5) that horizons exist for black hole masses large enough to satisfy $G_N M \geq 2a$. We observe that in four dimensions the effect of angular momentum has two important consequences to the structure of black holes. Firstly, black hole solutions exist only up to a minimum mass M_c. Secondly, there exists an inner horizon.

In the five dimensional case, the term which is responsible for the gravitational attraction becomes constant and $\Delta(r)$ has only one positive root given by

$$r_+ = \sqrt{G_N M - a^2}\,. \tag{6.6}$$

Hence, black hole solutions exist only for sufficiently large masses $G_N\, M > a^2$ and the resulting spacetime has only one horizon.

In six or higher dimensions none of the two main features of the $4d$ Kerr black holes are conserved: The gravitational term of $\Delta(r)$ dominates as we approach $r \to 0$ and thus $\Delta(r)$ is always negative in this limit. This, together with the limit of $\Delta(r)$ when $r \to \infty$, imply that there is always a horizon independently of the mass, and independently of the angular momentum. Moreover, a check on the first derivative of $\Delta(r)$ with respect to r reveals exactly one event horizon, and no inner horizon.

A generic feature of rotating black hole solutions is that, for given mass, their horizon radii are always less than their non-rotating counterparts. In fact, the horizon radius of the non-rotating Schwarzschild-Tangherlini black hole is given by

$$r_{\rm cl} = (G_N M)^{\frac{1}{d-3}}. \tag{6.7}$$

Substituting (6.7) into (6.2) gives $\Delta(r_{cl}) = a^2 \geq 0$. For $d \geq 5$, since the first derivative $\Delta'(r)$ is always positive, it follows that the horizons of spinning black holes at given mass M (if they exist) are smaller of their non-rotating counterparts, $r_{\rm cl}(a) < r_{\rm cl}$. For $d = 4$, this observation can be read off from the horizons of the Schwarzschild and Kerr solutions (6.5), $r_+ \leq G_N M = r_{\rm cl}$.

case	short distance index	gravity	horizons	$\Delta(r \to 0)$
(i)	$s < d-5$	strong if $s<0$; weak if $s>0$	one or more	singular
(ii)	$s = d-5$	strong if $s<0$; weak if $s>0$	none, one or more	finite
(iii)	$s > d-5$	strong if $s<0$; weak if $s>0$	none, one or more	a^2

Table 6.1: Horizons of rotating black holes assuming a scale-dependent gravitational coupling strength (6.8) at short distances for various dimensions and in dependence on the short distance index s (see text).

6.2.2 Quantum effects

We expect that this picture changes when quantum gravity effects are taken into account and the black hole mass approaches the fundamental scale of quantum gravity. In what follows we will assume that the leading order quantum effects are captured from the renormalization of the gravitational coupling, which makes it a function of the momentum scale. We are going to extensively study these effects in the context of asymptotic safety scenario, but before doing that we would like to gain a qualitatively picture of what is implied from various forms of the running gravitational coupling.

Depending on the ultraviolet completion of gravity and the renormalization group, gravity can become "weak" or "strong" at short distances, or superseeded by an altogether different description. To investigate the behaviour of black holes for these cases, we parametrize the putative running of Newton's constant at short distances as

$$G_N \to G(r) = r_{\rm char}^{d-2} \left(\frac{r}{r_{\rm char}}\right)^s . \tag{6.8}$$

Here, $r_{\rm char}$ denotes the characteristic length scale for the on-set of quantum corrections, and the index s parametrizes whether the gravitational coupling remains classical ($s=0$), decreases ($s>0$) or increases ($s<0$) towards short distances. Then we substitute this form of $G(r)$ back to the expression (6.2) for $\Delta(r)$, we distinguish the following three cases

(i) $s < d-5$. The strength of the gravitational contribution to Δ increases (decreases) for negative (positive) $d-5$. The function $\Delta(r \to 0)$ is unbounded from below implying the existence of, at least, one horizon.

(ii) $s = d-5$. In this case, we find a finite limit $\Delta(r \to 0) \equiv \Delta_0 = a^2 - r_{\rm char}^3 M$. For $\Delta_0 < 0$, this necessarily implies the existence of a horizon, similar to case (i). For $\Delta_0 > 0$, the situation is similar to case (iii).

(iii) $s > d-5$. In this case the gravitational coupling becomes weaker for all $d \geq 5$. For $d<5$, gravity may even become strong. In either case $\Delta_0 = a^2 > 0$ implying that

the space-time can have none, one or more horizons, depending on the precise short distance behavior of $G(r)$ and the other parameters of the spacetime such as the mass and angular momentum.

The conclusions of the above considerations are summarised in Table. 6.1

6.2.3 Asymptotically safe gravity

The asymptotic safety scenario for gravity was first proposed by Weinberg [148] in 1979 and relies on the existence of a non-trivial UV fixed point which governs the renormalisation group flow of gravity. It was shown that this was indeed the case for Einstein gravity in $2+\epsilon$ dimensions. Since then it was verified that also in four [141, 130] and in higher dimensions [55, 100] the non-perturbative flow of gravity is governed by a UV fixed point.

Moreover, there exists a Gaussian (non-interacting) fixed point and a trajectory of the flow which connects the two fixed points so that general relativity and perturbation theory are recovered in the region of the Gaussian fixed point. Upon integration of the higher dimensional renormalisation group flow we find an implicit equation for the momentum dependent gravitational coupling given by

$$\frac{G_k}{G_N} = \left(1 - \frac{G_k}{g_*\, k^{2-d}}\right)^{\delta} \tag{6.9}$$

where $\delta = \theta_{\rm G}/\theta_{\rm NG}$ is the ratio of the universal scaling exponents θ at the Gaussian (non-Gaussian) fixed point, respectively and g_* is the value of the UV fixed point. In [99], it was found that $\theta_{\rm G} = (d-2)$ and $\theta_{\rm NG} = 2d\,\frac{d-2}{d+2}$, leading to

$$\delta = \frac{d+2}{2d}\,. \tag{6.10}$$

Hence, the index δ interpolates between $\frac{3}{4}$ and 2 for $d \in [4, \infty]$. In the linear approximation $\theta_{\rm G} = \theta_{\rm NG}$ we have $\delta = 1$, and consequently $G_k = G_N/(1 + k^{d-2}/g_*)$. In the quadratic approximation, $\theta_{\rm G} = \frac{1}{2}\theta_{\rm NG}$ [60].

The input from asymptotic safety provides us with the running Newton's coupling as a function of momentum. However, black hole solutions are found in coordinates of curved spacetime and we need to use a matching between momentum and position scales in order to make a replacement of Newton's constant, by a distance-dependent coupling

$$G_N \to G(r) \tag{6.11}$$

It is the central assumption this study that the leading quantum gravity corrections originate from this replacement. Following [54], we will identify $k = \xi/r$, where ξ is a non-universal parameter which also depends on the specific RG scheme used in the derivation of (6.9).

For the most part of this chapter we are going to use the linear approximation $\delta = 1$. In this case the running of gravitational coupling (6.9) takes the form

$$G(r) = G_N \frac{r^{d-2}}{r^{d-2} + \frac{G_N}{g_*}} \tag{6.12}$$

where the parameter ξ has been absorbed into g_*.

6.3 Horizons

After these preliminaries we study the horizon structure of black holes using a running for the Newton's constant dictated by the asymptotic safety scenario. We saw that classical black holes have two horizons under a condition for $d = 4$, one horizon under a condition for $d = 5$ and always one horizon when $d \geq 6$. This pattern is modified in our consideration and the existence of horizons depends on the precise form of $G(r)$. We start this section by presenting an analysis about the existence of horizons and their conditions. We are also interested to see if the possibility of ultra-spinning solutions still arises. Then, following from the fact that in the classical case $d = 5$ is a critical dimensionality, we examine separately the cases $d = 4$, $d = 5$ and $d \geq 6$.

6.3.1 Horizon structure

First, we examine how many horizons our solutions have. For this, we recall the structure of non-rotating black holes within asymptotic safety and we investigate the modifications due to rotation, while keeping $G(r)$ as general as possible.

We begin by looking at the relation which gives the horizons $\Delta(r) = 0$. It is more convenient and it provides more physical insight to look for roots of the dimensionless function

$$f(r) = \frac{\Delta(r)}{r^2} \equiv 1 + \frac{a^2}{r^2} - \frac{M\,G(r)}{r^{d-3}}. \tag{6.13}$$

In contrast to the classical case (6.2), the running of gravitational coupling $G(r)$ modifies the gravitational potential and in the context of asymptotic safety it makes it weaker at short distances. For given mass M and angular momentum a, the RG improved horizon radius $r_s(M, a)$ is obtained as the implicit solution(s) of

$$r_s^{d-3}(M, a) = M\,G(r_s(M, a)) - a^2\, r_s^{d-5}(M, a)\,, \tag{6.14}$$

provided it exists.

Assuming that $M\,G(r)\,r^{3-d}$ doesn't diverge when we approach $r \to 0$ but instead it vanishes, we can deduce the form of the gravitational potential $V(r) = -M\,G(r)\,r^{3-d}$. Its

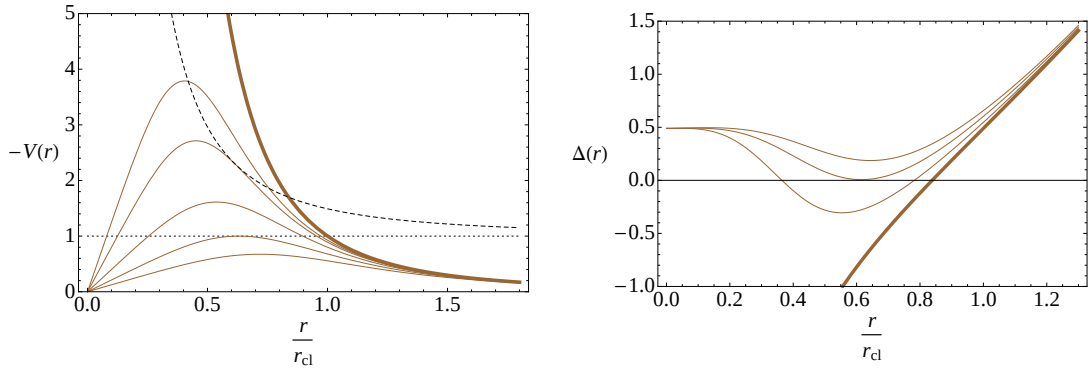

Figure 6.1: Left panel: The gravitational potential $-MG(r)/r^{d-3}$ (full lines) in comparison with the rotational barrier $1 + a^2/r^2$ ($a = 0$: dotted line, $a \neq 0$: dashed line). Right panel: the function $\Delta(r)$ (6.13) for a theory where gravity becomes weaker at small distances ($d = 6$ and $a = 0.7\, M_{\rm Pl}^{-2}$). In either case, the thick (brown) line denotes the classical limit, and thin lines denote decreasing values for M (top to bottom) in the case where $G(r)$ is weakening towards shorter distances.

first derivative with respect to r is given by

$$V'(r) = M\, G(r)\, r^{2-d}\, (d - 3 + \eta(r))\,, \tag{6.15}$$

where $\eta(r) = -r\, G'(r)/G(r)$ is the anomalous dimension of gravity. As implied by the previous section, in the context of asymptotic safety, $\eta(r)$ is a monotonically increasing function, which interpolates from $\eta(0) = 2-d$ to $\eta(\infty) = 0$. Thus, it is obvious from (6.15) that $V'(r)$ changes sign once and $V(r)$ decreases from $V(0) = 0$ down to a minimum value $V_{\rm min}$ and then it increases back to $V(\infty) = 0$. This behaviour reflects the weakening of gravity in our model, see Fig. 6.1.

In the absence of rotation, $V(r)$ competes with the constant barrier 1. Thus, if $V_{\rm min} < -1$ the spacetime has two horizons, if $V_{\rm min} = -1$ it has one degenerate horizon, while if $V_{\rm min} > -1$ there are no horizons. Which of the three cases is actually realised depends on the mass M and the precise form of $G(r)$ [23], [54].

When we consider rotating black holes, the gravitational potential $V(r)$ competes the constant term enhanced by the rotational term, see Fig. 6.1. In order to examine how many horizons we have, we look for roots of the derivative of $f(r)$, given by

$$f'(r) = r^{-3}\left[-2a^2 + M\, G(r)\, r^{5-d}\, (d - 3 + \eta(r))\right]. \tag{6.16}$$

Using the same assumptions as for the non-rotating case, we find that in four and five dimensions $f(r)$ has only one minimum and the spacetime can have either two, one degen-

erate, or no horizons. For six or higher dimensions we have to know more details about $G(r)$, but for the running of Newton's coupling given by (6.12), the same behaviour with either two, one degenerate or no horizons still holds (for details see Appendix C.1). The resulting form of $\Delta(r)$ is plotted in Fig. 6.1.

6.3.2 Critical mass

This behaviour of the function $f(r)$, implies that black hole solutions exist only for masses greater than a minimum mass M_c. For non-rotating black holes within asymptotic safety there is a map between the RG parameter g_* and a black hole which is characterised by some M_c. As we shall see in more detail later, for rotating black holes, M_c is also a function of angular momentum and so there is a map between ω and every $M_c(a)$. Black holes exist only for

$$M \geq M_c(a). \tag{6.17}$$

For the rest of this Chapter we will write M_c for the critical mass of the non-rotating black hole [54], while for a rotating black hole we will write explicitly $M_c(a)$. Moreover, when we encounter the RG parameter g_*, we will eliminate it in favour of $M_c(a)$. This allows us to be compatible with other theories where gravity becomes weaker at short distances and exhibit an M_c, but they are not parametrized by the specific parameter g_* (see for example [117], [110]).

Keeping the function $G(r)$ arbitrary, we solve simultaneously $f(r) = 0$ and $f'(r) = 0$ using (6.13) and (6.16) to find

$$\eta(r_c) = 3 - d + 2\frac{a^2}{r_c^2 + a^2} \tag{6.18}$$

where r_c is the radius of the critical (degenerate) horizon. This result is to be compared with the non rotating case where $\eta(r_c) = 3 - d$ [54]. Thus, without relying on any specific running for the Newton's coupling, we have concluded that the graviton anomalous dimension for a critical rotating black hole will be less than the one of the corresponding spherical black hole and in general it will satisfy

$$3 - d \leq \eta(r_c) < 5 - d. \tag{6.19}$$

6.3.3 Critical parameters

In order to quantitatively examine the properties of RG corrected black holes we express the relevant equations in terms of dimensionless variables. This is achieved by dividing every dimensionfull parameter by the appropriate power of a representative length, which

we take to be the horizon radius of classical, non-rotating black holes, i.e. $r_{\rm cl} = (G_N M)^{\frac{1}{d-3}}$. The mass dimensions of the parameters are $[G_N] = 2-d$, $[a] = -1$ and $[M] = 1$, leading to

$$x = \frac{r}{r_{\rm cl}}\,. \tag{6.20}$$

The parameter x defines the ratio of the radial coordinate to the horizon of *classical non-rotating* black holes $r_{\rm cl}$. If they exist, we denote the event horizon by x_+, the Cauchy (inner) horizon by x_-, and the degenerate (critical) horizon by x_c. The parameter

$$A = \frac{a^2}{r_{\rm cl}^2} \tag{6.21}$$

provides the dimensionless ratio of the angular momentum parameter a over the mass. Finally, we introduce the parameter

$$\Omega = \frac{1}{g_*\, M\, r_{\rm cl}(M)}\,. \tag{6.22}$$

It measures the deviation from classical gravity to which our equations reduce for $\Omega \to 0$ meaning either $M/M_P \to \infty$ or $g_* \to \infty$.

Degenerate (critical) black holes are achieved for $\Delta = 0 = \Delta'$ as this function is defined in (6.13). Using the expression (6.9) for the running of Netwton's coupling together with the above definitions, we obtain the critical values x_c and Ω_c for non-rotating black holes as

$$x_c = \left(\frac{\delta}{d-3+\delta}\right)^{\frac{\delta}{d-3}} \tag{6.23}$$

$$\Omega_c = \frac{d-3}{d-3+\delta}\left(\frac{\delta}{d-3+\delta}\right)^{\frac{\delta}{d-3}}\,. \tag{6.24}$$

Note that $\Omega_c = \frac{d-3}{d-3+\delta}\, x_c$. For $\delta = 1$, they reduce to expressions first derived in [54]. For δ as predicted by (6.10), the result is displayed in Fig. 6.2, also comparing the linear and quadratic approximations $\delta = 1$ and 2, respectively. We note that $x_c, \Omega_c \to 1$ with increasing dimensions. In the limiting case $d \to 3$, we have $x_c = \exp(-1)$ and $\Omega_c = 0$. With these findings, the meaning of the parameter Ω becomes clear, and we write it as

$$\Omega = \left(\frac{M_c}{M}\right)^{\frac{d-2}{d-3}}\,\Omega_c \tag{6.25}$$

with Ω_c given by (6.24). The significance of (6.25) is that black hole solutions exist for black hole masses down to the critical mass $M = M_c$, but not below. The mass scale M_c does not exist within the classical framework and is the central new ingredient here. It is expressed as

$$\frac{M_c}{M_P} = (g_*\,\Omega_c)^{-\frac{d-3}{d-2}}\,\xi^{d-3}. \tag{6.26}$$

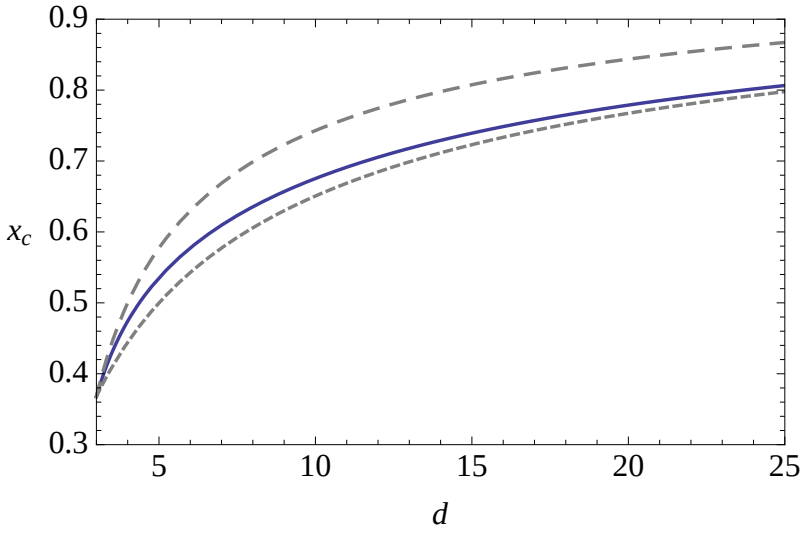

Figure 6.2: The ratio x_c of the outer horizon to the classical Schwarzschild horizon for critical non-rotating black holes as a function of the number of dimensions based on (6.9) in the linear approximation (dashed line, $\delta = 1$), quadratic approximation (short dashed line, $\delta = 2$), and with the full RG running (6.10) (solid line).

in terms of the Planck mass and the parameters of the RG. Below, we use the critical mass of the (non-rotating) black hole as a reference scale for the analysis of the rotating black holes.

In the sequel, it is often sufficient to use the approximation $\delta = 1$, in which case the expressions for $\tilde{\Delta}$ and Ω become

$$\tilde{\Delta} = A + x^2 - \frac{x^3}{x^{d-2} + \Omega}. \tag{6.27}$$

$$\Omega = (d-3)(d-2)^{-\frac{d-2}{d-3}} \left(\frac{M_c}{M}\right)^{\frac{d-2}{d-3}} \tag{6.28}$$

These equations and their solutions are the subject of the following sections.

6.3.4 Four dimensions

The RG-improved Kerr solution has been studied extensively in [134]. We recall this case for completeness, and in order to compare with the higher-dimensional results.

Classical Kerr black holes in four dimensions posses two horizons (see Section. 6.2.1), corresponding to $A \leq \frac{1}{4}$. Consequently, for every angular momentum J there is a minimum mass $M_c(A)$, below which there are no classical Kerr solutions. This structure remains unchanged even under the inclusion of RG corrections [134], except that the precise bounds depend, additionally, on the RG parameter Ω. Specifically, by solving simultaneously

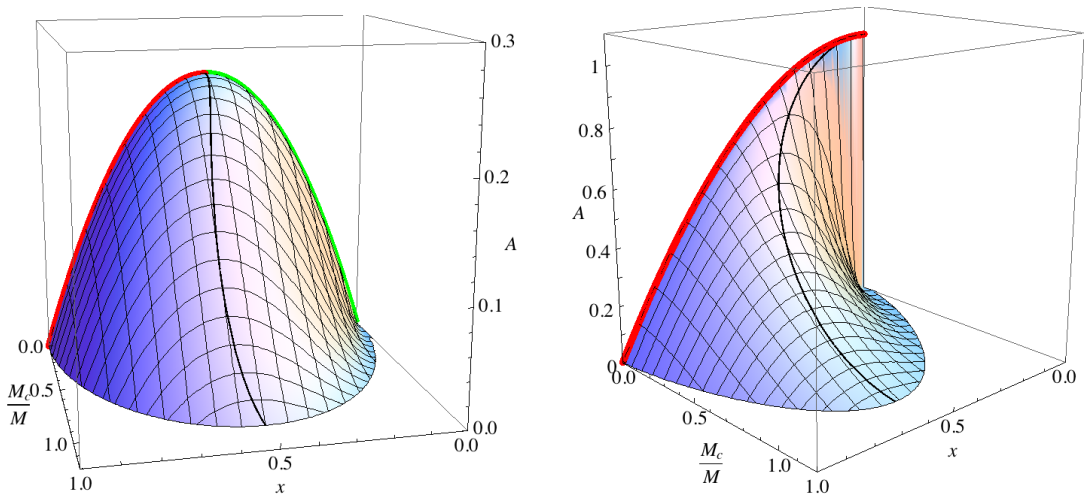

Figure 6.3: The phase space of black hole solutions in four dimensions (left panel) and five dimensions (right panel). The points on the 2-dimensional surface represent the horizon radii x as a function of angular momentum A and mass $M_{\rm c}$. The thick black line gives the radius of the critical horizon $x_{\rm c}$. The regions with $x > x_{\rm c}(A)$ ($x < x_{\rm c}(A)$) correspond to event (Cauchy) horizons. The red (green) lines represent the classical event (Cauchy) horizon, respectively.

$\tilde{\Delta} = 0$ and $\tilde{\Delta}' \geq 0$, we find a relation between the permitted values of A and Ω,

$$\begin{aligned} 0 \quad \leq \quad & \frac{3}{32} + \frac{1}{32}\sqrt{9 - 32(A+\Omega)} \\ & -\frac{1}{3}(A+\Omega) - \frac{1}{6}\sqrt{A^2 + \Omega^2 + 10A\Omega}\,. \end{aligned} \tag{6.29}$$

Inspection of the above condition shows that as Ω increases the upper limit of A decreases. This means, that as the mass of the black hole gets smaller and quantum effects become important, the maximally allowed value of the ratio A decreases. This is in contrast to the classical picture where the condition $A \leq \frac{1}{4}$ was sufficient for the existence of black holes at all mass scales. The quantum corrected picture implies that for every black hole mass there is a different bound of the angular momentum parameter $A_{\rm c}(M)$ as an upper limit in order to have horizons. When we go down to the critical mass for non rotating black holes $M_{\rm c}$ we find that the angular momentum parameter should vanish. For masses less than this there is no allowed phase space for black holes. The horizons and the allowed phase space of black hole solutions can be seen in Fig. 6.3.

We can view the criticality condition in the opposite way. It is evident from (6.29) that for every value of the ratio $A \leq \frac{1}{4}$, there is a maximum allowed value of Ω for which we can have black holes. This value corresponds to the minimum mass $M_{\rm c}(A)$. Moreover, we can deduce from (6.29) that as the angular momentum parameter A grows the minimum required mass for the existence of horizons $M_{\rm c}(A)$ increases. For the classically critical

black hole with $A = \frac{1}{4}$ we find that $\Omega = 0$ and so that $M_{\rm c}(A = \frac{1}{4}) \to \infty$ implying that only macroscopic black holes can reach this limit.

The vanishing of (6.29) defines the relation between A and Ω when we are at criticality. Then, we can find the radius of the critical horizon by solving $\tilde{\Delta}(x) = 0$ and $\tilde{\Delta}'(x) = 0$ simultaneously. This gives

$$x_{\rm c} = \frac{3}{8} + \frac{1}{8}\sqrt{9 - 32(A + \Omega)}, \tag{6.30}$$

where it should be kept in mind that A and Ω are implicitly related through the vanishing of (6.29) and the radius of the critical horizon is a function of only one parameter, $x_{\rm c}(A)$ or $x_{\rm c}(\Omega)$. This reflects the two directions of criticality in rotating black holes. After some analysis we find that the value of $x_{\rm c}$ for every possible A and Ω ranges from $x_{\rm c} = 0.5$ to $x_{\rm c} \simeq 0.55$.

From Fig. 6.3 we can observe how the horizons vary when we change A and Ω. As any of these two parameters grows, the radius of the event horizon gets smaller and that of the inner Cauchy horizon gets bigger. The two horizons meet, when we have reached the extreme configuration, at the critical horizon $x_{\rm c}$. This behaviour is verified if we look at the variation of the roots with respect to A and Ω

$$\partial_\Omega x_\pm = -\frac{\partial_\Omega \tilde{\Delta}|_{x_\pm}}{\tilde{\Delta}'(x_\pm)}, \qquad \partial_A x_\pm = -\frac{\partial_A \tilde{\Delta}|_{x_\pm}}{\tilde{\Delta}'(x_\pm)}. \tag{6.31}$$

Since, $\partial_\Omega \tilde{\Delta}|_{x_\pm}$ and $\partial_A \tilde{\Delta}|_{x_\pm}$ are always positive while $\tilde{\Delta}'(x_\pm)$ is positive at x_+ and negative at x_-, it is implied that $\partial_\Omega x_\pm$ and $\partial_A x_\pm$ are negative at the event horizon and positive at the Cauchy horizon. Note that this result is independent of dimensionality and it is true for every d.

6.3.5 Five dimensions

Classical Myers-Perry black holes with $d = 5$ is a marginal case where there is only one horizon if a condition between angular momentum and mass is satisfied. In terms of dimensionless variables this condition reads $A \leq 1$.

Now, the result of quantum effects is both to alter the horizon structure and to modify the condition for the existence of horizons. The horizon structure is modified as soon as we leave the classical limit. This is seen from the equation (6.27) which gives the horizons. As soon as Ω takes any non-zero value, spacetime develops a second (Cauchy) horizon provided that solutions to (6.27) exist. When we reach the critical black hole configurations these two horizons meet at $x_{\rm c}$. This structural change can be observed in Fig. 6.3.

The condition for the existence of horizons changes from being a simple bound on the ratio of angular momentum over the mass to a more complicated condition which depends on the mass scale of the black hole. We find this condition by solving simultaneously the two equations $\tilde{\Delta}(x) \leq 0$ and $\tilde{\Delta}'(x) = 0$. Then we obtain the following relation for the allowed values of Ω and A

$$\Omega \leq \frac{5 - \sqrt{24A+1}}{1 + \sqrt{24A+1}} \left(\frac{1}{6} - A + \frac{1}{6}\sqrt{24A+1} \right)^{3/2} . \tag{6.32}$$

The relation reflects the two directions of criticality. For every angular momentum parameter $A \leq 1$ there exist a minimum mass $M_c(A)$ for which we can have black holes. As A increases then $M_c(A)$ grows and the classically critical black hole with $A = 1$ can be reached only by macroscopic black holes, since in that case $M_c(A = 1) \to \infty$. Similarly, we can read the condition (6.32) as it defines the maximum allowed ratio $A_c(M)$ for every mass. The horizons and the allowed phase space of five dimensional black holes are plotted in Fig. 6.3.

Solving for $\tilde{\Delta}(x) = 0$ and $\tilde{\Delta}'(x) = 0$ simultaneously we find that for the radius of critical horizon is given by

$$x_c = \left(\frac{1}{6} - A + \frac{1}{6}\sqrt{24A+1} \right)^{1/2} . \tag{6.33}$$

Similarly, the radius of the critical horizon can be expressed in terms of the mass scale Ω if we solve (6.32) for A and substitue back to (6.33). In either case the critical horizon ranges from $x_c = \sqrt{6}/4$ to $x_c = 0$.

The general behaviour of the horizons is the same as in four dimensions. This can be confirmed by looking again at the equations (6.31). As either A or Ω increases the radius of the event horizon gets smaller, the radius of the Cauchy horizon grows and they meet when we reach $M_c(A)$ or $A_c(M)$.

6.3.6 Six and more dimensions

Six and higher dimensional black holes are exceptional in the classical case. This is because they have always one horizon without any restriction to the angular momentum. As a result, there exist black holes with arbitrary large angular momentum, the so-called ultra-spinning black holes. Their horizon structure is similar to that of the Schwarzschild black holes, where there is always one simple event horizon.

The result of quantum effects is to destroy both of these features. In the quantum corrected picture, six or higher dimensional black holes have two horizons (an event horizon and a Cauchy horizon) only if a condition between the mass and the angular momentum

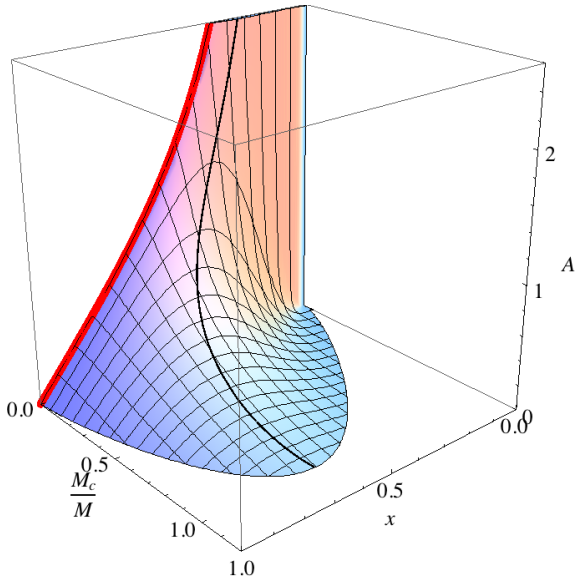

Figure 6.4: The allowed phase space of black hole solutions in six dimensions. The points of the 2-dimensional surface represent the radius of the horizon x, as a function of A and M_c. The thick black line gives the radius of the critical horizon x_c. The regions with $x > x_c(A)$ ($x < x_c(A)$) correspond to event (Cauchy) horizons. The red line represents the classical event horizon.

is satisfied. An arbitrary small value of Ω implies that there is a maximum of the gravitational potential (see Section 6.3.1) and so that there is a maximum value for the angular momentum parameter A. This change of behaviour takes place as soon as we leave from the classical limit as it is seen from the equation (6.27).

In principle, we could solve again the two relations $\tilde{\Delta}(x) \leq 0$ and $\tilde{\Delta}'(x) = 0$ to obtain the condition between A and Ω for the existence of the horizons. However, for arbitrary dimensionality we get the expression

$$3 - d + 2\frac{A}{x_c^2 + A} - (d-2)\frac{\Omega}{x_c^{d-2} + \Omega} \leq 0 \tag{6.34}$$

where we have to keep in mind that x_c and A are implicitly related through the equation

$$1 + \frac{2A}{x_c^2 + A} - (d-2)x_c^{d-5}(x_c^2 + A) = 0 \tag{6.35}$$

A very interesting consequence of quantum effects is that they impose an upper bound in the angular momentum and in addition, that the smaller the black hole mass is, this maximum angular momentum gets smaller and smaller until it should vanish. This has as a result that ultra-spinning black holes do not exist in the presence of quantum effects. To see this more clearly, we make the approximation $\frac{A}{x} \gg 1$ (which corresponds to the ultra-spinning regime) and we solve the two relations $\tilde{\Delta}(x) \leq 0$ and $\tilde{\Delta}'(x) = 0$ in order to find the condition for the existence of horizons in this regime. Then we get

$$\Omega \leq \frac{d-5}{3}\left[A\left(1+\frac{d-5}{3}\right)\right]^{-\frac{d-2}{d-5}}. \tag{6.36}$$

It is evident from the above inequality, that for $d \geq 6$ and $\frac{A}{x} \gg 1$ the maximum allowed Ω gets extremely small, since it scales as an inverse power of A. This means that ultra-spinning black holes exist only in the classical regime, where $M \gg M_c$ and $\Omega \to 0$. We can interpret this feature as the ultra-spinning black holes being unstable under small quantum fluctuations. This behavior of $d \geq 6$ black holes and their allowed phase space of solutions can be observed in Fig. 6.4.

The behaviour of the event and Cauchy horizons as we vary the parameters A and Ω is the same as in the four and five dimensional case. This is verified by looking at the equations (6.31). Then, we observe that for greater A or Ω the event horizon shrinks and the inner horizon grows until they meet for the critical values of the parameters $A_c(M)$ or $M_c(A)$ at the critical horizon.

6.3.7 Ergosphere

From the form of the corrected metric ((6.1) with the substitution $G_N \to G(r)$) we observe that it still possesses the timelike Killing vector $k = \frac{\partial}{\partial t}$. The ergosphere is the region outside the event horizon, where k becomes spacelike,

$$k^\mu k_\mu = g_{tt} = \frac{a^2 \sin^2\theta - \Delta(r)}{\Sigma(r)} > 0 \tag{6.37}$$

with $\Sigma(r)$ and $\Delta(r)$ defined by (6.2). This is a region where an observer cannot remain stationary. All observers in the ergosphere are forced to rotate in the direction of rotation of the black hole. Furthermore, it has been suggested that the ergosphere can be used to extract energy from rotating black holes through the Penrose process [30], [31].

The boundary of ergoregion is modified due to quantum corrections. First, note that we are interested in finding the roots of a new function $E(r) = a^2 \sin^2\theta - \Delta(r)$, which is the original $\Delta(r)$ shifted by an angular-dependent term. Revisiting the analysis of Section 6.3.1 we conclude that $E(r)$ has either two, one or no roots, depending on the values of its parameters. We denote (in dimensionless variables) the larger root of (6.37) as x_{E+} and the smaller as x_{E-}. Then the ergoregion will be the region $x_+ < x < x_{E+}$.

In order to examine the properties of x_{E+}, we write down the function $\tilde{E}(x)$ in terms of dimensionless variables

$$\tilde{E}(x) = -x^2 - A\cos^2\theta + \frac{x^3}{x^{d-2}+\Omega} \tag{6.38}$$

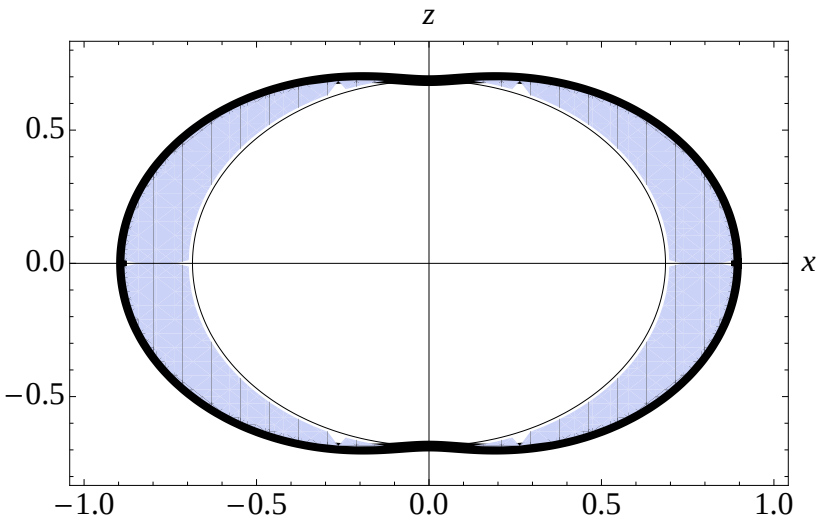

Figure 6.5: The ergosphere in six dimensions with $A = 1/5$ and $\frac{M}{M_c} = 1.56$, plotted in the dimensionless $x - z$ plane with the angular coordinate θ starting from the axis of rotation z. The ergoregion is represented by the shaded region between the event horizon (inner solid line) and the boundary x_{E+} (outer thick line).

and we find its largest root. The form of this equation shows that the solution we are seeking will depend on the angular coordinate θ. The analysis for $\tilde{\Delta}(x)$ is easily extended for $\tilde{E}(x)$ noticing that their only difference is the substitution of the angular momentum term by $A\cos^2\theta$. This means that $\tilde{E}(x)$ interpolates from the zero angular momentum $\tilde{\Delta}(x)|_{A=0}$ at the equatorial plane to the full $\tilde{\Delta}(x)$ at the poles. Moreover, we know from the analysis of $\tilde{\Delta}(x)$ that as the angular momentum parameter A increases the largest root x_+ decrease. Thus, the outer boundary of ergoregion x_{E+} coincides with the event horizon at the poles and as the angle θ grows, x_{E+} grows until it reaches the horizon of the non-rotating limit at $\theta = \pi/2$. The outer boundary of the ergoregion x_{E+} and the event horizon are plotted in the $x - z$ plane in Fig. 6.5.

Next, we should answer the question wether x_{E+} is bigger or smaller than its classical value. This is straightforward if we consult the analysis of the previous sections. Since $\tilde{E}(x)$ is just $\tilde{\Delta}(x)$ with a different angular momentum parameter, its behaviour with varying Ω is the same. That is, if we go to smaller masses and quantum effects become important (Ω gets bigger) then x_{E+} gets smaller. This can be observed also in Fig. 6.6 where we have plotted x_{E+} for different values of Ω.

Finally, we have to comment if any modifications to the structure of ergosphere are coming from different dimensions. It should be clear by now that this is not the case. The

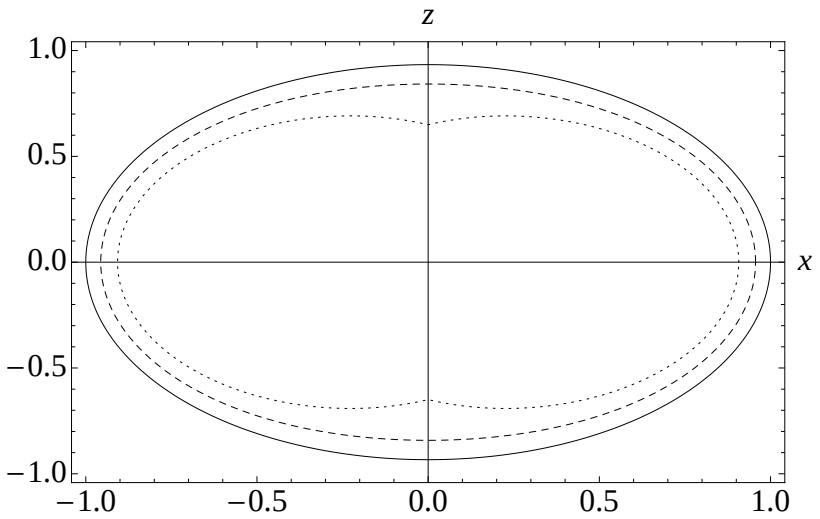

Figure 6.6: The boundary of the ergoregion x_{E+} for rotating black holes with $A = 1/4$ in six dimensions for various black hole masses in the dimensionless $x - z$ plane. Classical, quantum, and critical black holes are represented by a solid, dashed, and dotted line corresponding to the parameters $\frac{M_c}{M} \to 0$, $\frac{M}{M_c} = 2.77$ and $\frac{M}{M_c} = 1.72$, respectively.

function $\tilde{E}(x)$ follows the behaviour of $\tilde{\Delta}(x)$ and it has always two, one or no horizons for every dimensionality. Since we are interested only for the larger root x_{E+} of $\tilde{E}(x)$, it makes no difference if classically $\tilde{E}(x)$ had only one root (as is the case for $d \geq 5$) or more (as in $d = 4$). Moreover, as the angular momentum term in $\tilde{E}(x)$ is always less or equal to that of $\tilde{\Delta}(x)$, the condition for the existence of the event horizon is enough to guarantee the existence of the ergosphere. It also follows that if the function $\tilde{E}(x)$ will have a second root (as in the quantum corrected case) this will always be smaller than x_- and thus will be irrelevant for the ergosphere, which is the region $x_+ < x < x_{E+}$.

6.4 Thermodynamics

The second part of our analysis will deal with the thermodynamical properties of the quantum corrected black holes. First, we present some basic properties of our spacetime, such as the angular velocity, the area and the surface gravity of the horizon. Then, we examine the temperature and the specific heat.

6.4.1 Killing vectors

For studying the thermodynamical properties of black holes we make use of the Killing vectors of the spacetime. We observe from the corrected form of (6.1) that we still have both Killing vectors present in the classical case, namely $k = \frac{\partial}{\partial t}$ and $m = \frac{\partial}{\partial \phi}$ associated with time translations and axisymmetry, respectively. We note that the results of this section are applicable for a generic form of the function $G(r)$ which parametrizes the running of Newton's constant.

We begin by finding the null generator of the event horizon. In order to avoid a coordinate singularity at the horizon, we proceed with the coordinate transformation

$$du = dt + \frac{r^2 + a^2}{\Delta} dr, \qquad d\chi = d\phi + \frac{a}{\Delta} dr. \tag{6.39}$$

In these coordinates the Killing vectors are $k = \frac{\partial}{\partial u}$ and $m = \frac{\partial}{\partial \chi}$. The vector field normal to a hypersurface $S = const.$ is given by $l = f(x)\,(g^{\mu\nu}\partial_\nu S)\,\frac{\partial}{\partial x^\mu}$, where $f(x)$ is an arbitrary function. Using $S = r - r_+$ we find the normal vector at the event horizon

$$l_+ = \frac{a^2 + r_+^2}{r_+^2 + a^2 \cos^2\theta} \cdot f(r_+) \cdot \xi \tag{6.40}$$

where the vector ξ is given by

$$\xi = \frac{\partial}{\partial u} + \frac{a}{a^2 + r_+^2} \cdot \frac{\partial}{\partial \chi}. \tag{6.41}$$

It is easy to verify that the normal vector l_+ is null ($l_+^2 = 0$) and that the vector ξ is a Killing vector of the metric transformed by (6.39). As a result, we have that the event horizon is a Killing horizon of the Killing vector field ξ.

6.4.2 Angular velocity

The angular velocity of the horizon Ω_H is found by comparing orbits of the Killing vector k (which correspond to static particles), with orbits of the Killing vector ξ (which generates the event horizon). We find

$$\Omega_H = \left.\frac{d\phi}{dt}\right|_{r=r_+} = \frac{a}{r_+^2 + a^2}\,. \tag{6.42}$$

The functional form of this quantity is identical to its classical counterpart [113], except for the value of r_+ which is different from its classical value.

6.4.3 Horizon area

An expression for the area of the horizon is given by the integral $\int \sqrt{g^{(d-2)}} d\theta d\phi d\Omega_{d-4}$, performed at the event horizon, with $g^{(d-2)}$ the metric which corresponds to the geometry

of the horizon. We find

$$\mathcal{A}_H = r_+^{d-4}(r_+^2 + a^2)\Omega_{d-2}. \tag{6.43}$$

This expression is functionally the same as the classical one upon replacing the classical horizon radius by r_+.

6.4.4 Surface gravity

For a Killing horizon of a Killing vector ξ, the surface gravity κ is defined as

$$\xi^\nu \nabla_\nu \xi^\mu = \kappa\, \xi^\mu. \tag{6.44}$$

After substituting ξ as in (6.41) and performing the algebra we find the surface gravity as

$$\kappa = \frac{\partial_r \Delta|_{r=r_+}}{2(r_+^2 + a^2)} = \frac{1}{2r_+}\left(\frac{2r_+^2}{r_+^2 + a^2} + d - 5 + \eta(r_+)\right), \tag{6.45}$$

where $\eta(r_+) = -r_+\frac{G'(r_+)}{G(r_+)}$ is the anomalous dimension. The expression reduces to the classical one if, firstly, r_+ is replaced by the classical radius and, secondly, the term proportional to the anomalous dimension is dropped. We recall that (6.18)

$$\eta(r_c) = 5 - d - 2\frac{r_c^2}{r_c^2 + a^2} \tag{6.46}$$

in the case of a critical black hole where $r_+ = r_c$, independently of the specific RG running. We thus conclude that critical black holes have zero surface gravity. For future use, we note that $\eta(r_+)$, for a running Newton's constant given by (6.12) is a monotonically increasing function of g_*, starting from (6.46), when we are at $M_c(\alpha)$ and taking its maximum value $\eta(r_+) = 0$ in the classical limit.

6.4.5 Temperature

Using the techniques of quantum field theory in curved spacetime, Hawking showed that black holes radiate like thermal objects with temperature $T = \kappa/(2\pi)$, where κ is the surface gravity of the event horizon [77]. Another method for identifying the temperature with $\kappa/(2\pi)$ comes from Euclidean quantum gravity techniques [61] where an identification in imaginary time with period $\beta = 2\pi/\kappa$ is required in order to produce a smooth Euclidean manifold. In either case it is confirmed that the black hole temperature is a property of the spacetime itself, independent of which theory of gravity determines the geometry [19], [84].

Thus, it is straightforward to confirm that also in our case the formula for the temperature of the improved black holes is obtained by dividing the surface gravity (6.45) by

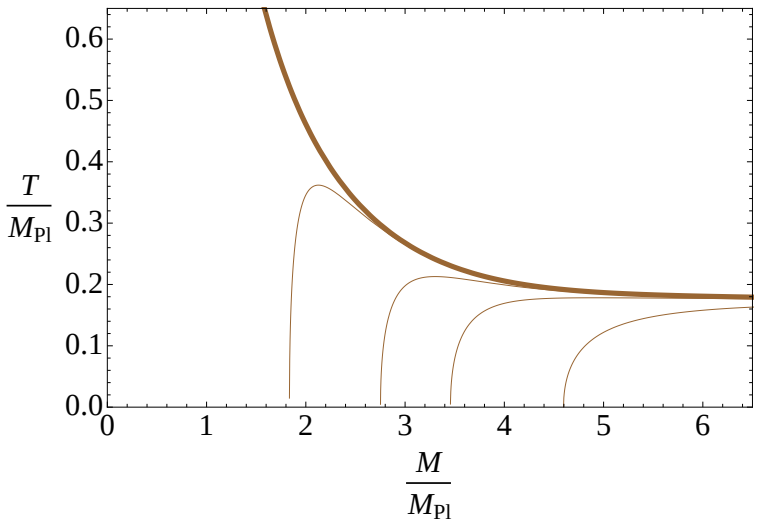

Figure 6.7: The temperature for various values of $M_c(a)$ in $d = 7$ and fixed angular momentum $J = 10$. The thick line corresponds to the classical temperature, while the other lines correspond to (from left to right) $M_c(a)/M_{Pl} = 1.83$, $M_c(a)/M_{Pl} = 2.75$, $M_c(a)/M_{Pl} = 3.45$ and $M_c(a)/M_{Pl} = 4.6$. We can verify that for smaller g_* (larger $M_c(a)$) the temperature gets smaller.

2π,

$$T = \frac{\kappa}{2\pi} = \frac{1}{4\pi r_+}\left(\frac{2r_+^2}{r_+^2 + a^2} + d - 5 + \eta(r_+)\right). \tag{6.47}$$

The temperature depends on all the parameters of the spacetime. Apart from its explicit dependence, it is also implicitly dependent on these parameters, since the event horizon is a function of mass, angular momentum parameter a and g_*, i.e. $r_+ = r_+(M, J, g_*)$.

From the expression (6.45) for surface gravity and the limit values of $\eta(r_+)$, we see that for large enough masses the temperature will be positive. If there exists an extremal black hole (i.e. $\Delta'(r_+) = 0$), then when mass gets its critical value $M_c(a)$, the temperature vanishes. If the spacetime does not exhibit an extremal solution, then the temperature remains positive, and it diverges as r_+ tends to zero.

We saw in the previous Sections that four and five dimensional black holes exist only up to a critical mass $M_c(a)$, both in the classical and the quantum regimes. Their temperature always reaches a maximum and vanishes when their mass reaches $M_c(a)$. However, in six or higher dimensions there are no extreme configurations in the classical limit and the temperature diverges as $r_+ \to 0$. The picture is modified once quantum corrections are taken into account, since then black holes only exist up to a critical value $M_c(a)$. Consequently, the temperature reaches a maximum. This change of behaviour can be seen in Fig. 6.7 where the temperature in seven dimensions is plotted both for the classical

and the improved black holes.

It is instructive to see how the temperature varies with the mass and g_*. We begin with the variation with respect to g_*. As explained before, this corresponds to changing the critical mass $M_c(a)$ at fixed angular momentum J, given by the relation

$$\frac{dT}{dg_*} = \frac{1}{4\pi}\left[\left(\frac{\Delta''(r_+)}{r^2+a^2} - \frac{2r_+\Delta'(r_+)}{(r^2+a^2)^2}\right)\frac{\partial r_+}{\partial g_*} - \frac{1}{r_+}\frac{\partial \eta(r_+)}{\partial g_*}\right] \tag{6.48}$$

It follows that for a running of the form (6.12) the above expression is always negative. Moreover it is checked that by restoring the power γ in our matching the same holds true for $\gamma > (\sqrt{2}-1)/(2d-4)$. Thus, for fixed mass and angular momentum a larger $M_c(a)$ implies a smaller temperature. Consequently, when quantum corrections are considered the temperature is always smaller than the classical one, i.e. $T_{\rm cl}(M,J) > T_{g_*}(M,J)$. We can observe the dependence of temperature to the critical mass $M_c(a)$ by looking at the Fig. 6.7.

6.4.6 Specific heat

The specific heat at constant angular momentum is defined as

$$C_J = \left.\frac{\partial M}{\partial T}\right|_J . \tag{6.49}$$

We are particularly interested on the sign of this quantity, since a positive specific heat implies a thermodynamically stable system. After some algebra we find

$$C_J = -(d-2)\,\pi\,\Omega_{d-2}\,G(r_+)\,\frac{r_+^{d-3}(a^2+r_+^2)^3\,T}{D(r_+)}, \tag{6.50}$$

where T is the temperature, and $D(r_+)$ is given by

$$\begin{aligned} D(r_+) = {} & \left[3(d-5)a^4 - 6a^2r_+^2 + (d-3)r_+^4\right]G(r_+)^2 \\ & - r_+^2(a^2+r_+^2)(3a^2+r_+^2)G'(r_+)^2 + r_+^2 G(r_+)\left[4a^2 r_+ G'(r_+) + (a^2+r_+^2)(3a^2+r_+^2)G''(r_+)\right]. \end{aligned} \tag{6.51}$$

In the classical limit we have $G'(r_+) = 0 = G''(r_+)$ and the last two terms of (6.51) vanish. The fact that the temperature reaches a maximum and then vanishes at M_c in four and five dimensions is reflected by a pole and a change of sign in the specific heat (see Fig. 6.8). For six or higher dimensions the temperature is a monotonically decreasing function of mass, and the specific heat remains always negative (see Fig. 6.9).

When quantum corrections are considered in four and five dimensions the qualitative behaviour of the specific heat is not changed. However, the point where specific heat

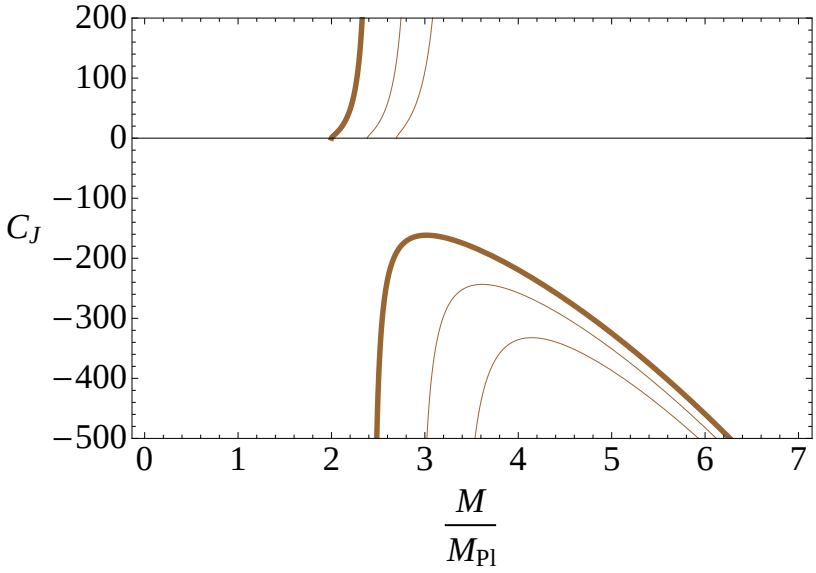

Figure 6.8: The specific heat for various values of $M_{\rm c}(a)$ in $d = 4$ and fixed angular momentum $J = 10$. The thick line corresponds to the classical specific heat, while the thin lines correspond to (from left to right) $M_{\rm c}(a)/M_{\rm Pl} = 2.4$ and $M_{\rm c}(a)/M_{\rm Pl} = 2.7$. We observe that due to the fact that both in the classical and quantum cases there exist an extreme black hole there is no change in the qualitative behaviour of C_J.

becomes positive is shifted to bigger masses. For six or higher dimensions the effect of the quantum correction terms in (6.51) is that they induce always one pole at C_J for some value of the mass. For masses sufficiently small, the specific heat becomes positive and vanishes at $M_{\rm c}(a)$. It is seen from (6.51) that the bigger the value of $M_{\rm c}$ is, the pole is shifted towards bigger masses.

6.5 Mass and energy

6.5.1 Energy momentum tensor

Myers-Perry black holes represent vacuum solutions of rotating spacetimes in higher dimensions. However, when we consider quantum corrections, the resulting spacetimes are not vacuum solutions of Einstein's equations and we can think of them as arising from an effective energy momentum tensor $T^{(\rm eff)}_{\mu\nu}$. We find this tensor by substituting the improved

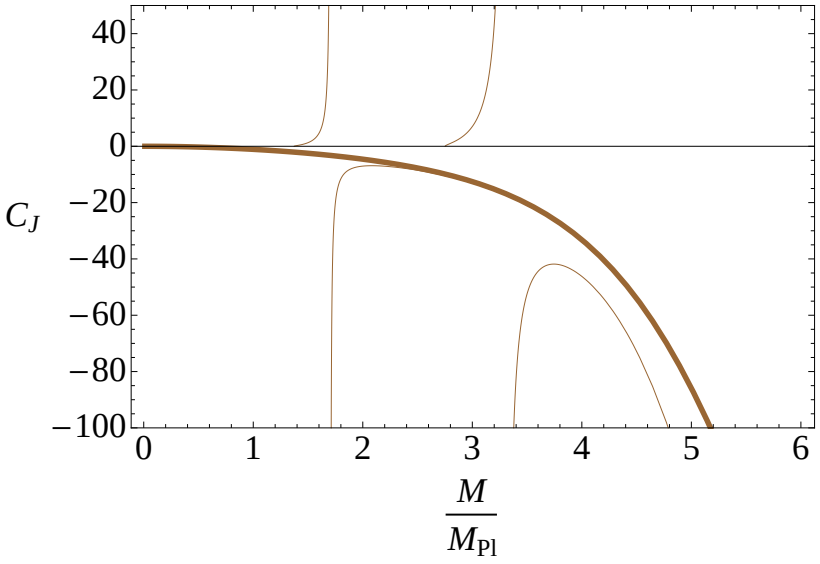

Figure 6.9: The specific heat for various values of $M_{\rm c}(a)$ in $d = 7$ and fixed angular momentum $J = 10$. The thick line corresponds to the classical specific heat which is always negative, while the thin lines correspond to (from left to right) $M_{\rm c}(a)/M_{\rm Pl} = 1.83$, $M_{\rm c}(a)/M_{\rm Pl} = 2.75$ and have a pole where C_J becomes positive for small masses.

metric into Einstein's equation $G_{\mu\nu} = 8\pi G_N T^{(\rm eff)}_{\mu\nu}$, leading to

$$T^{\mu(\rm eff)}_{\nu} = \begin{pmatrix} T^t_t & 0 & 0 & T^t_\phi & 0 & \cdots & 0 \\ 0 & T^r_r & 0 & 0 & \vdots & & \vdots \\ 0 & 0 & T^\theta_\theta & 0 & \vdots & & \vdots \\ T^\phi_t & 0 & 0 & T^\phi_\phi & 0 & & \vdots \\ 0 & \cdots & \cdots & 0 & \ddots & 0 & \vdots \\ \vdots & & & & 0 & T^i_i & 0 \\ 0 & \cdots & \cdots & \cdots & \cdots & 0 & \ddots \end{pmatrix} \tag{6.52}$$

where $4 \leq i \leq d-1$ label the extra dimensions. We write a general entry of $T^{\mu(\rm eff)}_{\nu}$ as

$$T^{\mu}_{\nu} = U^{\mu}_{\nu} G'(r) + V^{\mu}_{\nu} G''(r), \tag{6.53}$$

where in the classical limit $G'(r) = 0 = G''(r)$ and $T^{\mu}_{\nu} = 0$ as expected. Then, we calculate the components and we find the coefficients U^{μ}_{ν} and V^{μ}_{ν}. Their values are given in Appendix C.2.

In order to examine the properties of the energy-momentum tensor we diagonalize (6.52) and check the energy-conditions. After diagonalising the energy momentum tensor

we get

$$T = \text{diag}(p_i), \qquad i = \{0, \cdots, d-1\} \tag{6.54}$$

where $p_0 \equiv -\rho$ is minus the energy density, $p_1 = p_r$ and $p_2 = p_3 = p_\perp$, and p_i for $i \geq 4$ arise from the higher dimensions. The energy density ρ and p_3 arise after diagonalisation of (6.52) while p_r and p_2 originate directly from the T^r_r and T^θ_θ. We refer to the Appendix C.2 for explicit expressions of these quantities. Note that $\rho = -p_r$ and that $p_2 = p_\perp = p_3$.

In classical general relativity many properties of the spacetime depend on the energy conditions which are expressed as inequalities between the components of the energy momentum tensor. For this reason we compute the following relations relevant to these conditions:

$$\rho \geq 0 : \qquad \left[(d-2)r^2 + (d-4)a^2\cos^2\theta\right] G'(r) \geq 0 \tag{6.55}$$

$$\rho + p_\perp \geq 0 : \quad \left[(d-2)r^2 + (d-6)a^2\cos^2\theta\right] G'(r) - r\left(r^2 + a^2\cos^2\theta\right) G''(r) \geq 0 \tag{6.56}$$

$$\rho + p_i \geq 0 : \quad \left[(d-2)r^2 + (d-4)a^2\cos^2\theta\right] G'(r) - r\left(r^2 + a^2\cos^2\theta\right) G''(r) \geq 0 \tag{6.57}$$

$$\rho - p_\perp \geq 0 : \qquad (d-2)G'(r) + r\, G''(r) \geq 0 \tag{6.58}$$

$$\rho - p_i \geq 0 : \quad \left[(d-2)r^2 + (d-4)a^2\cos^2\theta\right] G'(r) + r\left(r^2 + a^2\cos^2\theta\right) G''(r) \geq 0 \tag{6.59}$$

with the index i being equal or greater than 4. The sign of the above inequalities and consequently the validity of the energy conditions strongly depend on the running of Newton's coupling through its first and second derivative.

We now turn to the energy conditions. For a diagonalised energy-momentum tensor the *weak energy condition* reads

$$\rho \geq 0 \qquad \text{and} \qquad \rho + p_i \geq 0, \qquad 1 \leq i \leq d-1. \tag{6.60}$$

From the relation (6.55) we conclude that the sign of ρ depends only on the sign of $G'(r)$ and in our case we have that $G'(r) > 0$ so that the first requirement of the weak energy condition is always satisfied. Moreover, as stated above we have that $\rho + p_r = 0$ and so for the validity of the weak energy condition we have to examine the remaining two relations $\rho + p_\perp \geq 0$ and $\rho + p_i \geq 0$ with $i \geq 4$. The first of them is given by (6.56) and for a function $G(r)$ given by (6.12) this expression has one root (denoted by r_{w1}). The condition is violated for $0 < r < r_{w1}$. It is interesting to note that in the limit of zero angular momentum this condition is not violated. Moreover, the same holds true in the special case where $\theta = \pi/2$. The second relation we need to examine takes the form (6.57). This relation has exactly the same behaviour as $\rho + p_\perp$ and is violated for $0 < r < r_{w2}$

only when $a \neq 0$ and $\theta \neq \pi/2$. Here, r_{w2} denotes the root of the expression on the LHS of (6.57).

Next we examine the validity of the *dominant energy condition* which reads

$$\rho \geq 0 \qquad \text{and} \qquad -\rho \leq p_i \leq \rho, \qquad 1 \leq i \leq d-1. \tag{6.61}$$

For this condition to hold, the weak energy condition should be fulfilled. We saw that there exist special cases that this is true. So, now we have to examine the relations $\rho - p_i \geq 0$. Again, the condition $\rho - p_r \geq 0$ is always satisfied. The requirement that $\rho - p_\perp \geq 0$ takes the form (6.58) and for $G(r)$ given by (6.12) is violated for $r > r_{d1}$, where r_{d1} is the only root of this expression. The remaining relations of the dominant energy condition are $\rho - p_i \geq 0$ with $i \geq 4$, and they take the form of (6.59). However, for the only case where the weak energy condition is satisfied ($a = 0$ or $\theta = \pi/2$), the above condition reduces to (6.58) and does not give any new information.

6.5.2 Curvature singularities

In classical general relativity, singularity theorems [75] state that whenever an event horizon is formed, a curvature singularity is hidden behind this horizon. However, their derivation relies on the positivity conditions of any energy momentum present in the spacetime. The fact that the RG-improved black holes violate some of these conditions opens the possibility that the spacetime may not exhibit any singularities.

Here we are going to briefly comment on the fate of the singularities in our improved spacetime. We compute two curvature invariants, the Ricci scalar R and the Kretschmann invariant $K = R_{\mu\nu\rho\sigma}R^{\mu\nu\rho\sigma}$, and examine their behaviour in the region of the classical ring singularity at $r = 0$ and $\theta = \frac{\pi}{2}$. Analytic expressions for these two quantities are given in Appendix C.3.

We begin with the Ricci scalar where classically we have $R = 0$. Now, we substitute (6.12) and find that a divergence at $r = 0$, $\theta = \frac{\pi}{2}$ as

$$R \sim \frac{1}{\epsilon} \tag{6.62}$$

for $\epsilon \to 0$. We observe that there is a ring singularity. For the Kretschmann invariant we have

$$K \sim \frac{1}{\epsilon^2} \tag{6.63}$$

for $\epsilon \to 0$. We observe that there is still a ring singularity at $r = 0$, $\theta = \frac{\pi}{2}$ but it is significantly softened compared to the classical case where $K \sim \frac{1}{\epsilon^{2d-2}}$.

In order to study the effects of different matchings between momentum and position scales on the behaviour of the singularities we approximate the running of the gravitational coupling near the origin by

$$M\,G(r) = \mu^{\sigma}\, r^{\sigma+d-3}, \tag{6.64}$$

as it was done in [54], where μ is a parameter which is fixed by the renormalisation group with dimensions of mass. Then, by substituting this into our expressions in Appendix C.3 we find that the Ricci scalar diverges as

$$R \sim \frac{1}{\epsilon^{2-\sigma}} \tag{6.65}$$

and the Kretschmann invariant as

$$K \sim \frac{1}{\epsilon^{4-2\sigma}}. \tag{6.66}$$

The above results indicate that quantum corrections have the property to significantly soften the black hole singularities. The matching we are using in here corresponds to $\sigma = 1$ and it already brings down the divergence of the ring singularity from order 6 to order 2. By using slightly different matchings we observe that the singularities can be cured even further and we point out that the spacetime is regular when $\sigma \geq 2$. This results have already been obtained for the non-rotating case [23], [54] and we observe that the addition of rotation does not alter this picture, apart from the fact that the singularity is now a ring singularity at $r = 0$, $\theta = \frac{\pi}{2}$.

6.5.3 Mass and angular momentum

The notion of mass and angular momentum in general relativity is quite puzzling. However, in stationary, asymptotically flat spacetimes we can use the Killing vectors associated with time translations and rotations to define the total mass and angular momentum of the spacetime, respectively. This is done by associating a conserved charge to each Killing vector through the Komar integrals [90]

$$Q_{\xi}(\partial\Sigma) = c \oint_{\partial\Sigma} \nabla^{\mu}\xi^{\nu} d\Sigma_{\mu\nu} \tag{6.67}$$

where ξ is the Killing vector, Σ is a spacelike hypersurface, $\partial\Sigma$ its boundary, $d\Sigma_{\mu\nu}$ is the surface element of $\partial\Sigma$ and c is a constant. In order to get the total mass of the spacetime, the boundary $\partial\Sigma$, which is a two-sphere, is taken at infinity or at any exterior vacuum region.

This result was generalized [13] for a spacetime containing a black hole and it is now given in terms of a boundary integral at the horizon and a hypersurface integral at the

region between the horizon and $\partial\Sigma_\infty$ at infinity. After fixing the constant c, we have the following formula for the mass of a stationary asymptotically flat spacetime in d dimensions [113]

$$M = -\frac{1}{16\pi G_N}\frac{d-2}{d-3}\left[2\int_\Sigma R^\mu_\nu k^\nu d\Sigma_\mu + \oint_{\mathcal{H}} \nabla^\mu k^\nu d\Sigma_{\mu\nu}\right] \tag{6.68}$$

where the integral over Σ is performed from the horizon until $\partial\Sigma_\infty$ and $d\Sigma_\mu$ is the surface element on Σ. We consider the first integral as it gives the contribution to the total mass of the matter outside the event horizon and the second integral as the mass of the black hole. Using Einstein's equations one can express the first integral in terms of the energy momentum tensor as $\int_\Sigma \left(T^\mu_\nu k^\nu - \frac{1}{2}Tk^\mu\right) d\Sigma_\mu$. Similarly, the angular momentum of a stationary and asymptotically flat spacetime is defined as

$$J = -\frac{1}{16\pi G_N}\left[2\int_\Sigma R^\mu_\nu m^\nu d\Sigma_\mu + \oint_{\mathcal{H}} \nabla^\mu m^\nu d\Sigma_{\mu\nu}\right]. \tag{6.69}$$

We note, that classical Myers-Perry black holes are vacuum solutions of Einstein's equations. Then, it is straightforward to find that the Komar integrals performed at the horizon return the physical mass and angular momentum of the black holes. As we saw in the previous section, our spacetime features an effective energy momentum tensor and we would like to know how this affects the mass and the angular momentum of the black holes. In what follows we are going to denote the boundary integrals at the horizon by

$$\begin{aligned} M_{\mathcal{H}} &= -\frac{1}{16\pi G_N}\frac{d-2}{d-3}\oint_{\mathcal{H}} \nabla^\mu k^\nu d\Sigma_{\mu\nu} \\ J_{\mathcal{H}} &= -\frac{1}{16\pi G_N}\oint_{\mathcal{H}} \nabla^\mu m^\nu d\Sigma_{\mu\nu}. \end{aligned} \tag{6.70}$$

At first, we would like to verify that the total mass and angular momentum of the spacetime remain the same. To do this we perform the integral (6.67) at $\partial\Sigma_\infty$ for the two Killing vectors and we find that they indeed return $Q_k(\partial\Sigma_\infty) = M_{\text{phys}}$ and $Q_m(\partial\Sigma_\infty) = \frac{2}{d-2}\, a\, M_{\text{phys}} = J$.

Now, it is interesting to see the modifications to the mass and angular momentum of the black holes, due to quantum corrections. Performing the boundary integral for the timelike Killing vector, we get the following expression for the mass of a black hole

$$M_{\mathcal{H}} = M_{\text{phys}}\frac{G(r_+)}{G_N}\left[1 + \frac{\eta(r_+)}{d-3}\cdot F\right], \tag{6.71}$$

where $F = {}_2F_1\left(1, 1; \frac{d-1}{2}; \frac{a^2}{r_+^2+a^2}\right)$ is the Gaussian hypergeometric function. By substituting $d = 4$ in (6.71) we recover the Komar mass of the four dimensional black holes as found in [134].

We note some interesting properties of this expression. Since all its parameters are positive, the hypergeometric function in (6.71) will be positive. Thus, for a theory where

the gravitational coupling becomes weaker (so $\eta(r)$ is negative) the mass of the black hole will be less than the physical mass $M_{\rm phys}$.

We are now interested on how $M_{\mathcal{H}}$ varies when we change the parameters a and g_*. We find that as either of them grow the Komar mass gets smaller. Thus, the black holes will have their minimum mass when they are in a critical configuration. Moreover, it is easily shown that the Komar mass reaches an absolute minimum value $M_{\mathcal{H}} = 0$ when the black holes are in one of the two following critical configurations. First, for every dimension, for a critical non-rotating black hole we have $M_{\mathcal{H}} = 0$, since the term inside the square brackets becomes $1 + \eta(r_{\rm c})/(d-3)$, which vanishes. The second case where the horizon mass vanishes, is when we have a critical ultra-spinning black hole. In this case we have $\frac{r_{\rm c}}{a} \to 0$ and again we get from (6.71) that $M_{\mathcal{H}} \to 0$.

Similarly, we can compute the Komar integral for the Killing vector m to find the angular momentum of the black holes. This is given by the expression

$$J_{\mathcal{H}} = J\frac{G(r_+)}{G_N}\left[1 + \frac{1}{2}\eta(r_+)\left(\frac{r_+^2}{a^2} + 1\right)(F-1)\right]. \tag{6.72}$$

Again, the limit $d = 4$ reduces this formula to that obtained in [134] for the Komar angular momentum of the RG-improved Kerr solution. Inspection of the above formula shows that the angular momentum of the horizon is always less than the classical value J. However, in contrast to the Komar mass, this formula can turn negative for some values of the parameters, which implies that the effective rotation of the horizon is in the opposite direction.

6.5.4 Remarks on the laws of black hole mechanics

Having reviewed the basic thermodynamical properties of the quantum corrected space-times, we are able to discuss their implications to the laws of black hole mechanics. Here, we are going to briefly comment on possible deviations from these classical laws.

First, we want to examine the validity of the integral formula

$$M_{\mathcal{H}} - 2\Omega_H J_{\mathcal{H}} = \frac{\kappa}{4\pi}\mathcal{A}_H. \tag{6.73}$$

This is the analogue of Smarr's formula [140] for a stationary axisymmetric spacetime (not necessary in vacuum) which contains a black hole. Then, the values of mass, angular momentum and area at the horizon are related through the relation (6.73). It follows directly from the derivation of [13] that the integral formula is a concequence only of the properties of the Killing vectors and of the constancy of surface gravity on the horizon. Thus, we expect that in the case of quantum corrections parametrized by $G(r)$ this will

still hold true. Indeed, we can also verify the validity of the integral formula by using the expressions of $M_{\mathcal{H}}$ and $J_{\mathcal{H}}$ obtained in the previous section.

The zeroth law states that the surface gravity of a stationary black hole is constant over the event horizon. It is easily seen, directly from the expression for the surface gravity

$$\kappa = \frac{1}{2\,r_+}\left(\frac{2\,r_+^2}{r_+^2+a^2} + d - 5 + \eta(r_+)\right), \tag{6.74}$$

that the zeroth law holds in our case. It is interesting to note, that the proof given in [13] relies on the dominant energy condition. However, there are other proofs [27], [127], which instead of this requirement rely on other conditions such as the existence of a bifurcate Killing horizon. Moreover, the proofs can go the opposite way implying that if the surface gravity is constant then there exists a bifurcate Killing horizon.

In the previous two cases we saw that classical relations hold when we consider asymptotically safe black holes. However, this is not in general true for the first law of black hole mechanics. This is the differential law relating variations of the mass, the angular momentum and the area of the black hole

$$dM = \frac{\kappa}{4\pi} d\mathcal{A}_H + \Omega_H dJ. \tag{6.75}$$

In classical Einstein gravity this relation, was first used to identify the entropy of the black hole with the area of the horizon, $S = \mathcal{A}_H/(4\pi)$. Corrections to this simple form of the entropy are well known to exist in theories of modified gravity or when quantum corrections are considered and various techniques have been developed for its calculation [147], [78], [84].

In what concerns us here, we note that it is evident from the original derivation [13], that when Einstein's equations imply an effective EM tensor, we have extra contributions, which take the form

$$dM = \frac{\kappa}{4\pi} d\mathcal{A}_H + \Omega_H dJ_H + d\int T^{\mu}_{\nu} k^{\nu} d\Sigma_{\mu}. \tag{6.76}$$

The term involving the energy-momentum tensor gives a contribution from the angular momentum outside the horizon and also contributions from the energy density and the pressures of the effective matter. It is evident that in general the first law doesn't hold in its classical form given by (6.75). For defining the entropy we should in principle include the additional contributions following the general procedure highlighted in [61], [146]. This is left for future work.

Recently, by studying the four dimensional Kerr black hole within asymptotic safety [134], the authors were motivated by the requirement that there exists an exact one-form

state function $S(M, J)$ and they were led to the modification of the Hawking temperature. However, it was shown by [53] that using a specific class of matchings between the momentum and position space, the first law of black hole mechanics holds in its classical form given by (6.75).

Finally, further investigation requires also the second law of black hole mechanics [76] which states that the area of the event horizon of a black hole does not decrease with time

$$d\mathcal{A}_H \geq 0. \tag{6.77}$$

The proof of the second law relies on the requirement that the energy momentum tensor of the spacetime obeys the dominant energy condition, which is not the case for black holes within asymptotic safety.

6.6 Conclusions

In this Chapter we have studied implications to the physics of rotating black holes due to quantum gravity effects. We have assumed that the leading order corrections come from the renormalisation of the Newton's constant and we implemented a specific running dictated by the asymptotic safety scenario for gravity. These techniques have been previously applied to four dimensional Schwarzschild [23], four dimensional Kerr [133, 134], and higher dimensional spherical symmetric black holes [54]. Here we examined quantum gravity effects in rotating black holes for spacetime dimensions $d \geq 4$.

Our findings show that in contrast to the classical case, in every dimensionality we get the same horizon structure. There always exist a critical mass M_c which is a function of angular momentum and below this mass there are no black hole horizons. Rotating black holes with exactly that mass have one degenerate horizon, while for masses above M_c there are two horizons, an event horizon and a Cauchy horizon, just like in the four dimensional Kerr black holes. These findings imply that there is a qualitative difference from macroscopic black holes for dimensions $d \geq 5$.

The existence of a critical mass M_c means that solutions of rotating black holes with arbitrarily high angular momentum in six or more dimensions cease to exist as the mass gets smaller. This can be interpreted as ultra-spinning black holes being unstable under small quantum fluctuations. We found that the critical mass is growing as a power of angular momentum and so that ultra-spinning black holes can only be macroscopic.

Subsequently, we computed thermodynamic quantities related to quantum corrected black holes such as the temperature and the specific heat. Since the form of the tem-

perature always follows the structure of the horizons we found that for every spacetime dimension we get the same behaviour. For large masses the temperature follows the classical curve, while as we approach M_c it reaches a maximum and then vanishes resulting in a cold remnant. Consequently the specific heat changes sign at the maximum of the temperature and it becomes positive for small masses.

Finally, we studied the implications of the quantum corrections to the singularities and the energy of the black holes. The ring singularity at the centre persist, although it is significantly softened compared to the classical case. The effective energy momentum tensor of our black holes doesn't satisfy the weak and the dominant energy condition, opening up the possibility that the usual laws of thermodynamics do not hold in our case. We found that this is indeed the general case for the first law.

Chapter 7

Conclusion

In this thesis we investigated the quantisation of metric gravity and its applications using renormalisation group techniques. Perturbative quantisation of gravity faces challenges which stem from the negative mass dimension of Newton's coupling. However, since the conjecture of Weinberg [148] and the development of non-perturbative techniques [153], asymptotic safety emerged as a candidate theory of quantum gravity. Based on the assumption that the renormalisation group flow of gravity approaches a non-trivial fixed point at the UV, it provides a well defined high energy limit for the quantum system. In addition, the requirement that the number of relevant operators remains finite in the vicinity of the fixed point ensures that the theory retains its predictive power.

Every attempt to investigate the renormalisation group flow of gravity has relied on some approximation scheme with the expansion in powers of the Ricci scalar being the most popular. However, in an asymptotically safe theory there is no a-priori ordering principle for the operators and one has to perform a detailed analysis to determine the relevancy of each curvature invariant. Here we developed a new strategy for testing the asymptotic safety conjecture and the validity of the approximation scheme by using a bootstrap approach. We performed a systematic search for fixed points and critical exponents for every order of the expansion up to an unprecedent R^{34}. A self-consistent UV fixed point and three relevant directions were found at each order of the approximation in support of the asymptotic safety conjecture. Moreover, we were able for the first time to estimate the radius of convergence of the expansion and to perform a high precision analysis for the stability of the approximation. More interestingly, it was found that curvature invariants become increasingly irrelevant with increasing mass dimension and that their critical exponents take almost gaussian values. These results provide an ordering principle for the operators based on their canonical dimension and indicate that the situation where

infinitely many eigenvalues become negative is unlikely.

In order to go beyond the $f(R)$ approximation, we investigated the effect from the inclusion of more complicated tensor structures, other than the Ricci scalar. We considered the square of the Ricci tensor and we successively added those terms in the effective average action. The flow equation was computed and a self-consistent UV fixed point was found for every order in the expansion up to order 7. The critical exponents were also calculated and it was found that there are always three attractive directions in the vicinity of the fixed point. These findings suggest that the dynamics of more involved tensors, like the Ricci tensor, do not show the tendency to invalidate the requirements of asymptotic safety.

In the third part of this thesis we investigated the implications of asymptotic safety scenario to the physics of rotating black holes. Classical black holes are fascinating objects with very rich structure but their description within general relativity faces limitations when we approach the scale of quantum gravity. Under the assumption that the leading order quantum corrections come from the replacement of Newton's constant with a momentum dependent coupling we examined the effects of a running gravitational coupling as it is dictated by the asymptotic safety scenario. Interestingly, it was found a qualitative difference in the horizon structure for spacetime dimensions $d \geq 5$. As a result, in every dimension we observe the same picture, with horizons existing down to a minimum mass $M_{\rm cr}$. Moreover, the seminal ultra-spinning black holes which are allowed classically cease to exist under the inclusion of quantum corrections. Implications to curvature singularities and thermodynamical properties were also discussed.

The formulation of a quantum theory for gravity remains an open challenge in theoretical physics. Despite recent advances in the front of asymptotic safety, there are still many open questions associated with the various steps of approximation. In this thesis we have contributed to the understanding of polynomial expansions and of the physics of black holes. Among the many directions that future research can take, we find most intriguing the examination of background dependence, the inclusion of more complicated operators and the investigation of the spacetime structure in the vicinity of the ultra-violet fixed point.

Bibliography

[1] Aad, G. et al. (2012). Observation of a new particle in the search for the Standard Model Higgs boson with the ATLAS detector at the LHC. *Phys.Lett.*, B716:1–29. 3

[2] Adler, S. L. (1982). Einstein Gravity as a Symmetry Breaking Effect in Quantum Field Theory. *Rev.Mod.Phys.*, 54:729. 18

[3] Aida, T. and Kitazawa, Y. (1997). Two loop prediction for scaling exponents in (2+epsilon)-dimensional quantum gravity. *Nucl.Phys.*, B491:427–460. 7

[4] Ambjorn, J., Goerlich, A., Jurkiewicz, J., and Loll, R. (2012). Nonperturbative Quantum Gravity. *Phys.Rept.*, 519:127–210. 5

[5] Antoniadis, I., Arkani-Hamed, N., Dimopoulos, S., and Dvali, G. R. (1998). "New dimensions at a millimeter to a Fermi and superstrings at a TeV". *Phys. Lett.*, B436:257–263. 4

[6] Aoki, K.-I., Morikawa, K., Souma, W., Sumi, J.-I., and Terao, H. (1998). Rapidly converging truncation scheme of the exact renormalization group. *Prog.Theor.Phys.*, 99:451–466. 16

[7] Arkani-Hamed, N., Dimopoulos, S., and Dvali, G. R. (1998). "The hierarchy problem and new dimensions at a millimeter". *Phys. Lett.*, B429:263–272. 4

[8] Ashtekar, A. (1986). New Variables for Classical and Quantum Gravity. *Phys.Rev.Lett.*, 57:2244–2247. 5

[9] Avramidi, I. (2000). Heat kernel and quantum gravity. *Lect.Notes Phys.*, M64:1–149. 12, 22, 134

[10] Babic, A., Guberina, B., Horvat, R., and Stefancic, H. (2005). Renormalization-group running cosmologies. A Scale-setting procedure. *Phys.Rev.*, D71:124041. 8

[11] Baez, J. C. (2000). An Introduction to spin foam models of quantum gravity and BF theory. *Lect.Notes Phys.*, 543:25–94. 5

[12] Ball, R. D., Haagensen, P. E., Latorre, Jose, I., and Moreno, E. (1995). Scheme independence and the exact renormalization group. *Phys.Lett.*, B347:80–88. 16

[13] Bardeen, J. M., Carter, B., and Hawking, S. W. (1973). The Four laws of black hole mechanics. *Commun. Math. Phys.*, 31:161–170. 2, 111, 113, 114

[14] Becker, D. and Reuter, M. (2012). Running boundary actions, Asymptotic Safety, and black hole thermodynamics. *JHEP*, 1207:172. 8, 86

[15] Bekenstein, J. D. (1973). Black holes and entropy. *Phys.Rev.*, D7:2333–2346. 2

[16] Benedetti, D., Machado, P. F., and Saueressig, F. (2009a). Asymptotic safety in higher-derivative gravity. *Mod.Phys.Lett.*, A24:2233–2241. 8, 39, 68, 75, 86

[17] Benedetti, D., Machado, P. F., and Saueressig, F. (2009b). Four-derivative interactions in asymptotically safe gravity. 8, 39, 75

[18] Bervillier, C., Juttner, A., and Litim, D. F. (2007). High-accuracy scaling exponents in the local potential approximation. *Nucl.Phys.*, B783:213–226. 57

[19] Birrell, N. and Davies, P. (1982). *Quantum fields in curved space*. 104

[20] Bjerrum-Bohr, N., Donoghue, J. F., and Holstein, B. R. (2003a). Quantum gravitational corrections to the nonrelativistic scattering potential of two masses. *Phys.Rev.*, D67:084033. 5

[21] Bjerrum-Bohr, N. E. J., Donoghue, J. F., and Holstein, B. R. (2003b). Quantum corrections to the Schwarzschild and Kerr metrics. *Phys.Rev.*, D68:084005. 5

[22] Bonanno, A., Contillo, A., and Percacci, R. (2011). Inflationary solutions in asymptotically safe f(R) theories. *Class.Quant.Grav.*, 28:145026. ix, 40, 54, 58, 65

[23] Bonanno, A. and Reuter, M. (2000). Renormalization group improved black hole spacetimes. *Phys. Rev.*, D62. 8, 86, 92, 111, 115

[24] Burgess, C. (2004). Quantum gravity in everyday life: General relativity as an effective field theory. *Living Rev.Rel.*, 7:5. 5

[25] Burgess, C. (2007). Introduction to Effective Field Theory. *Ann.Rev.Nucl.Part.Sci.*, 57:329–362. 11

[26] Cai, Y.-F. and Easson, D. A. (2010). Black holes in an asymptotically safe gravity theory with higher derivatives. *JCAP*, 1009:002. 8, 86

[27] Carter, B. (1973). Properties of the Kerr metric. In: Black Holes. *Gordon and Breach Science Publishers, New York–London–Paris*, pages 125–214. 114

[28] Chatrchyan, S. et al. (2012). Observation of a new boson at a mass of 125 GeV with the CMS experiment at the LHC. *Phys.Lett.*, B716:30–61. 3

[29] Christensen, S. and Duff, M. (1978). Quantum gravity in two + epsilon dimensions. *Phys.Lett.*, B79:213. 7

[30] Christodoulou, D. (1970). Reversible and irreversible transforations in black hole physics. *Phys.Rev.Lett.*, 25:1596–1597. 100

[31] Christodoulou, D. and Ruffini, R. (1971). Reversible transformations of a charged black hole. *Phys.Rev.*, D4:3552–3555. 100

[32] Codello, A. and Percacci, R. (2006). Fixed points of higher derivative gravity. *Phys.Rev.Lett.*, 97:221301. 8, 39, 86

[33] Codello, A., Percacci, R., and Rahmede, C. (2008). Ultraviolet properties of f(R)-gravity. *Int.J.Mod.Phys.*, A23:143–150. ix, 8, 9, 17, 26, 39, 40, 54, 86

[34] Codello, A., Percacci, R., and Rahmede, C. (2009). Investigating the Ultraviolet Properties of Gravity with a Wilsonian Renormalization Group Equation. *Annals Phys.*, 324:414–469. 8, 21, 39, 40, 44, 86, 134

[35] Contillo, A., Hindmarsh, M., and Rahmede, C. (2011). Renormalisation group improved early universe cosmology and transition to classicality. *AIP Conf.Proc.*, 1458:355–358. 8

[36] Contillo, A., Hindmarsh, M., and Rahmede, C. (2012). Renormalisation group improvement of scalar field inflation. *Phys.Rev.*, D85:043501. 8

[37] De Felice, A. and Tsujikawa, S. (2010). f(R) theories. *Living Rev.Rel.*, 13:3. 39

[38] Dias, O. J., Figueras, P., Monteiro, R., Reall, H. S., and Santos, J. E. (2010a). An instability of higher-dimensional rotating black holes. *JHEP*, 1005:076. 85

[39] Dias, O. J., Figueras, P., Monteiro, R., and Santos, J. E. (2010b). Ultraspinning instability of rotating black holes. *Phys.Rev.*, D82:104025. 85

[40] Dias, O. J., Figueras, P., Monteiro, R., Santos, J. E., and Emparan, R. (2009). Instability and new phases of higher-dimensional rotating black holes. *Phys.Rev.*, D80:111701. 85

[41] Dietz, J. A. and Morris, T. R. (2013). Asymptotic safety in the f(R) approximation. *JHEP*, 1301:108. 8, 39

[42] Dou, D. and Percacci, R. (1998). The running gravitational couplings. *Class.Quant.Grav.*, 15:3449–3468. 8, 25, 26, 39

[43] Eichhorn, A. (2012). Quantum-gravity-induced matter self-interactions in the asymptotic-safety scenario. *Phys.Rev.*, D86:105021. 8, 40

[44] Eichhorn, A. and Gies, H. (2010). Ghost anomalous dimension in asymptotically safe quantum gravity. *Phys.Rev.*, D81:104010. 8, 20, 40

[45] Eichhorn, A. and Gies, H. (2011). Light fermions in quantum gravity. *New J.Phys.*, 13:125012. 8, 40

[46] Eichhorn, A., Gies, H., and Scherer, M. M. (2009). Asymptotically free scalar curvature-ghost coupling in Quantum Einstein Gravity. *Phys.Rev.*, D80:104003. 8, 20, 40

[47] Emparan, R., Harmark, T., Niarchos, V., Obers, N. A., and Rodriguez, M. J. (2007). The Phase Structure of Higher-Dimensional Black Rings and Black Holes. *JHEP*, 10(110). 85

[48] Emparan, R. and Myers, R. C. (2003). Instability of ultra-spinning black holes. *JHEP*, 09. 85

[49] Emparan, R. and Reall, H. S. (2002). A rotating black ring in five dimensions. *Phys. Rev. Lett.*, 88. 85

[50] Emparan, R. and Reall, H. S. (2008). Black Holes in Higher Dimensions. *Living Rev. Rel.*, 11:6. 87

[51] Englert, F. and Brout, R. (1964). Broken Symmetry and the Mass of Gauge Vector Mesons. *Phys.Rev.Lett.*, 13:321–323. 3

[52] Falls, K., Litim, D., Nikolakopoulos, K., and Rahmede, C. (2013). A bootstrap towards asymptotic safety. 38, 39, 86

[53] Falls, K. and Litim, D. F. (2012). Black hole thermodynamics under the microscope. 115

[54] Falls, K., Litim, D. F., and Raghuraman, A. (2012). Black Holes and Asymptotically Safe Gravity. *Int.J.Mod.Phys.*, A27:1250019. 8, 86, 90, 92, 93, 94, 111, 115

[55] Fischer, P. and Litim, D. F. (2006a). Fixed points of quantum gravity in extra dimensions. *Phys.Lett.*, B638:497–502. 8, 39, 86, 90

[56] Fischer, P. and Litim, D. F. (2006b). Fixed points of quantum gravity in higher dimensions. *AIP Conf.Proc.*, 861:336–343. 8, 39

[57] Folkerts, S., Litim, D. F., and Pawlowski, J. M. (2012). Asymptotic freedom of Yang-Mills theory with gravity. *Phys.Lett.*, B709:234–241. 8, 40, 86

[58] Freire, F., Litim, D. F., and Pawlowski, J. M. (2000). Gauge invariance and background field formalism in the exact renormalization group. *Phys.Lett.*, B495:256–262. 18

[59] Gastmans, R., Kallosh, R., and Truffin, C. (1978). Quantum Gravity Near Two-Dimensions. *Nucl.Phys.*, B133:417. 7

[60] Gerwick, E., Litim, D., and Plehn, T. (2011). Asymptotic safety and Kaluza-Klein gravitons at the LHC. *Phys.Rev.*, D83:084048. 90

[61] Gibbons, G. W. and Hawking, S. W. (1977). Action Integrals and Partition Functions in Quantum Gravity. *Phys. Rev.*, D15:2752–2756. 104, 114

[62] Gies, H. (2012). Introduction to the functional RG and applications to gauge theories. *Lect.Notes Phys.*, 852:287–348. 12

[63] Gilkey, P. B. (1995). Invariance theory, the heat equation and the Atiyah-Singer index theorem. 12, 22, 134

[64] Goldstone, J. (1961). Field Theories with Superconductor Solutions. *Nuovo Cim.*, 19:154–164. 3

[65] Goldstone, J., Salam, A., and Weinberg, S. (1962). Broken Symmetries. *Phys.Rev.*, 127:965–970. 3

[66] Golner, G. R. (1986). Nonperturbative renormalization group calculations for continuum spin systems. *Phys.Rev.*, B33:7863–7866. 16

[67] Goroff, M. H. and Sagnotti, A. (1986). The Ultraviolet Behavior of Einstein Gravity. *Nucl.Phys.*, B266:709. 4

[68] Green, M. B., Schwarz, J., and Witten, E. (1987a). *Superstring theory. Vol. 1: Introduction*. Cambridge University Press. 5

[69] Green, M. B., Schwarz, J., and Witten, E. (1987b). *Superstring theory. Vol. 2: Loop amplitudes, anomalies and phenomenology*. Cambridge University Press. 5

[70] Groh, K. and Saueressig, F. (2010). Ghost wave-function renormalization in Asymptotically Safe Quantum Gravity. *J.Phys.*, A43:365403. 8, 20, 40

[71] Gross, D. and Wilczek, F. (1973). Ultraviolet Behavior of Nonabelian Gauge Theories. *Phys.Rev.Lett.*, 30:1343–1346. 3

[72] Gubser, S. S. and Mitra, I. (2001). The Evolution of unstable black holes in anti-de Sitter space. *JHEP*, 0108:018. 85

[73] Guralnik, G., Hagen, C., and Kibble, T. (1964). Global Conservation Laws and Massless Particles. *Phys.Rev.Lett.*, 13:585–587. 3

[74] Harst, U. and Reuter, M. (2011). QED coupled to QEG. *JHEP*, 1105:119. 8, 40, 86

[75] Hawking, S. and Ellis, G. (1973). *The Large scale structure of space-time*. 110

[76] Hawking, S. W. (1972). Black holes in general relativity. *Commun. Math. Phys.*, 26(152-166). 115

[77] Hawking, S. W. (1975). Particle Creation by Black Holes. *Commun. Math. Phys.*, 43:199–220. 2, 104

[78] Hawking, S. W. and Page, D. N. (1983). Thermodynamics of Black Holes in anti-De Sitter Space. *Commun. Math. Phys.*, 87:577. 114

[79] Higgs, P. W. (1964a). Broken Symmetries and the Masses of Gauge Bosons. *Phys.Rev.Lett.*, 13:508–509. 3

[80] Higgs, P. W. (1964b). Broken symmetries, massless particles and gauge fields. *Phys.Lett.*, 12:132–133. 3

[81] Hindmarsh, M., Litim, D., and Rahmede, C. (2011). Asymptotically Safe Cosmology. *JCAP*, 1107:019. 8

[82] Hindmarsh, M. and Saltas, I. D. (2012). f(R) Gravity from the renormalisation group. *Phys.Rev.*, D86:064029. 8

[83] J. Beringer, e. a. (2012). (particle data group). *Phys. Rev. D*, 86(010001). 3

[84] Jacobson, T., Kang, G., and Myers, R. C. (1994). On black hole entropy. *Phys.Rev.*, D49:6587–6598. 104, 114

[85] Kadanoff, L. (1966). Scaling laws for Ising models near T(c). *Physics*, 2:263–272. 3

[86] Kawai, H., Kitazawa, Y., and Ninomiya, M. (1993). Quantum gravity in (2+epsilon)-dimensions. *Prog.Theor.Phys.Suppl.*, 114:149–174. 7

[87] Kawai, H. and Ninomiya, M. (1990). Renormalization Group and Quantum Gravity. *Nucl.Phys.*, B336:115. 56

[88] Kerr, R. P. (1963). Gravitational field of a spinning mass as an example of algebraically special metrics. *Phys.Rev.Lett.*, 11:237–238. 2, 85

[89] Koch, B. and Saueressig, F. (2013). Structural aspects of asymptotically safe black holes. 86

[90] Komar, A. (1959). Covariant conservation laws in general relativity. *Phys. Rev.*, 113:934–936. 111

[91] Lauscher, O. and Reuter, M. (2002a). Flow equation of quantum Einstein gravity in a higher derivative truncation. *Phys.Rev.*, D66:025026. 8, 26, 39, 86, 134

[92] Lauscher, O. and Reuter, M. (2002b). Ultraviolet fixed point and generalized flow equation of quantum gravity. *Phys.Rev.*, D65:025013. 8, 39

[93] Litim, D. F. (1997). Scheme independence at first order phase transitions and the renormalization group. *Phys.Lett.*, B393:103–109. 16

[94] Litim, D. F. (2000). Optimization of the exact renormalization group. *Phys.Lett.*, B486:92–99. 11, 16, 17, 32, 44

[95] Litim, D. F. (2001a). Derivative expansion and renormalization group flows. *JHEP*, 0111:059. 17

[96] Litim, D. F. (2001b). Mind the gap. *Int.J.Mod.Phys.*, A16:2081–2088. 11, 17

[97] Litim, D. F. (2001c). Optimized renormalization group flows. *Phys.Rev.*, D64:105007. 16, 32, 44

[98] Litim, D. F. (2002). Critical exponents from optimized renormalization group flows. *Nucl.Phys.*, B631:128–158. 53, 57

[99] Litim, D. F. (2004). Fixed points of quantum gravity. *Phys.Rev.Lett.*, 92:201301. 8, 39, 86, 90

[100] Litim, D. F. (2006). On fixed points of quantum gravity. *AIP Conf.Proc.*, 841:322–329. 86, 90

[101] Litim, D. F. (2011). Renormalisation group and the Planck scale. *Phil.Trans.Roy.Soc.Lond.*, A369:2759–2778. 11

[102] Litim, D. F. and Pawlowski, J. M. (1999). On gauge invariance and Ward identities for the Wilsonian renormalization group. *Nucl.Phys.Proc.Suppl.*, 74:325–328. 18

[103] Litim, D. F. and Vergara, L. (2004). Subleading critical exponents from the renormalization group. *Phys.Lett.*, B581:263–269. 53

[104] Litim, D. F. and Zappala, D. (2011). Ising exponents from the functional renormalisation group. *Phys.Rev.*, D83:085009. 17

[105] Machado, P. F. and Saueressig, F. (2008). On the renormalization group flow of f(R)-gravity. *Phys.Rev.*, D77:124045. 8, 9, 17, 26, 39, 40, 86, 134

[106] Manrique, E. and Reuter, M. (2010). Bimetric Truncations for Quantum Einstein Gravity and Asymptotic Safety. *Annals Phys.*, 325:785–815. 20, 22

[107] Manrique, E., Reuter, M., and Saueressig, F. (2011a). Bimetric Renormalization Group Flows in Quantum Einstein Gravity. *Annals Phys.*, 326:463–485. 20

[108] Manrique, E., Reuter, M., and Saueressig, F. (2011b). Matter Induced Bimetric Actions for Gravity. *Annals Phys.*, 326:440–462. 20

[109] Marchais, E. (2011). Private communication. 47

[110] Modesto, L. and Nicolini, P. (2010). "Charged rotating noncommutative black holes". *Phys.Rev.*, D82:104035. 93

[111] Monteiro, R., Perry, M. J., and Santos, J. E. (2009). "Thermodynamic instability of rotating black holes". *Phys.Rev.*, D80:024041. 85

[112] Morris, T. R. (1998). Elements of the continuous renormalization group. *Prog.Theor.Phys.Suppl.*, 131:395–414. 12

[113] Myers, R. C. and Perry, M. J. (1986). "Black Holes in Higher Dimensional Space-Times". *Ann. Phys.*, 172:304. 2, 85, 87, 103, 112

[114] Nambu, Y. (1960). Quasiparticles and Gauge Invariance in the Theory of Superconductivity. *Phys.Rev.*, 117:648–663. 3

[115] Narain, G. and Percacci, R. (2010). Renormalization Group Flow in Scalar-Tensor Theories. I. *Class.Quant.Grav.*, 27:075001. 8, 40

[116] Narain, G. and Rahmede, C. (2010). Renormalization Group Flow in Scalar-Tensor Theories. II. *Class.Quant.Grav.*, 27:075002. 8, 40

[117] Nicolini, P., Smailagic, A., and Spallucci, E. (2006). "Noncommutative geometry inspired Schwarzschild black hole". *Phys.Lett.*, B632:547–551. 93

[118] Niedermaier, M. and Reuter, M. (2006). "The Asymptotic Safety Scenario in Quantum Gravity". *Living Rev.Rel.*, 9:5. 11, 86

[119] Nordström, G. (1918). On the energy of the gravitational field in einstein's theory. *Verhandl. Koninkl. Ned. Akad. Wetenschap., Afdel. Natuurk.* 2

[120] Percacci, R. (2007). Asymptotic Safety. 11

[121] Percacci, R. and Perini, D. (2003a). Asymptotic safety of gravity coupled to matter. *Phys.Rev.*, D68:044018. 8, 20, 40, 86

[122] Percacci, R. and Perini, D. (2003b). Constraints on matter from asymptotic safety. *Phys.Rev.*, D67:081503. 8, 40, 86

[123] Polchinski, J. (1992). Effective field theory and the Fermi surface. 11

[124] Polchinski, J. (1998a). *String theory. Vol. 1: An introduction to the bosonic string.* Cambridge University Press. 5

[125] Polchinski, J. (1998b). *String theory. Vol. 2: Superstring theory and beyond.* Cambridge University Press. 5

[126] Politzer, H. D. (1973). Reliable Perturbative Results for Strong Interactions? *Phys.Rev.Lett.*, 30:1346–1349. 3

[127] Racz, I. and Wald, R. M. (1992). "Extension of space-times with Killing horizon". *Class. Quant. Grav.*, 9:2643–2656. 114

[128] Randall, L. and Sundrum, R. (1999). "A large mass hierarchy from a small extra dimension". *Phys. Rev. Lett.*, 83:3370–3373. 4

[129] Reissner, H. (1916). Über die eigengravitation des elektrischen feldes nach der einsteinschen. *Theorie. Ann. Phys.* 2

[130] Reuter, M. (1998). "Nonperturbative evolution equation for quantum gravity". *Phys.Rev.*, D57:971–985. 5, 8, 9, 11, 17, 18, 19, 20, 21, 26, 39, 86, 90

[131] Reuter, M. and Saueressig, F. (2005). From big bang to asymptotic de Sitter: Complete cosmologies in a quantum gravity framework. *JCAP*, 0509:012. 8

[132] Reuter, M. and Saueressig, F. (2007). Functional Renormalization Group Equations, Asymptotic Safety, and Quantum Einstein Gravity. 11

[133] Reuter, M. and Tuiran, E. (2006). Quantum Gravity Effects in Rotating Black Holes. pages 2608–2610. 8, 86, 115

[134] Reuter, M. and Tuiran, E. (2011). "Quantum Gravity Effects in the Kerr Spacetime". *Phys.Rev. D*, 83. 8, 86, 95, 112, 113, 114, 115

[135] Reuter, M. and Weyer, H. (2004). Renormalization group improved gravitational actions: A Brans-Dicke approach. *Phys.Rev.*, D69:104022. 8

[136] Rosten, O. J. (2012). Fundamentals of the Exact Renormalization Group. *Phys.Rept.*, 511:177–272. 12

[137] Rovelli, C. (2004). *Quantum gravity.* Cambridge University Press. 5

[138] Rovelli, C. and Smolin, L. (1990). Loop Space Representation of Quantum General Relativity. *Nucl.Phys.*, B331:80. 5

[139] Schwarzschild, K. (1916). "On the gravitational field of a mass point according to Einstein's theory". *Sitzungsber.Preuss.Akad.Wiss.Berlin (Math.Phys.)*, pages 189–196. 2, 85

[140] Smarr, L. (1973). "Mass formula for Kerr black holes",. *Phys. Rev. Lett.*, 30:71–73. 113

[141] Souma, W. (1999). Nontrivial ultraviolet fixed point in quantum gravity. *Prog.Theor.Phys.*, 102:181–195. 8, 39, 86, 90

[142] 't Hooft, G. and Veltman, M. (1974a). One loop divergencies in the theory of gravitation. *Annales Poincare Phys.Theor.*, A20:69–94. 4

[143] 't Hooft, G. and Veltman, M. (1974b). "One loop divergencies in the theory of gravitation". *Annales Poincare Phys.Theor.*, A20:69–94. 85

[144] Tangherlini, F. R. (1963). "Schwarzschild field in n dimensions and the dimensionality of space problem". *Nuovo Cim.*, 27:636–651. 2, 85, 87

[145] Turyshev, S. G. (2008). Experimental Tests of General Relativity. *Ann.Rev.Nucl.Part.Sci.*, 58:207–248. 2

[146] Visser, M. (1993). "Dirty black holes: Entropy versus area". *Phys.Rev.*, D48:583–591. 114

[147] Wald, R. M. (1993). "Black hole entropy is the Noether charge". *Phys.Rev.*, D48:3427–3431. 114

[148] Weinberg, S. (1979). *General Relativity: An Einstein centenary survey*, chapter Ultraviolet dirvergences in quantum theories of gravity, pages 790– 831. Cambridge University Press. 5, 6, 7, 39, 40, 66, 72, 85, 90, 117

[149] Weinberg, S. (1980). Effective Gauge Theories. *Phys.Lett.*, B91:51. 11

[150] Weinberg, S. (1995). *The quantum theory of fields. Vol. 1: Foundations.* Cambridge University Press. 3

[151] Weinberg, S. (1996). *The quantum theory of fields. Vol. 2: Modern applications.* Cambridge University Press. 3

[152] Weinberg, S. (2008). *Cosmology.* OUP Oxford. 2

[153] Wetterich, C. (1993). Exact evolution equation for the effective potential. *Phys.Lett.*, B301:90–94. 8, 11, 12, 117

[154] Wilson, K. and Kogut, J. B. (1974). The Renormalization group and the epsilon expansion. *Phys.Rept.*, 12:75–200. 3, 11

[155] Wilson, K. G. (1971a). Renormalization group and critical phenomena. 1. Renormalization group and the Kadanoff scaling picture. *Phys.Rev.*, B4:3174–3183. 3, 11

[156] Wilson, K. G. (1971b). The Renormalization Group and Strong Interactions. *Phys.Rev.*, D3:1818. 3, 11

[157] Wilson, K. G. (1975). The Renormalization Group: Critical Phenomena and the Kondo Problem. *Rev.Mod.Phys.*, 47:773. 3, 11

[158] York, James W., J. (1973). Conformatlly invariant orthogonal decomposition of symmetric tensors on Riemannian manifolds and the initial value problem of general relativity. *J.Math.Phys.*, 14:456–464. 25, 26

[159] Zanusso, O., Zambelli, L., Vacca, G., and Percacci, R. (2010). Gravitational corrections to Yukawa systems. *Phys.Lett.*, B689:90–94. 8, 40, 86

Appendix A

Variations and Hessians

A.1 Second variations

Here we present the variations for the various terms that appear in (4.5) evaluated on the sphere. These can be read from Table A.1

$\delta(\sqrt{g})$	$\frac{1}{2}\sqrt{g}h$
$\delta(R)$	$-\frac{R}{d}h + \nabla^\alpha\nabla^\beta h_{\alpha\beta} - \nabla^2 h$
$\delta(R_{\mu\nu}R^{\mu\nu})$	$-2\frac{R^2}{d^2}h - 2\frac{R}{d}\nabla^2 h + 2\frac{R}{d}\nabla^\mu\nabla^\nu h_{\mu\nu}$
$\delta^{(2)}(\sqrt{g})$	$\frac{1}{2}\sqrt{g}\left(\frac{1}{2}hh - h_{\mu\nu}h^{\mu\nu}\right)$
$\delta^{(2)}(R)$	$h_{\mu\nu}\left[\frac{1}{2}\nabla^2 + \frac{d-2}{d(d-1)}R\right]h^{\mu\nu}$ $+h\left[\frac{1}{2}\nabla^2 + \frac{R}{d(d-1)}\right]h$ $+(\nabla_\alpha h^{\alpha\beta})(\nabla^\mu h_{\mu\beta})$
$\delta^{(2)}(R_{\mu\nu}R^{\mu\nu})$	$h_{\mu\nu}\left[\frac{1}{2}\nabla^4 + \frac{R}{d}\frac{d-3}{d-1}\nabla^2 + 2\frac{R^2}{d^2}\frac{d^2-3d+3}{(d-1)^2}\right]h^{\mu\nu}$ $+h\left[\frac{1}{2}\nabla^4 + \frac{R}{d}\frac{3d+1}{2(d-1)}\nabla^2 + 2\frac{R^2}{d^2}\frac{2d-3}{(d-1)^2}\right]h$ $+(\nabla_\mu\nabla_\nu h^{\mu\nu})[-\nabla^2]h + (\nabla_\alpha h^{\alpha\beta})\left[\nabla^2 + \frac{3R}{d}\right](\nabla^\mu h_{\mu\beta}) + (\nabla_\alpha\nabla_\beta h^{\alpha\beta})^2$

Table A.1: Summary of the variations

A.2 The Hessians for the $f(R)$ approximation

Here we present the Hessians that arise from the gravitational part $\bar{\Gamma}_k^{\text{quad}}$ after substituting the metric decomposition (3.2) into the second variation (4.6). Then we get for the

corresponding matrix elements of the transverse-traceless part

$$\left(\bar{\Gamma}_k^{(2)}\right)^{h^T h^T} = \frac{1}{2}F_k'(R)\Box - \frac{1}{2}F_k(R) - \frac{d-2}{d(d-1)}R\,F_k'(R). \tag{A.1}$$

For the transverse vector part

$$\left(\bar{\Gamma}_k^{(2)}\right)^{\xi\xi} = \left[F_k(R) - 2F_k'(R)\frac{R}{d}\right]\Box + F_k(R)\frac{R}{d} - 2F_k'(R)\frac{R^2}{d^2}. \tag{A.2}$$

For the scalar part

$$\begin{aligned}\left(\bar{\Gamma}_k^{(2)}\right)^{\sigma\sigma} =& \frac{(d-1)^2}{d^2}\Box^4 - \frac{d-1}{2d^2}\left[(d-2)F_k'(R) - 4RF_k''(R)\right]\Box^3 \\ &- \frac{1}{2d^2}\left[d(d-1)F_k(R) - R(d\,F_k'(R) + 2RF_k''(R)\right]\Box^2 \\ &- \left[R\left(d\,F_k(R) - 2RF_k'(R)\right)\right]\Box.\end{aligned} \tag{A.3}$$

For the non-diagonal piece

$$\begin{aligned}\left(\bar{\Gamma}_k^{(2)}\right)^{\sigma h} =& -\frac{(d-1)^2}{d^2}F_k''(R)\Box^3 + \frac{(d-1)}{d^2}\left[\frac{(d-2)}{2}F_k'(R) - 2RF_k''(R)\right]\Box^2 \\ &+ \frac{1}{d^2}\left[\frac{(d-2)}{2}F_k'(R) - RF_k''(R)\right]R\,\Box.\end{aligned} \tag{A.4}$$

And finally for the trace part

$$\begin{aligned}\left(\bar{\Gamma}_k^{(2)}\right)^{hh} =& \frac{(d-1)^2}{d^2}F_k''(R)\Box^2 - \frac{1}{4d^2}\left[2(d-1)\left((d-2)F_k'(R) - 4R\,F_k''(R)\right)\right]\Box \\ &+ \frac{1}{4d^2}\left[(d-2)(d\,F_k(R) - 4RF_k'(R)) + 4R^2F_k''(R)\right].\end{aligned} \tag{A.5}$$

A.3 The Hessians for the $f(R^{\mu\nu}R_{\mu\nu}) + R\,z(R^{\mu\nu}R_{\mu\nu})$ approximation

Here we present the Hessians that arise from the gravitational part $\bar{\Gamma}_k^{\rm quad}$ after substituting the metric decomposition (3.2) into the second variation (5.7). Then we get for the corresponding matrix elements of the transverse-traceless part

$$\begin{aligned}\left(\bar{\Gamma}_k^{(2)}\right)^{h^T h^T} =& \frac{1}{2}(f' + R\,z')\Box^2 + \left[\frac{1}{2}z + \frac{R}{d}\frac{d-3}{d-1}(f' + R\,z')\right]\Box \\ &+ 2\frac{R^2}{d^2}\frac{d^2-3d+3}{(d-1)^2}(f' + R\,z') - \frac{1}{2}(f + R\,z) + \frac{d-2}{d(d-1)}R\,z\end{aligned} \tag{A.6}$$

For the transverse vector part

$$\left(\bar{\Gamma}_k^{(2)}\right)^{\xi\xi} = \left[-4\frac{R^2}{d^2}(f' + R\,z') + f + R\,z - 2\frac{R}{d}z\right]\Box - 4\frac{R^3}{d^3}(f' + R\,z') + \frac{R}{d}(f + R\,z) - 2\frac{R^2}{d^2}z \tag{A.7}$$

For the scalar part

$$\begin{aligned}\left(\bar{\Gamma}_k^{(2)}\right)^{\sigma\sigma} = &\left[\frac{1}{2}\frac{d-1}{d}(f'+R\,z') + 4\frac{R}{d}\left(\frac{d-1}{d}\right)^2\left(z'+\frac{R^2}{d}z''+\frac{R}{d}f''\right)\right]\Box^4\\ &+\left[-\frac{R}{d}\frac{d^2-10d+8}{2d^2}(f'+R\,z') + 8\frac{R^2}{d^2}\frac{d-1}{d}\left(z'+\frac{R^2}{d}z''+\frac{R}{d}f''\right)\right.\\ &\left.-\frac{(d-1)(d-2)}{2d^2}z\right]\Box^3\\ &+\left[\frac{R^2}{d^2}\frac{d+2}{d}(f'+R\,z') + 4\frac{R^3}{d^3}\left(z'+\frac{R^2}{d}z''+\frac{R}{d}f''\right) - \frac{1}{2}\frac{d-1}{d}(f+R\,z) + \frac{1}{2}\frac{R}{d}z\right]\Box^2\\ &+\left[2\frac{R^3}{d^3}(f'+R\,z') - \frac{1}{2}\frac{R}{d}(f+R\,z) + \frac{R^2}{d^2}z\right]\Box\end{aligned} \tag{A.8}$$

For the non-diagonal piece

$$\begin{aligned}\left(\bar{\Gamma}_k^{(2)}\right)^{\sigma h} = &\left[-\frac{d-1}{d}(f'+R\,z') - 8\frac{(d-1)^2}{d^3}R\left(z'+\frac{R^2}{d}z''+\frac{R}{d}f''\right)\right]\Box^3\\ &+\left[\frac{R}{d}\frac{d^2-10d+8}{d^2}(f'+R\,z') - 16\frac{R^2}{d^2}\frac{d-1}{d}\left(z'+\frac{R^2}{d}z''+\frac{R}{d}f''\right)\right.\\ &\left.+\frac{(d-1)(d-2)}{d^2}z\right]\Box^2\\ &+\left[2\frac{R^2}{d^2}\frac{d-4}{d}(f'+R\,z') - 8\frac{R^3}{d^3}\left(z'+\frac{R^2}{d}z''+\frac{R}{d}f''\right) + \frac{R}{d}\frac{d-2}{d}z\right]\Box\end{aligned} \tag{A.9}$$

And finally for the trace part

$$\begin{aligned}\left(\bar{\Gamma}_k^{(2)}\right)^{hh} = &\left[\frac{d-1}{2d}(f'+R\,z') + 4\frac{R}{d}\left(\frac{d-1}{d}\right)^2\left(z'+\frac{R^2}{d}z''+\frac{R}{d}f''\right)\right]\Box^2\\ &+\left[-\frac{R}{d}\frac{d^2-10d+8}{2d^2}(f'+R\,z') + 8\frac{R^2}{d^2}\frac{d-1}{d}\left(z'+\frac{R^2}{d}z''+\frac{R}{d}f''\right)\right.\\ &\left.-\frac{(d-1)(d-2)}{2d^2}z\right]\Box\\ &-2\frac{R^2}{d^2}\frac{d-3}{d}(f'+R\,z') + 4\frac{R^3}{d^3}\left(z'+\frac{R^2}{d}z''+\frac{R}{d}f''\right) + \frac{d-2}{4d}(f+R\,z) - \frac{R}{d}\frac{d-2}{d}\,z\end{aligned} \tag{A.10}$$

Appendix B

Heat Kernel coefficients

In this Appendix we summarise some technicalities of the heat kernel techniques. We examine how these are affected when we consider constrained fields. For a full overview of the heat kernel methods we refer to [9, 63]. Some of the information found here has also been discussed in [91, 34, 105].

B.1 Constrained fields

First we need to know how the trace evaluation is modified due to the fact that we decompose our original fields. For example, any vector field V^μ can be decomposed in its transverse and longitudinal part as

$$V^\mu = V^{T\mu} + \nabla^\mu \eta \tag{B.1}$$

with $\nabla_\mu V^{T\mu} = 0$. Similarly, any symmetric tensor $h_{\mu\nu}$ is decomposed according to

$$h_{\mu\nu} = h^T_{\mu\nu} + \nabla_\mu \xi_\nu + \nabla_\nu \xi_\mu + \nabla_\mu \nabla_\nu \sigma - \frac{1}{d} g_{\mu\nu} \nabla^2 \sigma + \frac{1}{d} g_{\mu\nu} h \tag{B.2}$$

subject to the constraints

$$g^{\mu\nu} h^T_{\mu\nu} = 0, \qquad \nabla^\mu h^T_{\mu\nu} = 0, \qquad \nabla^\mu \xi_\mu = 0, \qquad h = g_{\mu\nu} h^{\mu\nu} \tag{B.3}$$

so that $h^T_{\mu\nu}$ is the transverse-traceless part of $h_{\mu\nu}$, ξ_μ is a transverse vector, σ is a scalar and h is the trace part of $h_{\mu\nu}$. From now on we use the notation $(2T)$ for a transverse-traceless symmetric tensor, $(1T)$ for a transverse vector

In order to see how this affects the calculation, we need to know how the coefficients $\mathbf{b}_n$ are modified when the operator is restricted to act on $(2T)$ tensors and $(1T)$ vectors. For this, we are going to relate the spectrum of the constrained fields in terms of the unconstrained. We start with the transverse vectors and we note that the spectrum of

every vector can be expressed as the union of the spectrum of a $(1T)$ vector and of the longitudinal mode $\nabla_\mu\eta$. The spectrum of $\nabla_\mu\eta$ can be related to that of the scalar field η through the commutation relations

$$-\nabla^2\nabla_\mu\eta = -\nabla_\mu\left(\nabla^2 + \frac{R}{d}\right)\eta. \tag{B.4}$$

We note however that for a constant scalar η, the vector V^μ receives no contribution from the longitudinal mode. So we have to subtract from the scalar trace the constant mode. Thus we write for the trace of a transverse vector

$$\mathrm{Tr}_{(1)}\left[e^{t\nabla^2}\right] = \mathrm{Tr}_{(1T)}\left[e^{t\nabla^2}\right] + \mathrm{Tr}_{(0)}\left[e^{t\left(\nabla^2+\frac{R}{d}\right)}\right] - e^{t\frac{R}{d}}, \tag{B.5}$$

where the last term corresponds to the zero mode of the scalar field. Thus we can relate the spectrum of the transverse vector to that of the unconstrained vector.

Now we turn our attention to the constraints of the transverse traceless tensors. Then for the symmetric tensors we use the commutation relations

$$-\nabla^2\left(\nabla_\mu\xi_\nu + \nabla_\nu\xi_\mu\right) = \nabla_\mu\left(-\nabla^2 - \frac{d+1}{d(d-1)}R\right)\xi_\nu + \nabla_\nu\left(-\nabla^2 - \frac{d+1}{d(d-1)}R\right)\xi_\nu \tag{B.6}$$

and

$$-\nabla^2\left(\nabla_\mu\nabla_\nu - \frac{1}{d}g_{\mu\nu}\nabla^2\right)\sigma = \left(\nabla_\mu\nabla_\nu - \frac{1}{d}g_{\mu\nu}\right)\left(-\nabla^2 - \frac{2}{d-1}R\right)\sigma. \tag{B.7}$$

As in the case of the transverse vector there are modes that do not contribute to the trace. These modes are (i) the $\frac{d(d+1)}{2}$ Killing vectors for which $\nabla_\mu\xi_\nu + \nabla_\nu\xi_\mu = 0$ so that they do not contribute to $h_{\mu\nu}$. (ii) a constant scalar σ as in the case of vectors and (iii) the $d+1$ scalars which correspond to the second lowest eigenvalue of $-\nabla^2 - \frac{2}{d-1}R$. Thus we have for the trace of a symmetric tensor

$$\begin{aligned}\mathrm{Tr}_{(2)}\left[e^{t\nabla^2}\right] =& \mathrm{Tr}_{(2T)}\left[e^{t\nabla^2}\right] + \mathrm{Tr}_{(1T)}\left[e^{t\left(\nabla^2+\frac{d+1}{d(d-1)}R\right)}\right] + \mathrm{Tr}_{(0)}\left[e^{t\nabla^2}\right] + \mathrm{Tr}_{(0)}\left[e^{t\left(\nabla^2+\frac{2}{d-1}R\right)}\right] \\ & - e^{t\frac{2}{d-1}R} - (d+1)e^{t\frac{1}{d-1}R} - \frac{d(d+1)}{2}e^{t\frac{2}{d(d-1)}R}.\end{aligned} \tag{B.8}$$

Again we can relate the spectrum of the constrained transverse traceless tensor to that of the 2-tensor the vector and the scalar.

In order to clarify how the contributions from the exponents play a role in our calculation we expand the exponential in powers of R such as $\sum_{m=0}^{\infty} c_m R^m$. Taking into account that the volume of the sphere goes like $V \sim R^{-d/2}$ and that the heat kernel coefficients like $\mathbf{b}_n \sim R^{n/2}$ we find that

$$\int d^dx\sqrt{g}\,\mathbf{b}_n \sim R^{\frac{n-d}{2}}. \tag{B.9}$$

Since ultimately we are interested in comparing powers of R the exponentials contribute when $2m = n - d$ and the coefficients $\mathbf{b}_n$ receive contributions only when $n \geq d$. Another way to see where the excluded modes enter is from the expansion $e^{-tz} = 1 - tz + \frac{1}{2}t^2z^2 + ...$ In order for the parameter t to be included in $Q_i[W] = \int_0^\infty dt\, t^{-i}\tilde{W}(t)$ we see directly from (2.42) that the corresponding power m of the expansion $\sum_{m=0}^\infty c_m R^m$ is such that $2m = n - d$.

B.2 Summary

Here we summarise the trace of the heat kernel coefficients $\mathrm{tr}_s\mathbf{b}_n = b_n|_s$ for the fields that we will be interested in after taking into account their constraints. We write 0 for the scalars, 1 for the vectors and 2 for the tensors. For the scalars we have

$$b_0|_0 = 1 \tag{B.10}$$

$$b_2|_0 = \frac{1}{6}R \tag{B.11}$$

$$b_4|_0 = \frac{\left(5d^2 - 7d + 6\right)R^2}{360(d-1)d} \tag{B.12}$$

$$b_6|_0 = \frac{\left(35d^4 - 112d^3 + 187d^2 - 110d + 96\right)R^3}{45360(d-1)^2d^2} \tag{B.13}$$

$$b_8|_0 = \frac{\left(175d^6 - 945d^5 + 2389d^4 - 3111d^3 + 3304d^2 - 516d + 2160\right)R^4}{5443200(d-1)^3d^3}\,. \tag{B.14}$$

For the transverse vector fields we have

$$b_0|_1 = d - 1 \tag{B.15}$$

$$b_2|_1 = \frac{R(6\delta_{2,d} + (d-3)(d+2))}{6d} \tag{B.16}$$

$$b_4|_1 = \frac{R^2\left(360\delta_{2,d} + 720\delta_{4,d} + 5d^4 - 12d^3 - 47d^2 - 186d + 180\right)}{360(d-1)d^2} \tag{B.17}$$

$$b_6|_1 = R^3\left(\frac{\delta_{2,d}}{8} + \frac{\delta_{4,d}}{96}\right) + \frac{\left(35d^6 - 147d^5 - 331d^4 - 3825d^3 - 676d^2 + 10992d - 7560\right)R^3}{45360(d-1)^2d^3} \tag{B.18}$$

$$b_8|_1 = R^4\left(\frac{\delta_{2,d}}{96} + \frac{\delta_{4,d}}{768} + \frac{\delta_{6,d}}{2700} + \frac{15\delta_{8,d}}{175616}\right) + \frac{\left(175d^7 - 2345d^6 - 8531d^5 - 15911d^4 + 16144d^3 + 133924d^2 - 206400d + 75600\right)R^4}{75600(d-1)^3d^4} \tag{B.19}$$

Finally for the transverse traceless tensor fields we have

$$
\begin{aligned}
b_0|_2 &= \frac{1}{2}(d-2)(d+1) && \text{(B.20)}\\
b_2|_2 &= \frac{(d+1)(d+2)R(3\delta_{2,d}+d-5)}{12(d-1)} && \text{(B.21)}\\
b_4|_2 &= \frac{(d+1)R^2\left(1440\delta_{2,d}+3240\delta_{4,d}+5d^4-22d^3-83d^2-392d-228\right)}{720(d-1)^2 d} && \text{(B.22)}\\
b_6|_2 &= R^3\left(\frac{3\delta_{2,d}}{2}+\frac{5\delta_{4,d}}{36}\right) && \text{(B.23)}\\
&+ \frac{(d+1)\left(35d^6-217d^5-667d^4-7951d^3-13564d^2-10084d-28032\right)R^3}{90720(d-1)^3d^2}\\
b_8|_2 &= R^4\left(\frac{\delta_{2,d}}{2}+\frac{5\delta_{4,d}}{288}+\frac{\delta_{6,d}}{175}+\frac{675\delta_{8,d}}{175616}\right) && \text{(B.24)}\\
&+ \frac{\left(175d^{10}-945d^9+464d^8-150566d^7+478295d^6-2028005d^5\right)R^4}{453600(d-1)^4d^4}\\
&+ \frac{(-2945774d^4-5191124d^3-10359960d^2-7018560d-181440)R^4}{453600(d-1)^4d^4}.
\end{aligned}
$$

Finally, in Table B.1 we summarise the eigenvalues of the operator $-\nabla^2$ on scalars, transverse vectors and transverse-traceless symmetric tensors and their multiplicities.

	$\Lambda_l(d,s)$	$D_l(d,s)$
$T^{lm}_{\mu\nu}$ with $l\geq 2$	$\frac{l(l+d-1)-2}{d(d-1)}R$	$\frac{(d+1)(d-2)(l+d)(l-1)(2l+d-1)(l+d-3)!}{2(d-1)!(l+1)!}$
T^{lm}_{μ} with $l\geq 1$	$\frac{l(l+d-1)-1}{d(d-1)}R$	$\frac{l(l+d-1)(2l+d-1)(l+d-3)!}{(d-2)!(l+1)!}$
T^{lm} with $l\geq 0$	$\frac{l(l+d-1)}{d(d-1)}R$	$\frac{(2l+d-1)(l+d-2)!}{l!(d-1)!}$

Table B.1: Summary of the eigenvalues of the operator $-\nabla^2$ on scalars, transverse vectors and transverse-traceless symmetric tensors and their multiplicities

Appendix C

Black Holes

C.1 Horizons

In this Appendix we are going to show that under the assumptions discussed in section 6.3.1 the spacetime has always either two horizons (an event and a Cauchy horizon), one extreme, or no horizons at all depending on the values of its parameters.

First we want to define what are the assumptions for $G(r)$ that we are going to use and to extend them, so to cover the maximum possible variety of runnings. For this we review the relation which defines the horizons for non-rotating black holes. This reads

$$f(r)|_{a=0} = 1 - \frac{M\,G(r)}{r^{d-3}} = 0 \tag{C.1}$$

and its first derivative (which is the first derivative of the gravitational potential) is given by

$$V'(r) = M\,G(r)\,r^{2-d}\left[d - 3 + \eta(r)\right]. \tag{C.2}$$

In order for non-rotating black holes to have the usual behavior (either two, one critical or no horizons) we have to demand two things. First, that the limit $r \to 0$ of the lapse function is positive. This implies that

$$\lim_{r\to 0} V(r) = \lim_{r\to 0}\left(-\frac{M\,G(r)}{r^{d-3}}\right) > -1. \tag{C.3}$$

If this hold true then the limits of $f(r)$ as $r \to 0$ and as $r \to \infty$ are both positive. Consequently, if $f(r)$ has only one minimum, the spacetime has two horizons if this minimum is negative, one degenerate horizon if this minimum is 0 and no horizons if it is positive.

In order to achieve this behavior we need that $V'(r)$ changes from negative to positive values only once. For this to be true it is enough to postulate that the anomalous dimension for gravity $\eta(r)$ is a monotonically increasing function of r and that it satisfies

$$\lim_{r\to 0}\eta(r) < 3 - d, \qquad \lim_{r\to\infty}\eta(r) = 0. \tag{C.4}$$

Then, it is evident that if (C.3) and (C.4) hold, the spacetime for non-rotating black holes has the desired behavior.

In the case of asymptotic safety, the above two assumptions can be reduced to a single assumption for the matching of momentum and position scales. If, we make the identification

$$k(r) \sim \frac{\xi}{r^{\gamma}} \tag{C.5}$$

and use the running for $G(k)$ implied by asymptotic safety (6.9), then the two assumptions reduce to the single condition for the parameter γ

$$\gamma > \frac{d-3}{d-2} \tag{C.6}$$

We note, that the matching we are commonly using for our calculations is $k(r) = 1/r$, meaning $\gamma = 1$, which clearly satisfies the condition (C.6).

Now we are going to see that the above assumptions are enough to ensure that the spacetime of rotating black holes still has the same horizon structure in four and five dimensions. For six or higher dimensions we will see that we have to demand more details about the behavior of $G(r)$. Now, the relation which gives the horizons is

$$f(r) = 1 + \frac{a^2}{r^2} - \frac{M\,G(r)}{r^{d-3}}. \tag{C.7}$$

The limits of this function for $r \to 0$ and $r \to \infty$ are again both positive under the condition (C.3). Again, we need to show that this function has only one minimum and so that its first derivative changes from negative to positive values only once. So, we turn our attention to

$$r^3\, f'(r) = -2a^2 + M\,G(r)\,r^{5-d}\,[d-3+\eta(r)]\,. \tag{C.8}$$

In what follows we will need to find out also about the behaviour of the second term in (C.8), so we define the function $U(r) = M\,G(r)\,r^{5-d}\,[d-3+\eta(r)]$ and we write down its first derivative $U'(r) = -M\,G(r)\,r^{4-d}\,[(d-5+\eta(r))\,(d-3+\eta(r)) - r\,\eta'(r)]$. Moreover, we define r_1 as the value of r for which the anomalous dimension becomes $\eta(r_1) = 3-d$ and r_2 when we have $\eta(r_2) = 5-d$. Now, we need to distinguish between $d=4$, $d=5$ and $d \geq 6$ in order to find the behavior of $f'(r)$. We start with the four dimensional case.

d=4. Using both assumptions (C.3) and (C.4) we can see that the limit of $f'(r)$ as $r \to 0$ is negative and the limit of $f'(r)$ as $r \to \infty$ is positive. However, we need to know that $f'(r)$ changes sign only once. For the region of r between $0 \leq r \leq r_1$, $f'(r)$ is always negative. So, in order to change sign only once we have to assure that for $r > r_1$, $U(r)$ is

always a growing function of r. This is easily seen by looking at its first derivative $U'(r)$, since for $r > r_1$ then $\eta(r) > -1$ and $\eta'(r) > 0$ always.

d=5. In five dimensions the limit $r \to 0$ of $f'(r)$ is still negative, but the limit $r \to \infty$ has the sign of $M\,G_N - a^2$. This being positive, is just the condition for the existence of roots in the classical case. In the case where $M\,G_N - a^2 > 0$, the limit of $f'(r)$ when $r \to \infty$ is positive and is easily checked again from $U'(r)$ that for $r > r_1$, $U(r)$ is growing and so that the spacetime has the expected behavior. If on the other hand $M\,G_N - a^2 < 0$ then $f'(r)$ is always negative and there are no horizons.

d=6. Now the limit $r \to 0$ of $f'(r)$ is still negative, but the limit $r \to \infty$ is negative too. In order to have only one minimum for $f(r)$ we need that $f'(r)$ has the most two roots. This is satisfied if for $r > r_1$, $U(r)$ grows until a maximum value and then decreases to 0. For this we have to check the sign of the expression inside square brackets in $U'(r)$. For $r_1 < r < r_2$ then $U(r)$ is positive implying that $U(r)$ grows. Now, in order for rotating black holes in $d \geq 6$ dimensions to have the desired horizon structure we have to impose the condition that for $r > r_2$ the function $U'(r)$ has only one root. This condition is far stronger in terms of $\eta(r)$ than those that we have assumed so far, but in the case of asymptotic safety and for a running given by (6.9) with a matching that obeys $\gamma > \frac{d-3}{d-2}$ it is easily checked that this condition holds.

For completeness we state a derivation of the fact that the function of $G(k)$ given by (6.9) using the linear matching $k \sim 1/r$ gives the usual horizon structure with two, one critical or no horizons. In what follows we use dimensionless variables and we start looking for roots of the function $\tilde{\Delta}(x)$ (with G_N substituted by $G(x)$)

$$\tilde{\Delta}(x) = A + x^2 - \frac{x^3}{x^{d-2} + \Omega} \tag{C.9}$$

It is obvious, that now the limits $x \to 0$ and $x \to \infty$, (in contrast to the classical case for $d \geq 6$) do not guarantee the existence of a horizon in any dimensionality, since they always return $\tilde{\Delta} = A$ and $\tilde{\Delta} = \infty$ respectively. The next step is to look at the first derivative of $\tilde{\Delta}$ with respect to x, which is written

$$\begin{aligned} \tilde{\Delta}'(x) = &\frac{x}{(x^{d-2} + \Omega)^2} \cdot \Big[2x^{2(d-2)} + (d-5)x^{d-1} \\ &+4\Omega x^{d-2} - 3\Omega x + 2\Omega^2\Big] \end{aligned} \tag{C.10}$$

At first sight this doesn't look very helpful. In order to have horizons it is necessary (but not sufficient) that $\Delta'(x)$ becomes negative for some x. The limits $x \to 0$ and $x \to \infty$

of $\tilde{\Delta}'(x)$ give 0 and ∞ respectively, providing as with no information about the roots of $\tilde{\Delta}'(x)$.

Now we note, that the roots of $\tilde{\Delta}'(x)$ are the roots of the expression in square brackets in (C.10), which we call $N(x)$, and moreover that the sign of $\tilde{\Delta}'(x)$ is that of $N(x)$. A careful study of $N(x)$ and its derivatives shows that, for $d \geq 5$, it starts from a positive value ($2\Omega^2$), it decreases until some value $N(x_1)$ and then increases up to infinity. Whether or not $N(x_1)$ (and therefore $\tilde{\Delta}'(x_1)$) is negative, depends (for each dimensionality d) only on the value of Ω. If $\tilde{\Delta}'(x)$ becomes negative, then it has two roots x_2 and x_0, with $x_2 < x_1 < x_0$.

With this information we have what we need to determine the behavior of $\tilde{\Delta}(x)$. It begins from the positive value A and it starts increasing. If $\tilde{\Delta}'(x)$ remains positive for every x, then $\tilde{\Delta}(x)$ continues to increase and there are no horizons. If $\tilde{\Delta}'(x)$ becomes negative at some interval (x_2, x_0), then $\tilde{\Delta}(x)$ decreases until a value $\tilde{\Delta}(x_0)$ and then increases to infinity. When $\tilde{\Delta}(x_0) < 0$ the spacetime has two horizons. If $\tilde{\Delta}(x_0) = 0$ the spacetime has one degenerate horizon, while if $\tilde{\Delta}(x_0) > 0$ there are no horizons.

C.2 Energy-momentum tensor

The coefficients U^μ_ν in equation (6.53) are given by

$$
\begin{aligned}
U^t_t &= \frac{Mr^{4-d}}{8\Sigma^3}\left[(9-2d)a^4 + 2(8-3d)a^2r^2 - 4(d-2)r^4 - 2(d-4)a^2(a^2+r^2)\cos(2\theta) - a^4\cos(4\theta)\right] \\
U^r_r &= -\frac{Mr^{4-d}}{2\Sigma^2}\left[(d-2)r^2 + (d-4)a^2\cos^2\theta\right] \\
U^\theta_\theta &= -\frac{Mr^{4-d}}{\Sigma^2}a^2\cos^2\theta \\
U^\phi_\phi &= \frac{Mr^{4-d}}{8\Sigma^3}a^2\left[1/2(d-12)a^2 + 2(d-4)r^2 - 2(2a^2+dr^2)\cos(2\theta) - 1/2(d-4)a^2\cos(4\theta)\right] \\
U^t_\phi &= -\frac{Mr^{4-d}}{2\Sigma^3}a(a^2+r^2)\sin^2\theta\left[(d-2)r^2 + (d-6)a^2\cos^2\theta\right] \\
U^\phi_t &= \frac{Mr^{4-d}}{2\Sigma^3}a\left[(d-2)r^2 + (d-6)a^2\cos^2\theta\right] \\
U^i_i &= 0.
\end{aligned}
\tag{C.11}
$$

Similarly, for the coefficients V^μ_ν we get the following expressions

$$
\begin{aligned}
V_t^t &= \frac{Mr^{4-d}}{2\Sigma^2}\, a^2 r \sin^2\theta \\
V_r^r &= 0 \\
V_\theta^\theta &= -\frac{Mr^{4-d}}{2\Sigma}\, r \\
V_\phi^\phi &= -\frac{Mr^{4-d}}{2\Sigma^2}\, r(a^2+r^2) \\
V_\phi^t &= \frac{Mr^{4-d}}{2\Sigma^2}\, a\, r(a^2+r^2)\sin^2\theta \\
V_t^\phi &= -\frac{Mr^{4-d}}{2\Sigma^2}\, a\, r \\
V_i^i &= -\frac{Mr^{4-d}}{2\Sigma}\, r.
\end{aligned}
\tag{C.12}
$$

To check the energy conditions we have to diagonalise the EM tensor. The resulting diagonal $T^{\mu(\text{eff})}_{\nu(\text{diag})}$ is

$$
T^{\mu(\text{eff})}_{\nu(\text{diag})} = \frac{Mr^{4-d}}{8\Sigma^3}\text{diag}\left(T^0_0, T^r_r, T^\theta_\theta, T^3_3, T^4_4, \ldots, T^{d-1}_{d-1}\right) \tag{C.13}
$$

whith T^0_0 and T^3_3 being the diagonalised components given by

$$
T^0_0 = \tfrac{1}{2}\left(T^t_t + T^\phi_\phi - \sqrt{\left(T^t_t - T^\phi_\phi\right)^2 + 4T^t_\phi T^\phi_t}\right) \tag{C.14}
$$

$$
T^3_3 = \tfrac{1}{2}\left(T^t_t + T^\phi_\phi + \sqrt{\left(T^t_t - T^\phi_\phi\right)^2 + 4T^t_\phi T^\phi_t}\right). \tag{C.15}
$$

After substituting the expressions for the energy momentum components from equations (C.11) and (C.12) we get for T^0_0 and T^3_3

$$
T^0_0 = \begin{cases} -\frac{Mr^{4-d}}{2\Sigma^2}\left[(d-2)r^2 + (d-4)a^2\cos^2\theta\right] G'(r) & \text{if } Z(r) > 0, \\ -\frac{Mr^{4-d}}{2\Sigma^2}\left[2a^2\cos^2\theta\, G'(r) + r\Sigma G''(r)\right] & \text{if } Z(r) < 0. \end{cases} \tag{C.16}
$$

$$
T^3_3 = \begin{cases} -\frac{Mr^{4-d}}{2\Sigma^2}\left[2a^2\cos^2\theta\, G'(r) + r\Sigma G''(r)\right] & \text{if } Z(r) > 0, \\ -\frac{Mr^{4-d}}{2\Sigma^2}\left[(d-2)r^2 + (d-4)a^2\cos^2\theta\right] G'(r) & \text{if } Z(r) < 0. \end{cases} \tag{C.17}
$$

Here $Z(r)$ is an expression which has *always one* positive real root for a matching of the form (6.12) and is given by

$$
Z(r) = 2\left[(d-2)r^2 + (d-6)a^2\cos^2\theta\right] G'(r) - 2\, r\, \Sigma\, G''(r). \tag{C.18}
$$

It is essential to know at every point of the spacetime which is the timelike component of the diagonalised energy-momentum tensor which corresponds to the energy density. For this, we take the eigenvectors v_1^μ and v_2^μ used to diagonalise $T^{\mu(\text{eff})}_\nu$ and we compute $g_{\mu\nu}v_1^\mu v_1^\nu$ and $g_{\mu\nu}v_2^\mu v_2^\nu$. We find that when r is between the two horizons, T^r_r is the timelike

component. When r is not between the two horizons and $Z(r) > 0$ the timelike component is T^3_3, while when r is not between the horizons and $Z(r) < 0$ the timelike component is T^0_0. In any of these three cases the diagonal EM-tensor takes the form

$$T^{\mu(\text{eff})}_{\nu(\text{diag})} = \text{diag}\left(-\rho, p_r, p_\perp, p_\perp, p_4, \ldots, p_{d-1}\right), \tag{C.19}$$

where the timelike component is always given by

$$\rho = \frac{M\, r^{4-d}}{2\Sigma^2}\left[(d-2)r^2 + (d-4)a^2\cos^2\theta\right] G'(r) \tag{C.20}$$

and all the other components correspond to spacelike coordinates, with

$$p_\perp = -\frac{M\, r^{4-d}}{2\Sigma^2}\left[2a^2\cos^2\theta\, G'(r) + r\Sigma G''(r)\right]. \tag{C.21}$$

and

$$p_r = -\rho = T^r_r, \qquad\qquad p_i = T^i_i. \tag{C.22}$$

C.3 Kretschmann invariant

Here, we compute two of the curvature invariants, the Ricci scalar and the Kretschmann invariant and we examine the fate of the classical ring singularity at $r = 0, \theta = \pi/2$. The Ricci scalar in our case takes the form

$$R = M\, r^{4-d} \cdot \frac{r\, G''(r) + 2\, G'(r)}{r^2 + a^2\cos^2\theta}, \tag{C.23}$$

while the Kretschmann invariant $K = R_{\mu\nu\rho\sigma}R^{\mu\nu\rho\sigma}$ is given by the following formula

$$\begin{aligned} K =& \frac{M^2\, r^{6-2d}}{\left(r^2 + a^2\cos^2\theta\right)^6} \cdot \left[K_1\, G(r)^2 + K_2\, G(r)\, G'(r) + K_3\, G(r)\, G''(r)\right. \\ & \left. + K_4\, G'(r)^2 + K_5\, G'(r)\, G''(r) + K_6\, G''(r)^2\right] \end{aligned} \tag{C.24}$$

with the coefficients K_1, K_2, K_3, K_4, K_5 and K_6 given by

$$\begin{aligned}
K_1 =&(d-3)(d-2)^2(d-1)\,r^8+4(d-1)\left(-15+(-d+5)(d-4)\,d\right)\,r^6\,a^2\cos^2\theta+\\
&6\left(22+(d-6)\left(7+(d-6)\,d\right)\,d\right)\,r^4\,a^4\cos^4\theta+4(d-5)\left(3+(d-5)(d-4)\,d\right)\,r^2\,a^6\cos^6\theta+\\
&(d-5)(d-4)^2(d-3)\,a^8\cos^8\theta\\
\\
K_2 =&-4\,r\left(r^2+a^2\cos^2\theta\right)\cdot\left[(d-3)(d-2)^2r^6+\left(-48+d\left(64+3(d-9)\,d\right)\right)\,r^4\,a^2\cos^2\theta+\right.\\
&\left.\left(-68+d\left(104+3(d-11)\,d\right)\right)\,r^2\,a^4\cos^4\theta+(d-5)(d-4)^2\,a^6\cos^6\theta\right]\\
\\
K_3 =&2\,r^2(r^2+a^2\cos^2\theta)^2\cdot\left[(d-3)(d-2)\,r^4+2(9+(d-7)d)\,r^2\,a^2\cos^2\theta+\right.\\
&\left.(d-5)(d-4)a^4\cos^4\theta\right]\\
\\
K_4 =&2\,r^2(r^2+a^2\cos^2\theta)\cdot\left[(16+d(2d-11))\,r^4+2(23+d(2d-15))\,r^2\,a^2\cos^2\theta)+\right.\\
&\left.(46+d\,(2d-19))\,a^4\cos^4\theta)\right]\\
\\
K_5 =&16\,r\left(r^2+a^2\cos^2\theta\right)\cdot\left[(d-3)\,r^2+(d-5)\,a^2\cos^2\theta\right]\\
\\
K_6 =&32\,r^3\left(r^2+a^2\cos^2\theta\right)^3
\end{aligned}\tag{C.25}$$

If we approximate the running of the gravitational coupling near the origin as $G(r)=\mu^\sigma\,r^{\sigma+d-3}$, we find the following expression in terms of σ

$$\begin{aligned}
K =&\frac{16\,M^2\,\mu^2\,r^{2\sigma}}{\Sigma^6}\left[384\,r^8-192r^6(\sigma+4)\Sigma+8\,r^4\left(51+2d+38\sigma+6\sigma^2\right)\Sigma^2\right.\\
&-4\,r^2(\sigma+2)(3+2d+2\sigma(5+\sigma))\Sigma^3\\
&\left.+\left(12+2d^2+2d\,(\sigma-1)(\sigma+5)+\sigma(-20+\sigma(\sigma+1)(\sigma+5))\right)\Sigma^4\right]
\end{aligned}\tag{C.26}$$

and for the Ricci scalar

$$R=\frac{M\,\mu\,r^\sigma(d+\sigma-3)(d+\sigma-2)}{r^2+a^2\cos^2\theta}.\tag{C.27}$$